Universitat Politècnica de Catalunya

Microscopic description of two dimensional dipolar quantum gases

Ph. D. Thesis by:

Adrián Macía Rey

Thesis advisors:

Jordi Boronat Médico
Ferran Mazzanti Castrillejo

Departament de física i enginyeria nuclear

November 24, 2014

A Carmen y Alfonso

Aknowledgements

Hay tantas personas a las que tengo tanto que agradecer que podría ocupar la extensión de otra tesis únicamente para los agradecimientos de forma que intentaré ser breve.

En primer lugar quisiera dar las gracias a mis directores de tesis: Jordi Boronat y Ferran Mazzanti. De ellos he aprendido mucho durante los últimos cinco años, mucho de ciencia y también mucho sobre la vida. Han dedicado mucho tiempo y esfuerzo en intentar que me sienta orgulloso del trabajo desarrollado durante todo este tiempo y lo cierto es que lo han conseguido, me siento orgulloso de todo el trabajo que aquí se presenta y aún más de haber podido subir a hombros de estos gigantes. Espero, en el futuro, poder seguir aprendiendo de ellos como amigo.

Quisiera también dedicar un profundo agradecimiento a Grigori Astrakharchik y a Joaquim Casulleras, los otros dos miembros permanentes del grupo de simulación de sistemas cuánticos, por la multitud de charlas y discusiones profundamente enriquecedoras que hemos mantenido, así como también por haber sido unos grandes orientadores y compañeros durante todo este tiempo.

Mi siguiente agradecimiento va dirigido a mis compañeros doctorandos: Jonás, Riccardo, Oleg, Andrés, Guillem y, muy especialmente, a Ausias y Jordi que han sido mis compañeros de despacho a lo largo de todos estos años. A todos ellos les deseo la mejor de las suertes en el presente y en el futuro.

Quiero dedicar también unas palabras al resto de integrantes del departament de física i enginyeria nuclear, al resto de profesores y, sobretodo, al personal de secretaria: Ana, Cristina y Montserrat. Muchas gracias a todos por el trato recibido y por toda la ayuda que me habéis brindado en estos años.

Quiero aprovechar también este espacio para expresar mi gratitud a los grandes profesionales externos al departamento con los que he tenido el honor de colaborar en algunas partes de este trabajo: Stefano Giorgini, Robert E. Zillich y Diana Hufnaghl. Un verdadero placer colaborar con gente de esta dimensión profesional.

Fuera del entorno profesional también hay muchísima gente a la que debo unas palabras de gratitud. En primer lugar a Silvia, ella ha sido la persona

que más de cerca ha seguido los progresos de mi trabajo fuera del entorno laboral. Ha aguantado los momentos buenos y los malos, ha tenido siempre palabras de ánimo y muestras de cariño. No ha resultado fácil para ella tampoco y me atrevo a afirmar que sin ella esta tesis no existiría. Por esto y mucho más muchas gracias.

Quisiera agradecer también a mis padres, Blanca y Cristóbal, pues el camino hasta este momento no empezó con la concesión de una beca doctoral. Hasta este momento he llegado gracias al amor y a la pasión por la ciencia y, en esto, ellos tienen gran parte de culpa pues desde niño me han amamantado con ese interés y esa curiosidad.

Agradezco también al resto de mi entorno, familia y amigos, que han aguantado estoicamente mis charlas sobre las cosas en las que trabajaba, mis progresos y mis aventuras y desventuras. Muchas gracias a todos de corazón.

He dejado para el final los agradecimientos más especiales, quisiera agradecer muy especialmente a mis abuelos, Carmen y Alfonso, porque si hoy estoy aquí es sobre todo gracias a ellos. Mi abuelo me enseñó a apreciar la ciencia como el medio para llegar a conocer y comprender el mundo que me rodea, me enseñó a huir de los dogmatismos y a respetar y admirar el conocimiento científico. Hoy sólo queda uno de ellos para poder ver el resultado de todo el tiempo que han invertido en mí pero, aún así, quiero agradecerles todo lo que me han dado a lo largo de mi vida.

Abstract

A microscopic description of the many-body properties of anisotropic homogeneous gases of bosonic dipoles in two dimensions is presented and discussed. By changing the polarization angle with respect to the plane, we study the impact of the anisotropy, present in the dipole-dipole interaction on different physical quantities. We restrict the analysis to the range of polarization angles where the interaction is always repulsive, although the strength of the repulsion can be strongly dependent on the orientation with respect to the polarization field. We present a study of the zero energy two-body problem which allows us to find the scattering length of the interaction and to build a suitable Jastrow many-body wave function that will be used as a trial wave function for Monte Carlo simulations of the bulk two-dimensional system of bosonic dipoles. In the first part of this work we have studied the low-density dipolar Bose gas and we find that the anisotropy has an almost negligible impact on the ground state properties of the many-body system in the universal regime where the scattering length governs the physics of the system. We also show that scaling in the gas parameter persists in the dipolar case up to values where other isotropic interactions with the same scattering length yield different predictions. We also evaluate the excitation spectrum of the dipolar Bose gas in the context of the Feynman approximation and compare the results obtained with the Bogoliubov ones. As expected, we find that these two approximations agree at very low densities, while they start to deviate from each other as the density increases.

When the density of the system is increased we find that the behavior of the system depends on the value of the polarization angle of the dipolar moments of the system. At large densities and moderate values of the polarization angle the system undergoes a first-order quantum phase transition from a gas and a crystal phase. We also find that the anisotropy of the dipole-dipole potential causes an elongation of the crystalline lattice of the system in the direction where the interaction is stronger. At large polarization angles and moderate densities the system undergoes a second-order quantum phase transition from a gas to a stripe phase. Interestingly, the critical exponents of this second order transition are nearly independent of the tilting angle and are compatible with the 3D Ising and 3D XY model

universality classes within the statistical uncertainty of our simulations. Finally, at high densities and large tilting angles the system shows a first order phase transition between the crystal and stripe phases. The slope of this transition curve is extremely large indicating that, due to the anisotropy of the interaction, the crystal phase of the system is no longer stable if the dipole - dipole potential is highly anisotropic.

We consider the ground state of a bilayer system of dipolar bosons, which is a configuration consisting in the confinement of the particles in two paralel planes by means of a trapping potential. We consider the simplest situation where dipole moments are oriented by an external field in the direction perpendicular to the parallel planes. Quantum Monte Carlo methods are used to calculate the ground-state energy, the one-body and two-body density matrix as a function of the separation between layers. We find that by decreasing the interlayer distance for fixed value of the strength of the dipolar interaction, the behavior of all the physical observables studied are compatible with the existence of a second order phase transition modulated by the inter-layer distance. In this sense, the results presented in this work are in good agreement with some previous studies of dipolar gases in a bilayer setup.

Contents

Chapter 1

Introduction

In 1995 Bose-Einstein condensation of dilute Bose gases was achieved [1, 2]. This fact was the starting point for a new era in the field of experimental quantum physics. Since that pioneering works the interest in the study of ultracold quantum systems has grown up allowing to achieve also the regime of quantum degeneracy in fermionic systems [3, 4, 5, 6] which made possible to observe Fermi superfluidity.

At present, ultracold atomic and molecular physics are at the edge of both theoretical and experimental research, allowing for an unprecedented control over the system. It is nowadays commonly accepted that ultracold systems will soon show applications in the field of quantum information. From the theoretical point of view, ultracold systems are kind of a meeting point for researchers coming from different fields like: condensed matter, nuclear physics, high energy physics and many others.

Despite that quantum gases are extremely dilute systems (their typical density is about 10^{14} - 10^{15} cm^{-3}) most of their properties are strongly influenced by the presence of inter-atomic interactions. The experimental conditions required to bring gases to the quantum degenaracy regime, where temperatures are of the order of nK, imply that the energy involved in the scaterring processes are low enough to be governed by s-wave physics. With this consideration, the exact inter-particle interaction can be approached by an s-wave pseudo potential of the form [7]:

$$U(\mathbf{r}) = \frac{4\pi\hbar^2 a_S}{m}\delta(\mathbf{r}) \tag{1.1}$$

where m is the mass of the particles, a_S is the s-wave scattering length and $\delta(\mathbf{r})$ is the Dirac delta function. The overall factor multiplying the Dirac delta function is the coupling constant, g, so one can write $U(\mathbf{r}) = g\delta(\mathbf{r})$. In many of the atomic species commonly used in experiments the s-wave scattering length can be tuned by means of a Feshbach resonance [8, 9].

In recent years there has been an increasing interest in the study of quantum systems involving more complex interactions than the simple pseudo

potential of Eq. (1.1). One of these new systems is the dipolar quantum gas. The dipolar interaction between particles having an electric or magnetic dipole moment has two properties that are radically different from short range Van der Waals forces more commonly found in other condensed matter systems:

- It is anisotropic, which means that the interaction strength, and even the its sign (attractive or repulsive), depends on the relative orientation appart from the distance between particles.
- Contrarily to the Van der Waals forces, dipole-dipole interaction are long ranged in three dimensional systems, which means that in dipolar systems the scattering properties are radically different when compared with other systems.

In 2005, it was reported the first Bose-Einstein condensate of ^{52}Cr atoms [10, 11], where the magnetic dipole moment of the atoms is large enough ($\sim 6\mu_B$) to produce observable effects in the collapse of the condensate. More recently, new and exciting results have been achieved with polar molecules of Rubidium and Potassium (^{40}K^{87}Rb) [12], which have not been easy to bring down to quantum degeneracy due to strong loss rates in the population induced by chemical reactions [13, 14]. A promising route towards a molecular Bose-Einstein condensate is the Feshbach association of Rubidium and Cesium, which are not reactive [15]. In the field of atomic condensates, recent efforts have also been focused on exotic lanthanide magnetic systems, like ^{164}Dy [16, 17] and ^{168}Er [18]. The main interest in achieving the quantum degeneracy regime using polar molecules is the fact that the electric dipole moments of molecules are usually much larger than in the magnetic case, and, additionally they can be tuned by the application of an external electric field.

The dipole-dipole interaction for particles with a (magnetic or electric) dipole moment is given by:

$$V_{dd}(\mathbf{r}) = \frac{C_{dd}}{4\pi} \frac{\hat{\mathbf{p}}_1 \cdot \hat{\mathbf{p}}_2 - 3(\hat{\mathbf{p}}_1 \cdot \hat{\mathbf{r}})(\hat{\mathbf{p}}_2 \cdot \hat{\mathbf{r}})}{r^3} \tag{1.2}$$

where C_{dd} is $\mu_0\mu^2$ for particles having a permanent magnetic dipole moment μ and d^2/ϵ_0 for particles having a permanent electric dipole moment d; $\hat{\mathbf{p}}_1$ and $\hat{\mathbf{p}}_2$ point along the direction of the dipolar moments of particles 1 and 2, and $\hat{\mathbf{r}}$ is the relative position vector $\mathbf{r}/r$. The common setup employed in the experiments usually involves polarized samples where all the dipole moments of the particles point in the same direction (see Fig. 1.1). In this situation the general dipole-dipole interaction can be written in the following simpler form:

$$V_{dd}(\mathbf{r}) = \frac{C_{dd}}{4\pi} \frac{1 - 3\cos^2\theta}{r^3} \tag{1.3}$$

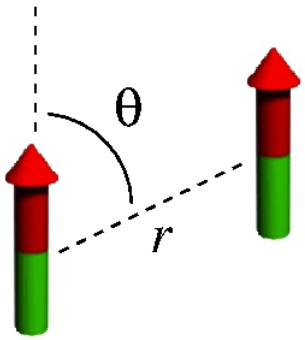

Figure 1.1: Dipoles in three dimensions polarized along z-axis.

It can be seen from (1.3) that dipole-dipole interaction is repulsive for dipoles that are side by side configuration, while for dipoles in a head to tail arrangement it is strongly attractive. This implies that a three dimensional quantum system of particles interacting only via the dipolar potential will be unstable due to this head to tail pairs that make the system collapse of the system. There are two different ways to overcome this problem: On one hand, one can introduce an additional two-body hard core interaction which mimics the well known short range behavior of interparticle interactions. On the other hand the system can be confined along the direction of the dipole moments, such that head to tail configurations are essentially forbidden by the trapping potential, yielding an effective quasi-2D system. Along the rest of this work we have studied the second situation, where the system is confined to two spatial dimensions.

Two-dimensional or quasi-two dimensional dipolar gases have been a very active field in the last years. As we have commented, the scattering properties of the inter-particle interaction have strong influence in the behavior of the many-body system. For this reason, great effort has been devoted to the study of the dipolar scattering in two dimensions [19, 20, 21] using standard two dimensional scattering theory [22, 23] or by means of pseudo-potential approaches [24].

From the quantum many-body point of view, there are several works devoted to the study of the stability of the quasi-two dimensional dipolar gas by analyzing the emergence of a deep roton-like minimum in the elementary excitation spectrum [25, 26, 27] in the framework of mean-field theory. The emergence of this roton-like minimum is absent in the pure two dimensional dipolar gas when the dipolar interaction is isotropic (i. e. when dipole moments are aligned orthogonally to the plane) [28]. The phase diagram of two dimensional dipolar gases have been also extensively studied in the

isotropic situation, for the bosonic [29, 30, 31] and the fermionic case [32]. In both systems, bosonic and fermionic, there is a quantum phase transition from a gas (at low densities) to a crystalline solid (at high densities).

Although two dimensional isotropic dipolar gases have been a widely studied many-body system, not much effort has been devoted to the analysis of dipolar gases, where the dipole moments of the particles are polarized along a direction that is tilted with respect to the orthogonal direction to the plane. There are also mean-field studies of the superfluid properties of quasi two dimensional dipolar Bose gases polarized with a tilt [33], where it is shown that the anisotropy of the interaction can, potentially, induce observable macroscopic effects. There have been also several works devoted to the study of the stability and phase diagram of fermionic dipolar systems in two dimensions using analytical techniques [34, 35, 36, 37]. There is a common prediction in all these works: the appearance of a new phase for strongly interacting systems (i. e. large dipole moment or large density): the stripe phase. To the best of our knowledge, there is only one theoretical work devoted to the study of the many-body properties of a dipolar system of bosons that tries to describe the phase diagram of a trapped sample of dipoles [38]. The main conclusions of that work also point to the existence of a stripe phase.

Another interesting two-dimensional arrangement of dipoles is the bilayer dipolar system where the particles are confined in two paralel planes separated by a fixed distance. In this situation, the dipolar interaction between particles in different layers shows attractive regions that makes possible the formation of dimers [39]. There have been several works discussing fermionic dipoles in this setup and showing the existence of a BEC-BCS crossover [40, 41, 42, 43] and the emergence of pair superfluidity. In the case of a tight- binding model of hard-core bosons on a lattice, the phase diagram at zero temperature has been investigated using mean field [44] and quantum Monte Carlo methods [45], and it was found to include exotic phases around half filling such as the checkerboard solid and the pair supersolid. For a translationally invariant system of bosons the existence of a second order quantum phase transition from two essentially uncorrelated superfluids to a single pair superfluid has also been predicted [46].

In conclusion, we have seen that two-dimensional dipolar systems, the main topic of this Thesis, are a very active research field from both, theoretical and experimental sides.

1.1 Objectives and outline of this work

In the following chapters we present a detailed study of the physics of two dimensional quantum dipolar gases of bosons in two different situations. On one side, the major part of this work is devoted to the study of the two-

dimensional dipolar Bose gas with tilted polarization. On the other side, we have also performed a study of the bilayer system of dipoles which also show some new and interesting physical properties.

In order to accomplish these objectives, we have developed different quantum Monte Carlo codes that implement different Monte Carlo methods that cover the specific requirements of the system of study. We have used variational and diffusion Monte Carlo methods to analyse the physical situations where the anisotropy of the dipole-dipole interaction does not affect significantly the behavior of the system. Alternatively, in the study of strongly correlated anisotropic systems we have used the path integral ground state method since it is much less dependent in the a priori knowledge of the physical properties of the system.

The outline of this work is the following:

- In chapter 2 we present the quantum Monte Carlo methods that we have used in the study of the different many-body systems that are being analyzed in the Thesis. We give a detailed description of variational Monte Carlo and diffusion Monte Carlo methods that are then used in chapters 4 and 6. We also present the basic features of the path integral ground state method (also known as variational path integral) that is being used in chapter 5. After a general description of the Monte Carlo methods we also dicuss how to evaluate the main physical quantities of interest, from the energy of the system to the condensate fraction.

- Chapter 3 is devoted to the study of the two-body problem of a two-dimensional system of bosonic dipoles. We give a detailed description of the problem and show how to obtain a zero energy solution for the general situation of tilted polarized dipoles where the dipole-dipole interaction shows an angular dependent strength. We finally derive an approximate expression for the s-wave scattering length of the two-body problem that is later required in the study of the low density dipolar gas presented in chapter 4.The most relevant results of this Chapter are published in:
  A. Macia, F. Mazzanti, J. Boronat, and R. E. Zillich, *Microscopic description of anisotropic low-density dipolar Bose gases in two dimensions*, Phys. Rev. A **84**, 033625 (2011).

- In chapter 4 we analyse the many-body properties of a low density dipolar gas of bosons with a tilting angle non-orthogonal to the plane. We find that in the low density regime the anisotropy of the interaction does not influence the many-body behavior of the system. We provide an accurate description of the equation of state and the condensate fraction of the system in terms of the s-wave scattering length presented in chapter 3. We also evaluate the Bogoliubov excitation

spectrum of the system which can be compared with the Feynman spectrum obtained from the simulations only at very low densities. The results presented in this Chapter can be found in the following papers:
A. Macia, F. Mazzanti, J. Boronat, and R. E. Zillich, *Microscopic description of anisotropic low-density dipolar Bose gases in two dimensions*, Physical Review A **84**, 033625 (2011).
A. Macia, F. Mazzanti and J. Boronat, *Ground state properties and excitation spectrum of a two dimensional gas of bosonic dipoles*, The European Physical Journal D, **66**, 301, (2012).

- In chapter 5 we study the phase diagram of the two dimensional dipolar system with a tilt, discussing the influence of the anisotropy of the interaction in the strongly correlated system. We give both a qualitative and a quantitative description of the phase diagram by means of the path integral ground state method. We find that at moderate densities and tilting angles the system undergoes a first-order phase transition from a gas to a crystalline solid. At moderate densities and large values of the tilting angle there is a second-order phase transition from the gas phase to a new stripe phase. At large densities and large values of the tilting angle there is another first-order phase transition from a crystal to a stripe phase. This work was published in the following works:
A. Macia, D. Hufnagl, F. Mazzanti, J. Boronat, and R. E. Zillich, *Excitations and Stripe Phase Formation in a Two-Dimensional Dipolar Bose Gas with Tilted Polarization*, Physical Review Letters, **109**, 235307, (2012).
A. Macia, J. Boronat and F. Mazzanti, *Phase diagram of dipolar bosons in 2D with tilted polarization*, accepted for publication in Physical Review A Rapid Communications, available in arXiv: 1407.6960 [cond-mat.quant-gas], (2014).

- In chapter 6 we consider the ground state of a bilayer system of dipolar bosons, whith dipole moments oriented by an external field in the direction perpendicular to the parallel planes. Quantum Monte Carlo methods are used to calculate the ground-state energy and the one- and two-body density matrices as a function of the separation between layers. We find that by decreasing the interlayer distance for fixed value of the strength of the dipolar interaction, the system undergoes a quantum phase transition from a single-particle superfluid to a pair superfluid. The single-particle superfluid is characterized by a finite value of the atomic condensate. The pair superfluid phase is found to be stable against formation of many-body cluster states. Some of the results of this chapter are available in:

A. Macia, G. E. Astrakharchik, F. Mazzanti, S. Giorgini and J. Boronat, *Single-particle vs. pair superfluidity in a bilayer system of dipolar bosons*, Physical Review A **90**, 043623 (2014).

Chapter 2

Quantum Monte Carlo methods

In this chapter we will make a description of the numerical methods that we have been using in order to give a microscopic description of a quantum many body system.

We are interested in giving an accurate description of a quantum fluid of identical particles interacting by means of a pair potential. The complete description of such a system at zero temperature is given by the Schrödinger equation (SE):

$$H|\Psi>=E|\Psi> \tag{2.1}$$

where the hamiltonian H is given, in general, by

$$H=-\frac{\hbar^2}{2m}\sum_{i=1}^{N}\nabla^2+\sum_{i=1}^{N}V_1(\mathbf{r}_i)+\frac{1}{2}\sum_{i=1}^{N}\sum_{j=1,j\neq i}^{N}V_2(\mathbf{r}_i-\mathbf{r}_j) \tag{2.2}$$

where V_1 is an external potential corresponding to an externally applied field and V_2 is a pair interaction that describe the inter-particle interactions.

In the following, we will use the following notation. We call $\mathbf{R}$ the whole set of coordinates of the system, i. e., $\mathbf{R}=\{\mathbf{r}_1,...,\mathbf{r}_N\}$. With this definition, the operator $\nabla^2_{\mathbf{R}}=\sum_{i=1}^{N}\nabla_i^2$ is the laplacian needed for the kinetic term, and finally the potential term will be $V(\mathbf{R})=\sum_{i=1}^{N}V_1(\mathbf{r}_i)+\frac{1}{2}\sum_{i=1}^{N}\sum_{j=1,j\neq i}^{N}V_2(\mathbf{r}_i-\mathbf{r}_j)$.

2.1 Variational Monte Carlo

Variational Monte Carlo (VMC) [47] is the simplest and fastest Monte Carlo method that can be used to obtain an approximate solution to the many-body problem by using the variational principle.

2.1.1 Variational principle

The variational principle tells us that if we consider a trial wave function Ψ_T the expectation value

$$E[\Psi_T] = \frac{< \Psi_T|H|\Psi_T >}{< \Psi_T|\Psi_T >} \tag{2.3}$$

is an upper bound to the ground state energy of the Hamiltonian H. This statement can be easily shown by expanding the trial wave function Ψ in the basis of eigenstates of the Hamiltonian

$$|\Psi_T >= \sum_n a_n|\phi_n > \tag{2.4}$$

where the functions $|\phi_n >$ verify

$$H|\phi_n >= E_n|\phi_n > \qquad \text{and} \qquad < \phi_n|\phi_m >= \delta_{n,m} \tag{2.5}$$

We can use the eigenstate expansion (2.4) in the expectation value (2.1) obtaining the following

$$E[\Psi_T] = \frac{\left(\sum_n a_n^* < \phi_n|\right) H \left(\sum_m a_m|\phi_m >\right)}{\left(\sum_n a_n^* < \phi_n|\right) \left(\sum_m a_m|\phi_m >\right)} \tag{2.6}$$

where by using the properties (2.5) we can finally write the energy of the trial wave function as:

$$E[\Psi_T] = \frac{\sum_n |a_n|^2 E_n}{\sum_n |a_n|^2}. \tag{2.7}$$

In the last expression one can easily see that the expectation value of the energy for the trial wave function $|\Psi_T >$ is always greater than the ground state energy of the hamiltonian unless $|\Psi_T >= |\phi_0 >$. It is useful to consider trial (or variational) wave functions that depends on one or more parameters $(\lambda_1, ...\lambda_n)$ called variational parameters. Those parameters can be optimized to get the lowest energy for a given family of wave functions $|\Psi_T(\lambda_1, ...\lambda_n) >$. In the simplest case of an uniparametric family of variational wave functions $|\Psi_T(\lambda) >$ the energy expectation value will be given by

$$E[\Psi_T(\lambda)] = \frac{< \Psi_T(\lambda)|H|\Psi_T(\lambda) >}{< \Psi_T(\lambda)|\Psi_T(\lambda) >} \tag{2.8}$$

and we can find the optimal variational energy of the hamiltonian by simply minimising this energy expectation value:

$$\frac{dE[\lambda]}{d\lambda}|_{\lambda_{optimal}} = 0 \tag{2.9}$$

2.1.2 Monte Carlo sampling of a variational wave function

The idea behind the variational Monte Carlo method (VMC) is to perform the evaluation of the expectation value in (2.3), that is in general a high dimension integral, by means of an stochastic sampling of a given variational wave function using the Metropolis algorithm.

In position basis the expectation value in (2.3) can be written as

$$E[\Psi_T] = \frac{\int d\mathbf{R}\Psi_T^*(\mathbf{R})H\Psi_T(\mathbf{R})}{\int d\mathbf{R}\Psi_T^*(\mathbf{R})\Psi_T(\mathbf{R})}. \tag{2.10}$$

This integral expression can be written in a more convenient way for Monte Carlo sampling if we think that the square modulus of the wave function gives the propability of finding the system in the configuration $\mathbf{R}$,

$$< E >_{\Psi_T} = \int d\mathbf{R}E_L(\mathbf{R})P(\mathbf{R}), \tag{2.11}$$

where the following two quantities are defined: the probability distribution, $P(\mathbf{R})$

$$P(\mathbf{R}) = \frac{\Psi_T^*(\mathbf{R})\Psi_T(\mathbf{R})}{\int d\mathbf{R}\Psi_T^*(\mathbf{R})\Psi_T(\mathbf{R})}; \tag{2.12}$$

and the so-called local energy, $E_L(\mathbf{R})$

$$E_L(\mathbf{R}) = \frac{H\Psi_T(\mathbf{R})}{\Psi_T(\mathbf{R})}. \tag{2.13}$$

The function $P(\mathbf{R})$ is a well behaved probability distribution that can be sampled using the Metropolis algorithm in order to obtain a sequence of configurations of the system distributed according to it.

Given an ensemble of N_{MC} configurations drawn from $P(\mathbf{R})$ we can simply evaluate the energy expectation value of the hamiltonian as:

$$< E >_{\Psi_T} \approx \frac{1}{N_{MC}} \sum_{i=1}^{N_{MC}} E_L(\mathbf{R}_i), \tag{2.14}$$

and, in general, any observable O can be evaluated along the Monte Carlo sampling as:

$$< O >_{\Psi_T} \approx \frac{1}{N_{MC}} \sum_{i=1}^{N_{MC}} O(\mathbf{R}_i). \tag{2.15}$$

So, given a trial wave function one can compute any observable of interest simply by using expression (2.15).

2.1.3 Variational Monte Carlo algorithm

At this point we have all the ingredients to give an algorithmic description of the VMC method. Let's explain the steps of the VMC algorithm:

1. Draw an initial configuration of the system of interest, $\mathbf{R}$.
2. Guess a new configuration as $\mathbf{R}' = \mathbf{R} + \delta\mathbf{R}$, with $\delta\mathbf{R}$ coming from a uniform or gaussian probability distribution function that verifies $p(\mathbf{R}' \to \mathbf{R}) = p(\mathbf{R} \to \mathbf{R}')$.
3. Evaluate the transition probability as $Q = \frac{\Psi_T^2(\mathbf{R}')}{\Psi_T^2(\mathbf{R})}$
4. Accept or reject the new configuration using Metropolis algorithm.
5. Compute observables of interest.
6. Repeat 2 - 5 to achieve desired accuracy in the calculation.

2.2 Imaginary time propagation methods

VMC is a fast and simple method to compute properties of a quantum many - body system, but it has a very important limitation: all the expectation values of any observable in VMC is completely determined by the trial wave function. The quality of the results obtained in a VMC simulation is directly related to the quality of the variational wave function, so one can expect that for situations where the wave function is poorly known VMC method is not an accurate solution of the quantum problem.

To overcome the limitations of the VMC method we can consider a different family of Monte Carlo methods that can solve the Schrödinger equation by transforming it into an integral equation. The evolution of a quantum system is given by the time dependent Schrödinger equation:

$$i\hbar\frac{\partial\Psi}{\partial t} = -\frac{\hbar^2}{2m}\sum_{i=1}^{N}\nabla^2\Psi + \sum_{i=1}^{N}V_1(\mathbf{r}_i)\Psi + \frac{1}{2}\sum_{i=1}^{N}\sum_{j=1,j\neq i}^{N}V_2(\mathbf{r}_i - \mathbf{r}_j)\Psi. \quad (2.16)$$

We are mainly interested in the ground-state properties of the system. This can be done by defining the imaginary time as $\tau = \frac{it}{\hbar}$ and thus considering the imaginary-time dependent Schrödinger equation

$$-\frac{\partial\Psi}{\partial\tau} = -\frac{\hbar^2}{2m}\sum_{i=1}^{N}\nabla^2\Psi + \sum_{i=1}^{N}V_1(\mathbf{r}_i)\Psi + \frac{1}{2}\sum_{i=1}^{N}\sum_{j=1,j\neq i}^{N}V_2(\mathbf{r}_i - \mathbf{r}_j)\Psi. \quad (2.17)$$

The imaginary-time dependent Schrödinger equation can be written in operator form as:

$$-\frac{\partial|\Psi(\tau)>}{\partial\tau} = H|\Psi(\tau)> \quad (2.18)$$

whose formal solution is:

$$|\Psi(\tau)>=e^{-H\tau}|\Psi(0)>. \tag{2.19}$$

The wave function at $\tau = 0$ can be expanded in terms of the eigenstates of the hamiltonian

$$|\Psi(0)>=\sum_{i=0}^{\infty} a_i|\phi_i> \tag{2.20}$$

and introduce this eigenstate expansion in (2.19) to obtain

$$|\Psi(\tau)>=\sum_{i=0}^{\infty} a_i e^{-\tau\epsilon_i}|\phi_i>. \tag{2.21}$$

If the eigenvalues of the hamiltonian are ordered as $\epsilon_0 < \epsilon_1 < \epsilon_2 < ...$ one can see from (2.21) that for $\tau \to \infty$ all contributions are exponentially vanishing and the slowest decaying term is the corresponding to the ground state of the system. So we can write

$$|\Psi(\tau \to \infty)>\approx a_0 e^{-\tau E_0}|\phi_0>. \tag{2.22}$$

There are several ways to implement the imaginary time propagation of an initial wave function that correspond to different quantum Monte Carlo methods. We have used two main approaches to solve this problem that we will see in the following two sections.

2.2.1 Diffusion Monte Carlo

The first method that we present to implement the imaginary time propagation is the diffusion Monte Carlo method (DMC) [47, 48]. DMC exploits the analogy between the imaginary-time dependent Schrödinger equation and the diffusion equation to achieve the stationary regime of the problem. The stationary solution is proportional to the ground state of the many body quatum problem.

The starting point is the imaginary time dependent Schrödinger equation with an energy shift $H \to H - E_T$:

$$-\frac{\partial|\Psi(\tau)>}{\partial\tau} = (H - E_T)|\Psi(\tau)>, \tag{2.23}$$

If we write explicitly the hamiltonian operator in eq. (2.23) we can write the SE as:

$$-\frac{\partial\Psi}{\partial\tau} = -\frac{\hbar^2}{2m}\nabla^2_{\mathbf{R}}\Psi + (V(\mathbf{R}) - E_T)\Psi \tag{2.24}$$

That is a standard diffusion equation with an additional term that can be interpreted as a sink/source of probability.

If we write now the spectral decomposition of the time-dependent wave function in terms of the imaginary time τ we obtain the following expression:

$$\Psi(\mathbf{R},\tau) = \sum_n a_n \phi_n(\mathbf{R}) e^{-(\epsilon_n - E_T)\tau} \tag{2.25}$$

If we assume that the eigenvalues ϵ_n are ordered as $\epsilon_0 < \epsilon_1 < \cdots < \epsilon_n < \cdots$ we can infer that the asymptotic behavior of $\Psi(\mathbf{R},\tau)$ is given by:

- if $E_T > \epsilon_0$ the wave function Ψ diverges.
- if $E_T < \epsilon_0$ the wave function Ψ vanishes.
- if $E_T = \epsilon_0$ the wave function $\Psi \approx c_0\phi_0$.

The physical interpretation of the method is clear, we must perform an imaginary time evolution until the asymptotic regime is reached, and by a clever choice of the reference energy, E_T, we will find the ground state energy.

There are two practical considerations about the outline of the DMC method as it is presented here. The first one is that the initial many–body wave function $\Psi(\mathbf{R},0)$ must have a significant overlap with the ground state wave function $\phi_0(\mathbf{R})$ if we want a_0 being not too small. The second consideration is that this simple version of DMC requires that the ground state wave function must be positive definite as it effectively happens with the many-body ground state wave function for a system of bosons; for fermions the situation is different and some approximations must be done.

After this last considerations, we will explain how the many-body SE can be integrated using Monte Carlo techniques.

Monte Carlo integration of the many-body Schrödinger equation

For the suitable integration of the many-body SE we have to transform the differential equation in an equivalent integral equation, and, this is easily done by considering the Green's function formalism.

The Green's function of the SE can be defined in an operatorial formalism, and then we will find the equivalent coordinate representation and using it, a practical expression for the Green's function.

The independent-basis SE for our problem is given by:

$$\frac{\partial|\Psi>}{\partial\tau} = -(H - E_T)|\Psi> \tag{2.26}$$

that can be formally solved by means of the time evolution operator $U(\tau,0)$ as follows:

$$|\Psi(\tau)> = U(\tau,0)|\Psi(0)> \tag{2.27}$$

where $U(\tau, 0)$ is given by:

$$U(\tau, 0) = e^{-(H-E_T)\tau} \tag{2.28}$$

now we can project the solution of the SE given in eq. (2.27) in position basis

$$< \mathbf{R}|\Psi(\tau) >= \int d\mathbf{R}' < \mathbf{R}|U(\tau, 0)|\mathbf{R}' >< \mathbf{R}'|\Psi(0) > \tag{2.29}$$

that can be writen as:

$$\Psi(\mathbf{R}, \tau) = \int d\mathbf{R}' < \mathbf{R}|U(\tau, 0)|\mathbf{R}' > \Psi(\mathbf{R}', 0). \tag{2.30}$$

Then we finally have writen an integral equation, equaivalent to the many-body SE and the only problem is to determine the kernel of the integral equation given by $< \mathbf{R}|U(\tau, 0)|\mathbf{R}' >$ that we define as:

$$G(\mathbf{R}, \mathbf{R}', \tau) \equiv < \mathbf{R}|U(\tau, 0)|\mathbf{R}' > \tag{2.31}$$

that is the Green's function of the SE. This Green's function can be determined by solving the differential equation:

$$-\frac{\partial G}{\partial \tau} = -\frac{\hbar^2}{2m}\nabla^2_{\mathbf{R}} G + (V(\mathbf{R}) - E_T)G \tag{2.32}$$

with the initial condition:

$$G(\mathbf{R}, \mathbf{R}', 0) = \delta(\mathbf{R} - \mathbf{R}') \tag{2.33}$$

The SE is then written in terms of the Green's function as:

$$\Psi(\mathbf{R}, \tau) = \int d\mathbf{R}' G(\mathbf{R}, \mathbf{R}', \tau)\Psi(\mathbf{R}', 0) \tag{2.34}$$

This is an integral equation that can be solved using Monte Carlo integration. The problem with the previous integral equation is that the Green's function of the problem is not known. However, we can evaluate the imaginary time evolution of the wave function using the following property of the Green's function,

$$\int d\mathbf{R}'' G(\mathbf{R}, \mathbf{R}'', \tau)G(\mathbf{R}'', \mathbf{R}\text{'}, \tau) = G(\mathbf{R}, \mathbf{R}', 2\tau) \tag{2.35}$$

Then, we can consider the full propagation in imaginary time as successive propagations of time step $\Delta\tau$, and then, we only need to find some short-time approximation for the total Green's function. We can write the following expression for the propagation of the wave function:

$$\Psi(\mathbf{R}, \Delta\tau) = \int d\mathbf{R}' G(\mathbf{R}, \mathbf{R}', \Delta\tau)\Psi(\mathbf{R}', 0) \tag{2.36}$$

or generalizing this expression to an arbitrary step n,

$$\Psi(\mathbf{R}, n\Delta\tau) = \int d\mathbf{R}' G(\mathbf{R}, \mathbf{R}', \Delta\tau)\Psi(\mathbf{R}', (n-1)\Delta\tau) \tag{2.37}$$

And then, as we have seen before, we only need to find some suitable approximation for the Green's function for small $\Delta\tau$.

Short time Green's function

The differential equation that defines the Green's function is given by:

$$-\frac{\partial G(\mathbf{R}, \mathbf{R}', \tau)}{\partial \tau} = \left[-\frac{\hbar^2}{2m}\nabla^2_{\mathbf{R}} + (V(\mathbf{R}) - E_T)\right] G(\mathbf{R}, \mathbf{R}', \tau) \tag{2.38}$$

with the boundary condition $G(\mathbf{R}, \mathbf{R}', 0) = \delta(\mathbf{R} - \mathbf{R}')$.

Now the main problem to obtain an expression for the total Green's function comes from the non conmutativity of the kinetic and potential terms in the hamiltonian. However, the evaluation of the Green's function corresponding to each of the individual pieces is trivial to do. If we consider the two contributions to the Green's function separately we will have, for the kinetic term:

$$G_K(\mathbf{R}, \mathbf{R}', \tau) = < \mathbf{R}|e^{-\frac{\hat{P}^2}{2m}}|\mathbf{R}' > \tag{2.39}$$

That can be easily evaluated in position basis by means of gaussian integration, giving a final kinetic Green's function:

$$G_K(\mathbf{R}, \mathbf{R}', \tau) = \left(\frac{m}{2\pi\hbar^2\tau}\right)^{\frac{dN}{2}} \exp\left[-\frac{m}{\hbar^2}\frac{(\mathbf{R} - \mathbf{R}')^2}{2\tau}\right] \tag{2.40}$$

where d is the dimensionality of the studied system.

For the interaction term we have:

$$G_V(\mathbf{R}, \mathbf{R}', \tau) = < \mathbf{R}|e^{-(V - E_T)\tau}|\mathbf{R}' > \tag{2.41}$$

that in position basis is:

$$G_V(\mathbf{R}, \mathbf{R}', \tau) = \exp\left[-(V(\mathbf{R}) - E_T)\tau\right]\delta(\mathbf{R} - \mathbf{R}') \tag{2.42}$$

With the propagators G_K and G_V we can build short time approximations to the total Green's function.

The time evolution operator defined in (2.28) can be approximated in different ways. A possible approximation of order $\Delta\tau^2$ is the following:

$$U(\Delta\tau) = e^{-(K+V-E_T)\Delta\tau} \approx e^{-K\Delta\tau}e^{-(V-E_T)\Delta\tau} + O(\Delta\tau^2) \tag{2.43}$$

which gives an approximate Green's function given by:

$$G(\mathbf{R},\mathbf{R}',\Delta\tau) = \left(\frac{m}{2\pi\hbar^2\Delta\tau}\right)^{\frac{dN}{2}} e^{-(V(\mathbf{R})-E_T)\Delta\tau} \exp\left[-\frac{m}{\hbar^2}\frac{(\mathbf{R}-\mathbf{R}')^2}{2\Delta\tau}\right] + O(\Delta\tau^2) \tag{2.44}$$

that is exact at first order in $\Delta\tau$.
Another possible decomposition of the time evolution operator is the following:

$$U(\Delta\tau) = e^{-(K+V-E_T)\Delta\tau} \approx e^{-(V-E_T)\frac{\Delta\tau}{2}} e^{-K\Delta\tau} e^{-(V-E_T)\frac{\Delta\tau}{2}} + O(\Delta\tau^3) \tag{2.45}$$

which gives an approximate Green's function given by:

$$G(\mathbf{R},\mathbf{R}',\Delta\tau) = \left(\frac{m}{2\pi\hbar^2\Delta\tau}\right)^{\frac{dN}{2}} e^{-\left(\frac{V(\mathbf{R})+V(\mathbf{R}')}{2}-E_T\right)\Delta\tau} \exp\left[-\frac{m}{\hbar^2}\frac{(\mathbf{R}-\mathbf{R}')^2}{2\Delta\tau}\right] + O(\Delta\tau^3) \tag{2.46}$$

which is exact at second order in $\Delta\tau$.

Importance sampling

In real many body problems with hard-core-like interaction potentials the simple DMC algorithm shows a poor convergence to the ground state solution, with large statistical fluctuations in the mean values of the evaluated observables. However, this can be corrected by means of importance sampling.

In this section we will explain the trick that makes DMC a really powerful method to solve many-body problems: the importance sampling technique. In the previous section we have seen how the imaginary time-dependent Schrödinger equation can be solved by means of Monte Carlo techniques. In this section, we will rewrite it for a different wave function given by:

$$f(\mathbf{R},\tau) \equiv \Psi_T(\mathbf{R})\Psi(\mathbf{R},\tau) \tag{2.47}$$

where $\Psi_T(\mathbf{R})$ is a trial (or guiding) wave function that is expected to be a good approximation to the exact ground state wave function of the system and it is intended to guide the random walk process in order to obtain a faster convergence.

We can write the SE for the function $f(\mathbf{R},\tau)$ from equation (2.24) simply by substituting $\Psi(\mathbf{R},\tau) = \frac{f(\mathbf{R},\tau)}{\Psi_T(\mathbf{R})}$. This gives the following differential equation:

$$-\frac{\partial f}{\partial\tau} = -\frac{1}{2}\nabla^2_{\mathbf{R}} f + \nabla(\mathbf{F}f) + (E_L(\mathbf{R}) - E_T)\, f \tag{2.48}$$

where we have defined the drift force (or velocity) as:

$$\mathbf{F}(\mathbf{R}) \equiv \nabla_{\mathbf{R}} \log \Psi_T(\mathbf{R}) \tag{2.49}$$

and $E_L(\mathbf{R})$ is the local energy defined in (2.13) that can be written using the definition of the drift force as:

$$E_L(\mathbf{R}) = -\frac{\hbar^2}{2m}\left[\nabla^2_{\mathbf{R}} \log \Psi_T(\mathbf{R}) + (\mathbf{F}(\mathbf{R}))^2\right] + V(\mathbf{R}) \tag{2.50}$$

Equation (2.48) can be written in operator notation as:

$$-\frac{\partial f}{\partial \tau} = (K + D + B)f \tag{2.51}$$

where K is the kinetic (or diffusive) term, D is the drift term and B is the termed branching term. As in the non-importance sampling case, we can write the evolution in imaginary time of the new wave function $f(\mathbf{R}, \tau)$ as an evolution operator acting on the initial wave function:

$$|f(\tau) >= U(\tau, 0)|f(0) >= e^{-(K+D+B)\tau}|f(0) > \tag{2.52}$$

In position basis the previous equation is:

$$f(\mathbf{R}, \tau) = \int d\mathbf{R}' < \mathbf{R}|e^{-(K+D+B)\tau}|\mathbf{R}' > f(\mathbf{R'}, 0) \tag{2.53}$$

The Green's function of each individual term in the new hamiltonian are:

$$\begin{cases} G_K(\mathbf{R}, \mathbf{R}', \tau) = \left(\frac{m}{2\pi\hbar^2\Delta\tau}\right)^{\frac{dN}{2}} \exp\left[-\frac{(\mathbf{R}-\mathbf{R}')^2}{2\tau}\right] \\ G_D(\mathbf{R}, \mathbf{R}', \tau) = \delta(\mathbf{R} - \mathcal{R}(\tau)) \\ G_B(\mathbf{R}, \mathbf{R}', \tau) = e^{-(E_L(\mathbf{R})-E_T)\tau}\delta(\mathbf{R} - \mathbf{R}') \end{cases} \tag{2.54}$$

where $\mathcal{R}(\tau)$ is given by:

$$\frac{d\mathcal{R}(\tau)}{d\tau} = \mathbf{F}(\mathcal{R}(\tau)) \tag{2.55}$$

that is the classical trajectory of the configuration moving at a velocity given by the drift term.

As in the non-importance sampling case we can split the time evolution operator in several ways. A first order decomposition is given by:

$$U(\Delta\tau) = e^{-(K+D+B)\Delta\tau} = e^{-K\Delta\tau}e^{-D\Delta\tau}e^{-B\Delta\tau} + O(\Delta\tau^2) \tag{2.56}$$

which gives the approximate Green's function:

$$\begin{aligned} G(\mathbf{R}, \mathbf{R}', \Delta\tau) = &\left(\frac{m}{2\pi\hbar^2\Delta\tau}\right)^{\frac{dN}{2}} e^{-(E_L(\mathbf{R})-E_T)\Delta\tau} \\ &\exp\left[-\frac{m}{\hbar^2}\frac{(\mathbf{R} - \mathcal{R}'(\Delta\tau))^2}{2\Delta\tau}\right] + O(\Delta\tau^2) \end{aligned} \tag{2.57}$$

where $\mathcal{R}'(\Delta\tau)$ is the solution of (2.55) with the initial condition $\mathcal{R}'(0) = \mathbf{R}'$ solved at first order in $\Delta\tau$, this can be done for example by $\mathcal{R}'(\Delta\tau) = \mathbf{R}' + \mathbf{F}(\mathbf{R}')\Delta\tau$.

A higher order decomposition is given by [49]:

$$U(\Delta\tau) = e^{-B\frac{\Delta\tau}{2}} e^{-D\frac{\Delta\tau}{2}} e^{-K\Delta\tau} e^{-D\frac{\Delta\tau}{2}} e^{-B\frac{\Delta\tau}{2}} + O(\Delta\tau^3) \tag{2.58}$$

which gives the approximate Green's function:

$$\begin{aligned} G(\mathbf{R}, \mathbf{R}', \Delta\tau) = &\left(\frac{m}{2\pi\hbar^2\Delta\tau}\right)^{\frac{dN}{2}} e^{-\left(\frac{E_L(\mathbf{R})+E_L(\mathbf{R}')}{2} - E_T\right)\Delta\tau} \\ &\int d\mathbf{R}''\delta(\mathbf{R} - \mathcal{R}''(\Delta\tau/2)) \exp\left[-\frac{m}{\hbar^2}\frac{(\mathbf{R}'' - \mathcal{R}'(\Delta\tau/2))^2}{2\Delta\tau}\right] \\ &+ O(\Delta\tau^3) \end{aligned} \tag{2.59}$$

where $\mathcal{R}'(\Delta\tau/2)$ and $\mathcal{R}''(\Delta\tau/2)$ are the solutions of (2.55) with initial conditions $\mathbf{R}'$ and $\mathbf{R}''$ respectively. In this quadratic Green's function one must solve the differential equation 2.55 with a second order algorithm.

Diffusion Monte Carlo algorithm with importance sampling

In the DMC method the probability density function $f(\mathbf{R}, \tau)$ is represented as an ensemble of N_W points in the configuration space called walkers. A walker is defined by the positions of all the particles of the system $\mathbf{R} = \{\mathbf{r}_1, \mathbf{r}_2, ...\mathbf{r}_N\}$. In this approximation we can write the function f as:

$$f(\mathbf{R}, \tau) = \mathcal{N}\sum_{i=1}^{N_W} \delta(\mathbf{R} - \mathbf{R}_i(\tau)) \tag{2.60}$$

where $\mathcal{N}$ simply gives the normalization factor.

Once we have defined the function $f(\mathbf{R}, \tau)$ at the present time step we need to describe how the Green's function given in (2.59) acts over it. At this point we decompose the full effect of the Green's function in three different steps.

The first step is a free diffusion. This process describes the isotropic diffusion of a walker through the configuration space and can be easily implemented by

$$\mathbf{R}' = \mathbf{R} + \boldsymbol{\eta}\sqrt{\Delta\tau} \tag{2.61}$$

where $\boldsymbol{\eta}$ is a normalized gaussian random vector drawn from the free (or kinetic) Green's function G_K defined in eq. (2.54) with $\boldsymbol{\eta} = \mathbf{R}' - \mathbf{R}$. This gaussian diffusion must be performed for walkers in the ensemble at time τ.

After the gaussian diffusion process there is the drift step. This step represents the effect of the importance sampling technique in the DMC algorithm. This process tries to guide the imaginary time evolution of the

walkers to regions of the configuration space where the wave function is expected to be large. The implementation of this step is as follows, first one needs to evaluate the drift force defined in eq. (2.49) and then use some second order integration method to integrate the differential equation (2.55). In our case we use the second order Runge-Kutta method [49] given by the two following steps:

$$\begin{aligned} \mathbf{R}'' &= \mathbf{R}' + \Delta\tau \mathbf{F}(\mathbf{R}') \\ \mathbf{R}''' &= \mathbf{R}'' + \frac{\Delta\tau}{2}(\mathbf{F}(\mathbf{R}'') + \mathbf{F}(\mathbf{R}')) \end{aligned} \tag{2.62}$$

The last part of the effect of the Green's function over the probability distribution function is the key point of the DMC method, the branching process. Up to this point the two different contributions to the short time Green's function conserves the norm of the function f, but in order to solve exactly the many body Schrödinger equation we have to add a term that is a source/sink of walkers. The branching process duplicates walkers that best mimics the exact ground state distribution or alternatively kills walkers that are far from the desired solution.

The implementation of the branching process can by done by simply making N_{sons} copies of each walker where N_{sons} is given by

$$N_{sons} = int\left(e^{-(E_L(\mathbf{R})-E_T)\tau} + \chi\right) \tag{2.63}$$

where χ is a uniform random number in the range $[0, 1)$ and $int()$ is the integer part function.

At this point it is clear that we can adjust the reference energy E_T in order to reduce the fluctuations in the number of walkers and keep the population size in the desired range. Another important issue is that when the number of walkers remains statistically constant the trial energy E_T is an estimator of the ground state energy of the many body system.

At the end of an imaginary time step we will obtain a new probability distribution function given by:

$$f(\mathrm{R}, \tau + \Delta\tau) = \mathcal{N} \sum_{i=1}^{N'_W} \delta(\mathbf{R} - \mathbf{R}_i(\tau + \Delta\tau)) \tag{2.64}$$

So, in summary we can write the DMC algorithm as:

1. Generate an initial set of walkers.
2. Evaluate the drift force (2.49) and the local energy (2.50) for each walker.
3. For each walker perform the diffusion, drift and branching processes as explained above.
4. When asymptothic regime is reached repeat 2-3 until statistical accuracy is the desired.

2.2.2 Path integral ground state

In this section we introduce the last Monte Carlo method that we have used along this work. It is the path integral ground state (PIGS), also known as variational path integral [50, 51, 52, 53, 54]. This method has common points with the two methods discussed previously (VMC and DMC). We can describe briefly the PIGS method as a variational Monte Carlo method using an imaginary time propagated trial wave function.

As we have seen previously we can write the imaginary time dependent Schrödinger equation as an equivalent integral equation (2.30), and use that expression for the wave function $\Psi(\mathbf{R},\tau)$ as a variational wave function in a Monte Carlo calculation. In such a Monte Carlo calculation we can use as the probability distribution function the following expression

$$\Psi(\mathbf{R},\tau) = \int d\mathbf{R}' G(\mathbf{R},\mathbf{R}',\tau)\Psi(\mathbf{R},0) \tag{2.65}$$

The idea behind the PIGS method is similar to the previously commented in DMC. We can decompose the Green's function in several steps as:

$$G(\mathbf{R}_M,\mathbf{R}_0,\tau) \approx \int d\mathbf{R}_{M-1}...d\mathbf{R}_1 \prod_{j=0}^{M-1} G(\mathbf{R}_{j+1},\mathbf{R}_j,\Delta\tau) \tag{2.66}$$

where $\Delta\tau = \frac{\tau}{M}$. Using the decomposition of the Green's function we can write the ground state wave function as:

$$\Psi_0(\mathbf{R}) = \lim_{M\to\infty} \int d\mathbf{R}_{M-1}...d\mathbf{R}_0 \prod_{j=0}^{M-1} G(\mathbf{R}_{j+1},\mathbf{R}_j,\Delta\tau)\Psi(\mathbf{R}_0,0). \tag{2.67}$$

It is obvious that in a computational simulation one must work with a finite M value, so the point is to build a variational wave function with a finite number of convolution terms, using as initial condition a carefully chosen trial wave function, $\Psi(\mathbf{R},0) = \Psi_T(\mathbf{R})$. With these considerations the variational wave function in PIGS can be written as:

$$\Psi_{PIGS}(\mathbf{R},\tau) = \int d\mathbf{R}_{M-1}...d\mathbf{R}_0 \prod_{i=0}^{M-1} G(\mathbf{R}_{j+1},\mathbf{R}_j,\Delta\tau)\Psi_T(\mathbf{R}_0) \tag{2.68}$$

where $\mathbf{R}_M = \mathbf{R}$. With this last expression for the PIGS wave function we can evaluate the energy of the many body problem as

$$E_{PIGS}(\tau) = \frac{\int d\mathbf{R}\Psi_{PIGS}(\mathbf{R},\tau)\hat{H}\Psi_{PIGS}(\mathbf{R},\tau)}{\int d\mathbf{R}\Psi_{PIGS}(\mathbf{R},\tau)\Psi_{PIGS}(\mathbf{R},\tau)}. \tag{2.69}$$

The variational principle ensures that this expression is an strict upper bound of the ground state energy of the many body problem. At this stage

we can see that the advantage of PIGS over VMC is that within this method we have a systematic process that allows to obtain a variational energy that is in principle as close to the exact ground state function as we need. One only have to increase the number of convolution terms in order to obtain a better variational estimation for the ground state energy. One can compute the energy for increasing values of M and find an asymptotic regime where the bias introduced by considering a finite number of convolution terms is smaller than the statistical uncertainties introduced by the Monte Carlo process.

We have seen how to evaluate the energy of the system in terms of the variational function Ψ_{PIGS}. One can write the expectation value of any other operator as follows

$$< \hat{O} >= \frac{\int d\mathbf{R} O(\mathbf{R}) |\Psi_{PIGS}(\mathbf{R}, \tau)|^2}{\int d\mathbf{R} |\Psi_{PIGS}(\mathbf{R}, \tau)|^2}. \tag{2.70}$$

From the previous expression and the explicit form of Ψ_{PIGS} given in (2.68) we can write that expectation value as

$$< \hat{O} >= \int d\mathbf{R} O(\mathbf{R}) P(\mathbf{R}), \tag{2.71}$$

where the probability distribution function is given by

$$P(\mathbf{R}_0, ...\mathbf{R}_{2M}) = \frac{\Psi_T(\mathbf{R}_0) \prod_{j=0}^{2M-1} G(\mathbf{R}_{j+1}, \mathbf{R}_j, \Delta\tau) \Psi_T(\mathbf{R}_{2M})}{\int d\mathbf{R}_0 ... d\mathbf{R}_{2M} \Psi_T(\mathbf{R}_0) \prod_{j=0}^{2M-1} G(\mathbf{R}_{j+1}, \mathbf{R}_j, \Delta\tau) \Psi_T(\mathbf{R}_{2M})}. \tag{2.72}$$

An important issue of the PIGS method is the short-time approximation of the Green's function of the system, which is the representation of the time evolution operator in the position basis,

$$G(\mathbf{R}, \mathbf{R}', \Delta\tau) =< \mathbf{R} | e^{-\hat{H}\Delta\tau} | \mathbf{R}' > \tag{2.73}$$

where $\hat{H} = \hat{K} + \hat{V}$ is the hamiltonian of the system and $\hat{K}$ and $\hat{V}$ are the kinetic and potential energy operators respectively. The simplest short time approximation to the Green's function is the primitive approximation given by

$$e^{-\hat{H}\tau} = e^{-\hat{K}\Delta\tau} e^{-\hat{V}\Delta\tau} + O(\Delta\tau^2). \tag{2.74}$$

The representation of the kinetic and potential part of the Green's function is shown in the following epxpressions:

$$\begin{aligned} G_K(\mathbf{R}, \mathbf{R}', \Delta\tau) &= \left(\frac{m}{2\pi\hbar^2\Delta\tau}\right)^{\frac{dN}{2}} e^{-\frac{m}{\hbar^2}\frac{(\mathbf{R}-\mathbf{R}')^2}{2\Delta\tau}} \\ G_V(\mathbf{R}, \mathbf{R}', \Delta\tau) &= e^{-V(\mathbf{R})\Delta\tau} \delta(\mathbf{R} - \mathbf{R}') \end{aligned} \tag{2.75}$$

where d is the dimensionality of the system. Using the primitive approximation we can obtain the Green's function for any imaginary time value τ increasing the number of convolution terms in (2.72). The convergence to the exact result is guaranteed by the Trotter formula:

$$e^{-\tau\hat{H}} = \lim_{M\to\infty}\left(e^{-\Delta\tau\hat{K}}e^{-\Delta\tau\hat{V}}\right)^{M}. \tag{2.76}$$

The classical isomorphism

We have seen in the previous section the theoretical basis of the PIGS method. In this section we will show an important issue of the method, the classical isomorphism. The Green's function $G(\mathbf{R},\mathbf{R}',\tau)$ can be written explicitly in terms of the kinetic and potential contributions given in (2.75) as:

$$\begin{aligned} G(\mathbf{R}_0,\mathbf{R}_{2M},\tau) = &\left(\frac{m}{2\pi\hbar^2\Delta\tau}\right)^{\frac{dNM}{2}}\times \\ &\times\int d\mathbf{R}_1,\ldots d\mathbf{R}_{2M-1}\prod_{j=0}^{2M-1} e^{-\frac{m}{\hbar^2}\frac{(\mathbf{R}_{j+1}-\mathbf{R}_j)^2}{2\Delta\tau}-V(\mathbf{R}_j)\Delta\tau} \end{aligned} \tag{2.77}$$

where $\mathbf{R}_0=\mathbf{R}'$, $\mathbf{R}_{2M}=\mathbf{R}$ and $\tau = M\Delta\tau$. The exponent of the kinetic term can be written as:

$$-\frac{m}{\hbar^2}\frac{(\mathbf{R}_{j+1}-\mathbf{R}_j)^2}{2\Delta\tau} = -\frac{m}{2\hbar^2\Delta\tau}\sum_{i=1}^{N}(\mathbf{r}_{j+1,i}-\mathbf{r}_{j,i})^2 \tag{2.78}$$

while the potential term can be written as:

$$-V(\mathbf{R})\Delta\tau = -\Delta\tau\sum_{i=1}^{N}\left(V_1(\mathbf{r}_{i,j})+\frac{1}{2}\sum_{k=1,k\neq i}^{N}V_2(\mathbf{r}_{i,j}-\mathbf{r}_{k,j})\right) \tag{2.79}$$

where N is the number of particles of the system. Using the expressions (2.78) and (2.79) one can write explicitly the probability distribution function $P(\mathbf{R}_1,\ldots\mathbf{R}_M)$ from equation (2.72) as

$$\begin{aligned} P(\mathbf{R}_1,\ldots\mathbf{R}_{2M}) = &\frac{1}{\mathcal{Z}}\left(\frac{m}{2\pi\hbar^2\Delta\tau}\right)^{\frac{dNM}{2}}\times \\ &\times e^{\left[-\sum_{i=1}^{N}\frac{m}{2\hbar^2\Delta\tau}\sum_{j=0}^{2M-1}(\mathbf{r}_{i,j+1}-\mathbf{r}_{i,j})^2\right]}\times \\ &\times e^{\left[-\Delta\tau\sum_{i=1}^{N}\sum_{j=0}^{2M-1}\left(V_1(\mathbf{r}_{i,j})+\frac{1}{2}\sum_{k=1,k\neq i}^{N}V_2(\mathbf{r}_{i,j}-\mathbf{r}_{k,j})\right)\right]}\times \\ &\times e^{(\log\Psi_T(\mathbf{r}_{1,0},\ldots\mathbf{r}_{N,0})+\log\Psi_T(\mathbf{r}_{1,2M},\ldots\mathbf{r}_{N,2M}))} \end{aligned} \tag{2.80}$$

where $\mathcal{Z}$ is the following normalization integral

$$\begin{aligned}\mathcal{Z} = \int d\mathbf{R}_0, ...d\mathbf{R}_{2M} \left(\frac{m}{2\pi\hbar^2\Delta\tau}\right)^{\frac{dNM}{2}} \times \\ \times e^{\left[-\sum_{i=1}^{N} \frac{m}{2\hbar^2\Delta\tau} \sum_{j=0}^{2M-1} (\mathbf{r}_{i,j+1}-\mathbf{r}_{i,j})^2\right]} \times \\ \times e^{\left[-\Delta\tau \sum_{i=1}^{N} \sum_{j=0}^{2M-1} \left(V_1(\mathbf{r}_{i,j}) + \frac{1}{2}\sum_{k=1,k\neq i}^{N} V_2(\mathbf{r}_{i,j}-\mathbf{r}_{k,j})\right)\right]} \times \\ \times e^{(\log \Psi_T(\mathbf{r}_{1,0},...\mathbf{r}_{N,0}) + \log \Psi_T(\mathbf{r}_{1,2M},...\mathbf{r}_{N,2M}))}\end{aligned} \tag{2.81}$$

This last expression is completely analogous to the canonical partition function of a system of N classical open polimers each of them having $2M+1$ particles (or beads) bounded by harmonic springs (the kinetic energy terms). Each polymer interacts with the rest by means of the potential terms in a special way, there is only interaction between beads corresponding to equal imaginary times.

Basic path integral ground state algorithm

Using the classical isomorphism the PIGS method can be thought as a variational Monte Carlo method applied to a system of N linear polymers that interact between them. Starting from a set of initial configurations given by $\{\mathbf{X}_1, ..., \mathbf{X}_N\}$ where each $\mathbf{X}_i$ is the set of positions of one of these linear polymers, i. e. $\mathbf{X}_i = \{\mathbf{R}_0^{(i)}, ..., \mathbf{R}_{2M+1}^{(i)}\}$.

The PIGS algorithm is schematically given by:

1. Draw an initial configuration for each linear polymer $\{\mathbf{X}_1, ..., \mathbf{X}_N\}$ representing the full imaginary time path of each particle.
2. Guess a new configuration for the system by making $\mathbf{X}_i' = \mathbf{X}_i + \delta\mathbf{X}_i$.
3. Evaluate the transition probability to the new configuration as
$$Q = \frac{P(\mathbf{X}_1, ..., \mathbf{X}_i', ..., \mathbf{X}_N)}{P(\mathbf{X}_1, ..., \mathbf{X}_i, ..., \mathbf{X}_N)}. \tag{2.82}$$
4. Accept or reject the new configuration using Metropolis algorithm.
5. Compute observables of interest.
6. Repeat 2 - 5 to achieve the desired accuracy.

This is a basic PIGS algorithm build in complete analogy with the variational Monte Carlo method that can be improved in several ways. The first problem of this simple algorithm is that their efficiency can be not very high due to the presence of the kinetic terms connecting different beads in each polymer. In the following, we will see how to improve the efficiency of the sampling.

Staging algorithm

As we have commented previously, the simple sampling of the path integral can have some efficiency problems due to the presence of the kinetic springs. There are several methods to improve the efficiency of the sampling that can exploit the fact that the kinetic part of the action can be exactly sampled. In this work we have used the staging algorithm [55] with this purpose.

The staging algorithm works by purposing smart collective motions of several beads of each linear polymer. The positions of the new configuration are randomly generated using the kinetic part of the action and then the Metropolis test must only be applied to the potential part improving dramatically the efficiency of the algorithm.

In order to implement the collective motions let's consider the free (or kinetic) part of the action as a product of kinetic contributions involving all the beads of a single chain:

$$\begin{aligned} G_0(\mathbf{x}_0, \mathbf{x}_{2M}, \tau) = G_0(\mathbf{x}_0, \mathbf{x}_1, \Delta\tau) \times ... \times \\ \times G_0(\mathbf{x}_i, \mathbf{x}_{i+1}, \Delta\tau) \times ... \times \\ \times G_0(\mathbf{x}_{i+j-1}, \mathbf{x}_{i+j}, \Delta\tau) \times ... \times \\ \times G_0(\mathbf{x}_{2M-1}, \mathbf{x}_{2M}, \Delta\tau) \end{aligned} \tag{2.83}$$

where the $\mathbf{x}$ variable make reference to the d-dimensional coordinates of any of the N chains of the system. We are interested in build a new set of positions $\{\mathbf{x}_{i+1}, ..., \mathbf{x}_{i+j-1}\}$ generated randomly according to the free particle action. We can define the function S as:

$$S(\mathbf{x}_i, \mathbf{x}_{i+j}, j\Delta\tau) = \prod_{k=1}^{j} G_0(\mathbf{x}_{i+k-1}, \mathbf{x}_{i+k}, \Delta\tau) \tag{2.84}$$

and define a new set of coordinates $\mathbf{y}$ that allows us to write S in a decoupled form given by

$$S(\mathbf{x}_i, \mathbf{x}_{i+j}, j\Delta\tau) = G_0(\mathbf{x}_i, \mathbf{x}_{i+j}, j\Delta\tau) \prod_{k=1}^{j-1} G_0^{(k)}(\mathbf{x}_{i+k}, \mathbf{y}_{i+k}, \Delta\tau) \tag{2.85}$$

where the function $G_0^{(k)}$ is defined as

$$G_0^{(k)}(\mathbf{x}_{i+k}, \mathbf{y}_{i+k}, \Delta\tau) = \left(\frac{m_k}{2\pi\hbar^2\Delta\tau}\right)^{\frac{d}{2}} e^{-\frac{m_k}{\hbar^2}\frac{(\mathbf{x}_{i+k}-\mathbf{y}_{i+k})^2}{2\Delta\tau}}. \tag{2.86}$$

As it can be seen from (2.86) the new coordinates imply a redefinition of the mass term $m \to m_k$. So finally we can write the staging coordinates and the new mass term as:

$$\mathbf{y}_{i+k} = \frac{\mathbf{x}_{i+j} + \mathbf{x}_{i+k-1}(j - (k-1))}{j-k} \tag{2.87}$$

$$m_k = m\left(\frac{j-(k-1)}{j-k}\right) \tag{2.88}$$

Using this smart change of variables we can generate collective motions of several beads in a single chain by simply generating gaussian random numbers as:

$$\mathbf{x}'_{i+k} = \mathbf{y}_{i+k} + \eta\sqrt{\frac{\hbar^2\tau}{m_k}} \tag{2.89}$$

where η is a $U(0,1)$ random number.

Using this method we generate a set of new coordinates using the kinetic action as probability distribution function so we must sample only the potential action in the Metropolis algorithm.

High order approximation to the Green's function

Another aspect that can be improved in the simple PIGS method that we have explained is the approximation to the short time Green's function of the system. In the introduction of the method we have developed all the theory using the so-called primitive approximation that is accurate up to second order in $\Delta\tau$.

$$< \mathbf{R}|e^{(T+V)\Delta\tau}|\mathbf{R}' >=< \mathbf{R}|e^{\frac{V}{2}\Delta\tau}e^{T\Delta\tau}e^{\frac{V}{2}\Delta\tau}|\mathbf{R}' > \tag{2.90}$$

An obvious improvement is to consider some higher order decomposition for the propagator of the system.

A more accurate form of the Green's function allows for a faster convergence of the method and, as a consequence, a decrease in the required number of beads or a larger time step to achieve the convergence. In this work we have used the following approximation for the short time propagator [56, 57, 58]:

$$\begin{aligned} < \mathbf{R}|e^{(T+V)\Delta\tau}|\mathbf{R}' > =& < \mathbf{R}|e^{\frac{V}{6}\Delta\tau}e^{\frac{T}{2}\Delta\tau}e^{\frac{2W}{3}\Delta\tau}e^{\frac{T}{2}\Delta\tau}e^{\frac{V}{6}\Delta\tau}|\mathbf{R}' > \\ &+ O(\Delta\tau^5) \end{aligned} \tag{2.91}$$

where

$$W = V + \frac{1}{48}[V,[T,V]] \tag{2.92}$$

Using this high order decomposition for the short time propagator the Green's function can be written as:

$$G(\mathbf{R},\mathbf{R}',\Delta\tau) = G^{(0)}(\mathbf{R},\mathbf{R}'',\Delta\tau)G^{(1)}(\mathbf{R}'',\mathbf{R}',\Delta\tau) + O(\Delta\tau^5) \tag{2.93}$$

where the functions $G^{(0)}$ and $G^{(1)}$ are given by:

$$G^{(i)}(\mathbf{R},\mathbf{R}',\Delta\tau) = G_K(\mathbf{R},\mathbf{R}',\Delta\tau) \times G_V^{(i)}(\mathbf{R},\mathbf{R}',\Delta\tau) \tag{2.94}$$

and

$$G_V^{(i)}(\mathbf{R},\mathbf{R}',\Delta\tau)=\begin{cases}e^{-\frac{2}{3}V(\mathbf{R}')\Delta\tau} & i \text{ even}\\ e^{-\frac{4}{3}V(\mathbf{R}')\Delta\tau-\frac{\hbar^2\Delta\tau^3}{9m}\sum_{j=1}^{N}|\nabla_j V(\mathbf{R}')|^2} & i \text{ odd}\end{cases} \tag{2.95}$$

This expression for the short time Green's function is a particular case of a more general family of approximations derived from symplectic decompositions of the propagator [57].

Fourth order path integral ground state algorithm with staging

The improved PIGS algorithm that incorporates staging sampling to improve the convergence of the method is the following

1. Draw an initial configuration for each linear polymer $\{\mathbf{X}_1,...,\mathbf{X}_N\}$ representing the full imaginary time path of each particle.

2. Guess a new configuration for the system by making use of the staging method.

3. Evaluate the transition probability to the new configuration as

$$Q=\frac{P(\mathbf{X}_1,...,\mathbf{X}_i',...,\mathbf{X}_N)}{P(\mathbf{X}_1,...,\mathbf{X}_i,...,\mathbf{X}_N)}. \tag{2.96}$$

4. Accept or reject the new configuration using Metropolis algorithm.

5. Compute observables of interest.

6. Repeat 2 - 5 to achieve the desired accuracy.

The main difference between the improved and the basic algorithms is that in the improved algorithm the new configurations of the system are proposed using the staging method that, as we have seen, samples exactly the kinetic part of the action and therefore the transition probability involves only the evaluation of potential action.

In addition to the given steps it is convenient to accelerate the convergence by performing full chain translations of each chain between several steps of the simulation. This translations are proposed as:

$$\mathbf{X}_i'=\mathbf{X}_i+\delta\mathbf{X}_i \tag{2.97}$$

and then are accepted or rejected using the Metropolis algorithm.

2.3 Evaluating properties

In this section we will show how the observables of interest are evaluated from the Monte Carlo sampling. We are interested in the evaluation of the energy per particle of the system, that allows us to build the equation of state, and also in structural quantities like the pair distribution function and its Fourier transform, the static structure factor. Another important quantity to evaluate is the one-body density matrix that gives information about the Bose-Einstein condensation in the system.

2.3.1 Energy per particle

The energy of a quantum system can be evaluated as the expected value of the many body hamiltonian given by:

$$H = -\frac{\hbar^2}{2m}\sum_{i=1}^{N}\nabla^2 + \sum_{i=1}^{N}V_1(\mathbf{r}_i) + \sum_{i<j}V_2(\mathbf{r}_i - \mathbf{r}_j) \tag{2.98}$$

As we have seen the Schrödinger equation is given by:

$$< \Psi|H|\Psi >= E < \Psi|\Psi > \tag{2.99}$$

so the energy can be evaluated by the following expression

$$E[\Psi] = \frac{< \Psi|H|\Psi >}{< \Psi|\Psi >} \tag{2.100}$$

that can be put in integral form as:

$$E[\Psi] = \frac{\int d\mathbf{R}\Psi^*(\mathbf{R})H\Psi(\mathbf{R})}{\int d\mathbf{R}|\Psi(\mathbf{R})|^2} \tag{2.101}$$

and can be expressed in terms of the probability distribution as

$$E[\Psi] = \frac{\int d\mathbf{R}|\Psi(\mathbf{R})|^2\frac{H\Psi(\mathbf{R})}{\Psi(\mathbf{R})}}{\int d\mathbf{R}|\Psi(\mathbf{R})|^2} = \int d\mathbf{R}P(\mathbf{R})E_{loc}(\mathbf{R}) \tag{2.102}$$

where $P(\mathbf{R}) = \frac{|\Psi(\mathbf{R})|^2}{\int d\mathbf{R}|\Psi(\mathbf{R})|^2}$ and $E_{loc} = \frac{H\Psi(\mathbf{R})}{\Psi(\mathbf{R})}$.

The hamiltonian acting on the wave function can be split in the kinetic and potential terms, the potential term can be simply written as:

$$\frac{V\Psi(\mathbf{R})}{\Psi(\mathbf{R})} = \sum_{i=1}^{N}V_1(\mathbf{r}_i) + \sum_{i<j}V_2(\mathbf{r}_i - \mathbf{r}_j) \tag{2.103}$$

and the kinetic term:

$$\frac{K\Psi(\mathbf{R})}{\Psi(\mathbf{R})} = -\frac{\hbar^2}{2m}\frac{\nabla^2_{\mathbf{R}}\Psi(\mathbf{R})}{\Psi(\mathbf{R})}. \tag{2.104}$$

It is convenient to write the acting of the laplacian on the wave function as:

$$\frac{\nabla^2_{\mathbf{R}}\Psi(\mathbf{R})}{\Psi(\mathbf{R})} = \nabla^2_{\mathbf{R}} \log \Psi(\mathbf{R}) + (\nabla_{\mathbf{R}} \log \Psi(\mathbf{R}))^2 \tag{2.105}$$

Variational Monte Carlo

In a variational Monte Carlo sampling we have no access to the exact wave function of the system so, in general, we can evaluate the energy substituting the exact wave function by the trial wave function $\Psi_T(\mathbf{R})$, is we do this change the second term in (2.105) can be identified as the drift force and the total local energy can be written as:

$$E_{loc}(\mathbf{R}) = -\frac{\hbar^2}{2m}\left(\nabla^2_{\mathbf{R}} \log \Psi_T(\mathbf{R}) + F(\mathbf{R})^2\right) + V(\mathbf{R}) \tag{2.106}$$

In a VMC simulation this quantity is obviously an approximation to the exact ground state energy of the system.

Diffusion Monte Carlo

In a DMC simulation we sample the product of the exact wave function of the system times the trial (or guiding) wave function so the energy of the system can be written as:

$$E = \frac{\int d\mathbf{R}\Psi(\mathbf{R})\Psi_T(\mathbf{R})E_{loc}(\mathbf{R})}{\int \Psi_T(\mathbf{R})\Psi(\mathbf{R})} = \frac{\int d\mathbf{R}\Psi(\mathbf{R})\Psi_T(\mathbf{R})\frac{H\Psi_T(\mathbf{R})}{\Psi_T(\mathbf{R})}}{\int \Psi_T(\mathbf{R})\Psi(\mathbf{R})} \tag{2.107}$$

so finally we can write

$$E = \frac{\int d\mathbf{R}\Psi(\mathbf{R})H\Psi_T(\mathbf{R})}{\int \Psi_T(\mathbf{R})\Psi(\mathbf{R})} \tag{2.108}$$

thanks to the hermiticity the hamiltonian can act on the left or on the right and considering that $H|\Psi>= E_0|\Psi>$ we can write

$$E = E_0\frac{\int d\mathbf{R}\Psi(\mathbf{R})\Psi_T(\mathbf{R})}{\int \Psi_T(\mathbf{R})\Psi(\mathbf{R})} = E_0 \tag{2.109}$$

So in a DMC simulation we also have to evaluate the expectation value of the local energy function.

Path integral ground state

In a PIGS simulation the evaluation of the energy can be done in several ways. In this work, we have chosen the mixed estimator as in the case of DMC. In PIGS the physical observables must be evaluated at the mid-point

of the chain but in the case of the energy, as we are evaluating the expected value of the hamiltonian it can act on the extreme points ($\mathbf{R}_0$, $\mathbf{R}_M$) given that

$$\left[H, e^{-H\tau}\right] = 0 \tag{2.110}$$

So the mixed estimator of the energy on a PIGS simulation is given by:

$$E = \sum_{i=1}^{N} \frac{H\Psi_T(\mathbf{R}_0)}{\Psi_T(\mathbf{R}_0)} = \sum_{i=1}^{N} E_{loc}(\mathbf{R}_0) \tag{2.111}$$

2.3.2 Pair distribution function

Another observable of interest in the study of quantum gases is the so called pair distribution function that is given by the following expression:

$$g(\mathbf{r}_1, \mathbf{r}_2) = \frac{N(N-1)}{n^2} \frac{\int |\Psi(\mathbf{R})|^2 d\mathbf{r}_3 \cdots d\mathbf{r}_N}{\int |\Psi(\mathbf{R})|^2 d\mathbf{r}_1 \cdots d\mathbf{r}_N}. \tag{2.112}$$

In an homogeneous system the pair distribution function depends only in the relative position $\mathbf{r}_1 - \mathbf{r}_2$. The equation (2.112) can be written in the following form by defining $\mathbf{r} = \mathbf{r}_1 - \mathbf{r}_2$

$$g(\mathbf{r}) = \frac{N(N-1)}{n^2 L^d} \frac{\int \delta(\mathbf{r}_1 - \mathbf{r}_2 - \mathbf{r}) |\Psi(\mathbf{R})|^2 d\mathbf{R}}{\int |\Psi(\mathbf{R})|^2 d\mathbf{R}}. \tag{2.113}$$

where L is the size of the simulation box and d is the dimensionality of the system. This last expression is written in a more suitable form for a Monte Carlo evaluation.

In order to have more statistic and reduce the variance of the estimator it is common to sum over all possible pairs of particles in the system, if we do so the final expression that we will evaluate in our Monte Carlo simulations is

$$g(\mathbf{r}) = \frac{2}{nN} \frac{\int \sum_{i<j} \delta(\mathbf{r}_{ij} - \mathbf{r}) |\Psi(\mathbf{R})|^2 d\mathbf{R}}{\int |\Psi(\mathbf{R})|^2 d\mathbf{R}}. \tag{2.114}$$

where $\mathbf{r}_{ij} = \mathbf{r}_i - \mathbf{r}_j$.

The evaluation of the pair distribution function in the Monte Carlo sampling it is simply implemented by making an histogram of the relative distance of each pair of particles of the system.

2.3.3 Static structure factor

A quantity related with the pair distribution function that is very interesting in the study of the macroscopic state of a quantum gas is the static structure factor, that is also accessible experimentally.

The static structure factor is related with the Fourier transform of the pair distribution function

$$S(\mathbf{k}) = 1 + n \int d\mathbf{r} e^{-i\mathbf{q}\cdot\mathbf{r}}(g(\mathbf{r}) - 1). \tag{2.115}$$

Despite of its apparent simplicity, this expression is not the best way to evaluate the static structure factor in a Monte Carlo calculation. Instead of using (2.115) it is better to use the alternative definition of $S(\mathbf{k})$ that states that it is given by the correlation of the momentum distribution between $\mathbf{k}$ and $-\mathbf{k}$

$$NS(\mathbf{k}) =< \rho_{-\mathbf{k}}\rho_{\mathbf{k}} > - | < \rho_{\mathbf{k}} > |^2 \tag{2.116}$$

Using the property $\rho_{-\mathbf{k}} = \rho^*_{\mathbf{k}}$ we can write (2.116) as

$$NS(\mathbf{k}) =< |\rho_{\mathbf{k}}|^2 > - | < \rho_{\mathbf{k}} > |^2 \tag{2.117}$$

The density distribution in a Monte Carlo calculation is given by

$$n(\mathbf{r}) = \sum_{i=1}^{N} \delta(\mathbf{r} - \mathbf{r}_i) \tag{2.118}$$

that can be expressed in the momentum space as:

$$\rho_{\mathbf{k}} = \int e^{i\mathbf{k}\cdot\mathbf{r}} n(\mathbf{r}) = \sum_{i=1}^{N} e^{i\mathbf{k}\cdot\mathbf{r}_i} = \sum_{i=1}^{N} \cos\mathbf{k}\cdot\mathbf{r}_i + i\sum_{i=1}^{N} \sin\mathbf{k}\cdot\mathbf{r}_i \tag{2.119}$$

Using the definition of $\rho_{\mathbf{k}}$ we can write finally the expression for the evaluation of the static structure factor as:

$$\begin{aligned} NS(\mathbf{k}) = \langle \left(\sum_{i=1}^{N} \cos\mathbf{k}\cdot\mathbf{r}_i\right)^2 + \left(\sum_{i=1}^{N} \sin\mathbf{k}\cdot\mathbf{r}_i\right)^2 \rangle \\ - | < \sum_{i=1}^{N} \cos\mathbf{k}\cdot\mathbf{r}_i > |^2 - | < \sum_{i=1}^{N} \sin\mathbf{k}\cdot\mathbf{r}_i > |^2 \end{aligned} \tag{2.120}$$

In an homogeneous system the last two terms vanish.

The last consideration concerns the values of $\mathbf{k}$ in an homogeneous system, as we simulate the system in a finite simulation cell we must choose values of $\mathbf{k}$ that are compatible with the size of the box:

$$k_i = \frac{2\pi}{L_i} n_i \tag{2.121}$$

where $n_i = 1, 2, ...$ and L_i are the length of the box in the direction i.

2.3.4 One body density matrix

The last quantity that we are interested in is the one body density matrix that gives us information about the Bose - Einstein condensation in the system. In an homogeneous system the one body density matrix $\rho(\mathbf{r})$ is given by:

$$\rho(\mathbf{r}-\mathbf{r}') = N\frac{\int\cdots\int \Psi^*(\mathbf{r},\mathbf{r}_2,\cdots,\mathbf{r}_N)\Psi(\mathbf{r}',\mathbf{r}_2,\cdots,\mathbf{r}_N)d\mathbf{r}_2\cdots d\mathbf{r}_N}{\int\cdots\int|\Psi(\mathbf{r},\cdots,\mathbf{r}_N)|^2 d\mathbf{r}_1\cdots d\mathbf{r}_N} \quad (2.122)$$

In VMC the wave function that we are sampling is the $\Psi_T(\mathbf{R})$ so the previous expression can be written as:

$$\rho(\mathbf{r}-\mathbf{r}') = N\frac{\int\cdots\int \frac{\Psi_T^*(\mathbf{r},\mathbf{r}_2,\cdots,\mathbf{r}_N)}{\Psi_T^*(\mathbf{r}',\mathbf{r}_2,\cdots,\mathbf{r}_N)}|\Psi_T(\mathbf{r}',\mathbf{r}_2,\cdots,\mathbf{r}_N)|^2 d\mathbf{r}_2\cdots d\mathbf{r}_N}{\int\cdots\int|\Psi_T(\mathbf{r},\cdots,\mathbf{r}_N)|^2 d\mathbf{r}_1\cdots d\mathbf{r}_N} \quad (2.123)$$

where $P(\mathbf{R}) = \frac{|\Psi(\mathbf{R})|^2}{\int|\Psi(\mathbf{R})|^2 d\mathbf{R}}$.

On the other hand in the DMC method we are sampling the mixed function $f(\mathbf{R}) = \Psi_T(\mathbf{R})\Psi(\mathbf{R})$ so the expression (2.122) is

$$\rho(\mathbf{r}-\mathbf{r}') = N\frac{\int\cdots\int \Psi_T^*(\mathbf{r},\mathbf{r}_2,\cdots,\mathbf{r}_N)\Psi(\mathbf{r}',\mathbf{r}_2,\cdots,\mathbf{r}_N)d\mathbf{r}_2\cdots d\mathbf{r}_N}{\int\cdots\int|f(\mathbf{r},\cdots,\mathbf{r}_N)|^2 d\mathbf{r}_1\cdots d\mathbf{r}_N} \quad (2.124)$$

that can be written again as:

$$\rho(\mathbf{r}-\mathbf{r}') = N\frac{\int\cdots\int \frac{\Psi_T^*(\mathbf{r},\mathbf{r}_2,\cdots,\mathbf{r}_N)}{\Psi_T^*(\mathbf{r}',\mathbf{r}_2,\cdots,\mathbf{r}_N)}f(\mathbf{r}',\mathbf{r}_2,\cdots,\mathbf{r}_N)d\mathbf{r}_2\cdots d\mathbf{r}_N}{\int\cdots\int f(\mathbf{r},\cdots,\mathbf{r}_N)d\mathbf{r}_1\cdots d\mathbf{r}_N} \quad (2.125)$$

From the asymptotic behavior of the one body density matrix the condensate fraction of the system can be extracted as:

$$\lim_{|\mathbf{r}-\mathbf{r}'|\to\infty}\frac{\rho(\mathbf{r}-\mathbf{r}')}{n} = \frac{N_0}{N} \quad (2.126)$$

where N_0 is the number of particles on the condensate.

2.4 Trial wave functions

A key ingredient of the zero temperature quantum Monte Carlo methods is the trial wave function of the system. The trial function allows us to introduce all the a priory information about the physics of the system to improve the convergence and accuracy of the Monte Carlo sampling.

It is usual in the study of quantum bosonic fluids to consider the wave function as:

$$\Psi(\mathbf{r}_1,\cdots,\mathbf{r}_N) = \exp\left(U_1+U_2+U_3+\cdots+U_N\right) \quad (2.127)$$

where the different functions U_i are terms involving correlations of i particles,

$$\begin{aligned} U_1 &= \sum_{j=1}^{N} u_1(\mathbf{r}_j) \\ U_2 &= \sum_{i<j} u_2(\mathbf{r}_i, \mathbf{r}_j) \\ U_3 &= \sum_{i<j<k} u_3(\mathbf{r}_i, \mathbf{r}_j, \mathbf{r}_k) \end{aligned} \tag{2.128}$$

A common approximation is to consider a wave function containing only terms involving two body correlations, which implies $U_i = 0 \quad \forall i > 2$, such a wave function is called Jastrow wave function and can be written as:

$$\Psi(\mathbf{r}_1, \cdots, \mathbf{r}_N) = \exp\left(\sum_{i<j} u_2(\mathbf{r}_i, \mathbf{r}_j)\right) \tag{2.129}$$

where $u_2(\mathbf{r}_i, \mathbf{r}_j) = u_2(\mathbf{r}_i - \mathbf{r}_j)$ for an homogeneous system like a gas or a liquid. The two body correlation function $\exp(u_2(\mathbf{r}_i - \mathbf{r}_j))$ it is chosen to reproduce the exact behaviour of the two body problem at low distances in order to avoid the possible singularities of the local energy at short distances caused by interactions that are strongly repulsive at short distances. For a non homogeneous system like a crystalline solid we have to consider in general a one body term in addition to the two body Jastrow term in order to help the Monte Carlo sampling to find the ground state configuration of the system.

Chapter 3

Two-dipoles quantum problem

3.1 Introduction

The two-body scattering properties are of crucial importance in the study of low-density quantum gases since many properties of the many body system are directly related with two-body scattering parameters. In low-density quantum gases there are several important quantities that depend on the two-body scattering properties because the physics of the system is, in this situation, dominated by two body collisions as the probability of three body events vanishes as density is decreased.

Additionally to the intrinsic physical relevance of the two body scattering analysis there is another reason that motivates us to do this study. We are interested in perform Monte Carlo simulations of a quantum dipolar Bose gas and, as we have seen before, Monte Carlo methods need a trial many body wave function. A common approach to the many-body wave function is the Jastrow function built from two body correlations. It is also common to use the zero-energy solution of the two-body scattering problem as Jastrow correlation factor, so it will be useful for our purpose to have at hand this wave function to use it as input for our Monte Carlo simulations.

In the following sections we present our study of the zero-energy solutions of the two-body problem of two bosonic dipoles in two dimensions and in two different situations. First, we solve the well known isotropic two dipoles problem where the dipole moments of the particles are orthogonal to the plane. The second situation, and the most important for the purpose of this work, is when dipole moments are oriented with an angle α respect to the normal direction to the plane. Finally, we find an expression for the scattering length of the system that will be useful for the study of the low density dipolar gas of Bosons.

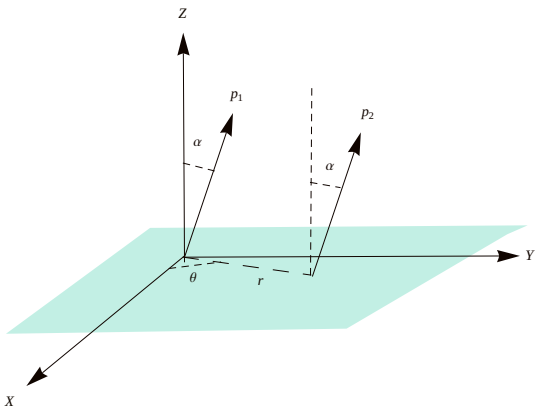

Figure 3.1: Two dipoles confined in the x-y plane and polarised along a direction that forms an angle α with the z axis are shown. In this system the interaction depends on the relative distance between particles and on the angle between their positions.

3.2 Interaction

General two-body interaction in a system of dipoles is given by the following expression

$$V(\mathbf{r}) = \frac{C_{dd}}{4\pi r^3}\left(\hat{\mathbf{p}}\cdot\hat{\mathbf{p}}' - 3\frac{(\hat{\mathbf{p}}\cdot\mathbf{r})\,(\hat{\mathbf{p}}'\cdot\mathbf{r})}{r^2}\right), \tag{3.1}$$

where $\hat{\mathbf{p}}$ and $\hat{\mathbf{p}}'$ are the unitary dipolar moment of each dipole. If dipoles are polarised in the same direction, figure 1 shows the system that we are studying. Then, the dipolar moments of each particle are given by:

$$\hat{\mathbf{p}} = \hat{\mathbf{p}}' = (\sin\alpha, 0, \cos\alpha) \tag{3.2}$$

while the vector $\mathbf{r}$ on the x-y plane is given by:

$$\mathbf{r} = (r\cos\theta, r\sin\theta, 0) \tag{3.3}$$

Applying this expressions in Equation (3.1), one can easily obtain an expression for the interaction that we are looking for, given by

$$V(r,\theta) = \frac{C_{dd}}{4\pi r^3}\left(1 - 3\lambda^2\cos^2\theta\right) \tag{3.4}$$

Where we have defined $\lambda \equiv \sin\alpha$.

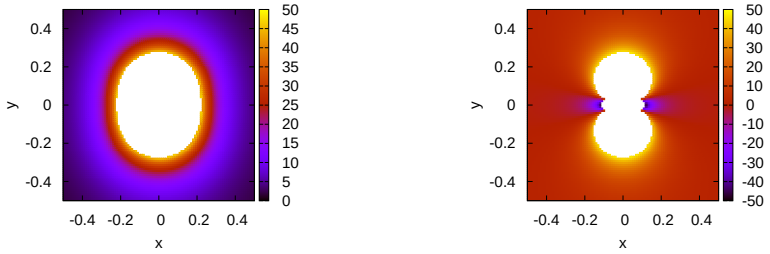

(a) Interaction potential for $\alpha < \alpha_c$. (b) Interaction potential for $\alpha > \alpha_c$.

Figure 3.2: Two dimensional dipolar interaction with a tilting angle below (a) and above (b) the critical angle.

In the case that we are studying, when we have two dipoles in the x-y plane it can be shown that the potential given in (3.4) is short ranged, provided that a necessary condition for a potential to be short-range is [59]:

$$\int_{|\mathbf{r}|\geq r_0} U(\mathbf{r}) d^D\mathbf{r} < \infty \tag{3.5}$$

where D is the dimensionality of the system and r_0 is some short distance cut off. Since we are working in a two dimensional system the integral above exists, and this allows us to state that we are working with a short ranged potential.

In addition our potential is anisotropic. For low values of λ (i. e. low values of polarisation angle) the potential is always repulsive, but with strength that depends of θ. If $\theta = 0$ the potential is less repulsive than for the $\theta = \frac{\pi}{2}$ direction.

There is a critical polarisation angle α_c: if $\alpha < \alpha_c$ the potential is always repulsive, but if $\alpha > \alpha_c$ the potential shows repulsive and attractive regions. One can easily calculate α_c solving the following equation for $\theta = 0$:

$$1 - 3\lambda^2 \cos^2\theta = 0 \Rightarrow 1 - 3\lambda^2 = 1 \Rightarrow \alpha_c = \arcsin\left(\frac{1}{\sqrt{3}}\right) \Rightarrow \alpha_c \approx 35.26 \tag{3.6}$$

In figure 3.2 we show the potential for $\alpha < \alpha_c$ and $\alpha > \alpha_c$.

3.3 Schrödinger equation

The Schrödinger equation for the two dipole system is:

$$-\frac{\hbar^2}{2\mu}\nabla^2\psi + V(r,\theta)\psi = E\psi \tag{3.7}$$

where μ is the reduced mass of the two body system, given by:

$$\mu = \frac{m_1 m_2}{m_1 + m_2} = \frac{m}{2} \tag{3.8}$$

where we used the fact that $m_1 = m_2 = m$.

We are interested in analysing scattering states, this implies that we consider only values of energy $E \geq 0$, hence we can write energy as:

$$E = \frac{\hbar^2 k^2}{2\mu} \tag{3.9}$$

If we write the Schrödinger equation explicitly in plane polar coordinates, we find the following partial differential equation:

$$\frac{\partial^2\psi}{\partial r^2} + \frac{1}{r}\frac{\partial\psi}{\partial r} + \frac{1}{r^2}\frac{\partial^2\psi}{\partial\theta^2} - \frac{2\mu}{\hbar^2}\frac{C_{dd}}{4\pi r^3}\left(1 - 3\lambda^2\cos^2\theta\right)\psi = -k^2\psi \tag{3.10}$$

Solving the above equation gives us a complete description of the physics of the two-dipole system, but unfortunately, the anisotropy of the interaction makes that the solutions of the partial differential equation are not separable, and this fact makes the resolution of the problem more difficult.

We are interested in the study of low energy solutions of the system, and in the following sections we show our approach to the solution of the problem.

3.3.1 Zero-energy solution for the $\alpha = 0$ case

The first problem that we have studied is the case of $\alpha = 0$. In this section we want to solve the following differential equation:

$$\frac{\partial^2\psi}{\partial r^2} + \frac{1}{r}\frac{\partial\psi}{\partial r} + \frac{1}{r^2}\frac{\partial^2\psi}{\partial\theta^2} - \frac{2\mu}{\hbar^2}\frac{C_{dd}}{4\pi r^3}\psi = -k^2\psi \tag{3.11}$$

This equation corresponds to a system of two dipoles whose dipole moments are polarised orthogonally to the x-y plane, as shows figure 3. In this situation the interaction potential is purely isotropic and repulsive. This fact allows us to find a solution of the problem using the method of separation of variables.

We are looking for a solution of the differential equation that can be written in the form:

$$\psi(r,\theta) = R(r)Q(\theta) \tag{3.12}$$

If we substitute the form (3.12) of the wave function in equation (3.11) and simplify the resulting expression we will find that we have converted the partial differential equation in the following system of two ordinary differential equations:

$$\begin{cases} Q_m''(\theta) = -m^2 Q_m(\theta) \\ R_m''(r) + \frac{1}{r}R_m'(r) - \left(\frac{m^2}{r^2} + \frac{2\mu}{\hbar^2}\frac{C_{dd}}{4\pi r^3}\right)R_m(r) = -k^2 R_m(r) \end{cases} \tag{3.13}$$

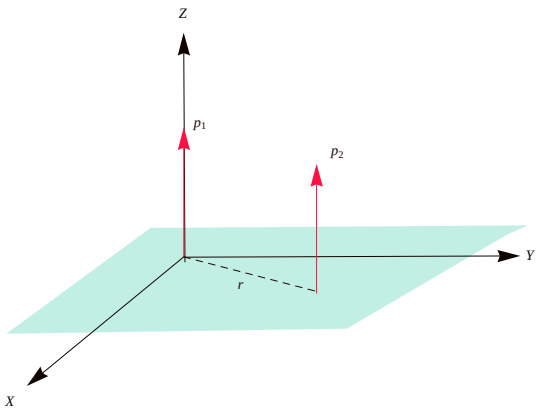

Figure 3.3: Physical situation when the interaction between dipoles is fully anisotropic and repulsive.

The angular equation has the following solutions:

$$Q_m(\theta) = A_m \cos m\theta + B_m \sin m\theta \tag{3.14}$$

Due to the Bosonic symmetry, the angular part of the wave function must verify $Q_m(\theta) = Q_m(-\theta)$, that implies $B_m = 0$ for each value of m, so the angular wave function will be

$$Q_m(\theta) = A_m \cos m\theta \tag{3.15}$$

Then the problem has been reduced to solve the radial equation given in (3.13).

We have to consider the equation for the radial wave function when $k = 0$. In this case the equation to solve is:

$$R_m''(r) + \frac{1}{r} R_m'(r) - \left(\frac{m^2}{r^2} + \frac{2\mu}{\hbar^2} \frac{C_{dd}}{4\pi r^3} \right) R_m(r) = 0 \tag{3.16}$$

In this situation the differential equation can be solved analytically. If we define $x \equiv \frac{2}{\sqrt{r}}$ we can rewrite the radial equation as:

$$x^2 \frac{d^2 R_m}{dx^2} + x \frac{dR_m}{dx} - \left[(2m)^2 + \frac{2\mu}{\hbar^2} \frac{C_{dd}}{4\pi} x^2 \right] R_m = 0 \tag{3.17}$$

The last equation can be easily identified as the modified Bessel equation given by:

$$x^2 y'' + xy' - (m^2 + k^2 x^2) y = 0 \tag{3.18}$$

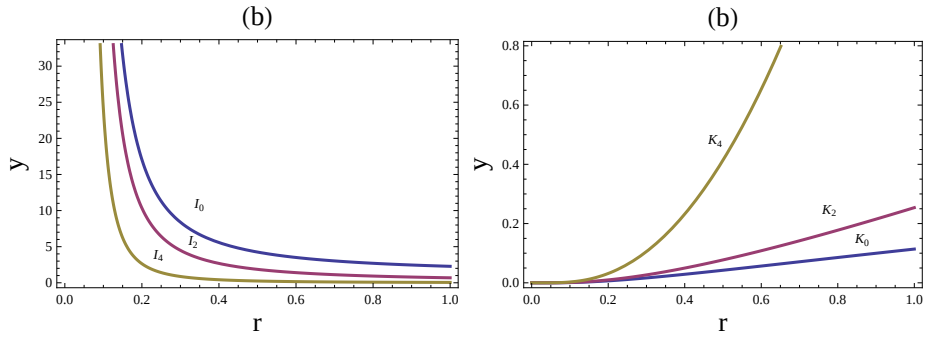

(a) Modified Bessel functions of the first kind and orders 0, 2 and 4.

(b) Modified Bessel functions of the second kind and orders 0, 2 and 4.

Figure 3.4: Modified Bessel functions of the argument $\frac{2}{\sqrt{r}}$.

This implies that the solution to the radial equation with $k = 0$ is:

$$R_m(x) = A_m I_{2m}\left(\sqrt{\frac{2\mu C_{dd}}{4\pi\hbar^2}}x\right) + B_m K_{2m}\left(\sqrt{\frac{2\mu C_{dd}}{4\pi\hbar^2}}x\right) \tag{3.19}$$

or in terms of the physical distance between dipoles:

$$R_m(r) = A_m I_{2m}\left(\sqrt{\frac{2\mu C_{dd}}{4\pi\hbar^2}}\frac{2}{\sqrt{r}}\right) + B_m K_{2m}\left(\sqrt{\frac{2\mu C_{dd}}{4\pi\hbar^2}}\frac{2}{\sqrt{r}}\right) \tag{3.20}$$

The solutions of the radial equations are shown in figure 3.4. The general solution of Schrödinger equation is the following:

$$\psi(r,\theta) = \sum_{m=0}^{\infty}\left[A_m I_{2m}\left(\sqrt{\frac{2\mu C_{dd}}{4\pi\hbar^2}}\frac{2}{\sqrt{r}}\right) + B_m K_{2m}\left(\sqrt{\frac{2\mu C_{dd}}{4\pi\hbar^2}}\frac{2}{\sqrt{r}}\right)\right]\cos m\theta \tag{3.21}$$

The last expression is the two dimensional equivalent of the familiar partial wave expansion in standard three dimensional scattering theory.

Now that we have the general solution of the zero-energy Schrödinger equation, we must consider the boundary conditions that must be applied to our solution.

Provided that the potential is strongly repulsive at $r = 0$, our wave function must vanish at the origin, i.e. $\psi(r = 0) = 0$. This condition implies that $A_m = 0$ for all m, because $I_{2m}\left(\sqrt{\frac{2\mu C_{dd}}{4\pi\hbar^2}}\frac{2}{\sqrt{r}}\right) \to \infty$ when $r \to 0$. So the solution reads as follows:

$$\psi(r,\theta) = \sum_{m=0}^{\infty} B_m K_{2m}\left(\sqrt{\frac{2\mu C_{dd}}{4\pi\hbar^2}}\frac{2}{\sqrt{r}}\right)\cos m\theta \tag{3.22}$$

The asymptotic behaviour of the wave function can be studied considering that the potential is short range in two dimensions. This implies that if $r >> 1$ dipoles don't see each other, and then Schrödinger equation at large distances becomes the Laplace equation:

$$\nabla^2 \psi \approx 0 \tag{3.23}$$

The solutions of the Laplace equation in ploar coordinates are given by:

$$\psi(r,\theta) = A_0 + B_0 \log r + \sum_{m=1}^{\infty} \left[A_m r^{-m} + B_m r^m\right] \cos m\theta \tag{3.24}$$

Setting $A_m = 0$ for all m one can see that this is exactly the long range behaviour of the wave function given in (3.22). The asymptotic behaviour of the modified Bessel function of the second kind $K_m(x)$ for small values of x are given by [60]:

$$\begin{cases} K_0(x) \approx -\log\left(\frac{x}{2}\right) - \gamma \\ K_m(x) \approx \frac{1}{2}\Gamma(m)\left(\frac{1}{2}x\right)^{-m} \end{cases} \tag{3.25}$$

The expressions above are valid for $x << 1$ what implies $r >> 1$, if we do the substitution $x \to \sqrt{\frac{2\mu C_{dd}}{4\pi\hbar^2}}\frac{2}{\sqrt{r}}$ we find the asymptotic behaviour of the wave function for large values of r:

$$\begin{cases} K_0\left(\sqrt{\frac{2\mu C_{dd}}{4\pi\hbar^2}}\frac{2}{\sqrt{r}}\right) \approx -\log\left(\frac{1}{2}\sqrt{\frac{2\mu C_{dd}}{4\pi\hbar^2}}\frac{2}{\sqrt{r}}\right) - \gamma = \\ \quad = \frac{1}{2}\log r - \gamma - \frac{1}{2}\log\left(\sqrt{\frac{2\mu C_{dd}}{4\pi\hbar^2}}\right) = \frac{1}{2}\log\left(\frac{r}{a_s}\right) \\ K_{2m}\left(\sqrt{\frac{2\mu C_{dd}}{4\pi\hbar^2}}\frac{2}{\sqrt{r}}\right) \approx \frac{1}{2}\Gamma(2m)\left(\sqrt{\frac{2\mu C_{dd}}{4\pi\hbar^2}}\frac{1}{2}\left(\frac{2}{\sqrt{r}}\right)\right)^{-2m} = \\ \quad = \frac{1}{2}\Gamma(2m)\left(\frac{4\pi\hbar^2}{2\mu C_{dd}}\right)^m r^m \end{cases} \tag{3.26}$$

The solution of the zero energy Schrödinger equation reproduces adequately the expected asymptotic behaviour. As an additional result of the asymptotic zero energy behaviour we have found the s-wave scattering wave of dipolar scattering:

$$a_s = e^{2\gamma + \log\left(\frac{2\mu C_{dd}}{4\pi\hbar^2}\right)}. \tag{3.27}$$

3.3.2 Zero energy solution for the $\alpha \neq 0$ case

In this section we consider the zero energy Schrödinger equation with the full anisotropic interaction. In this work we restrict ourselves to the regime

where $\alpha < \alpha_c$, this implies that the potential is anisotropic but repulsive for all $\mathbf{r}$.

The Schrödinger equation that we want to solve is:

$$-\frac{\hbar^2}{2\mu}\left[\frac{1}{r}\frac{\partial}{\partial r}\left(r\frac{\partial}{\partial r}\right)+\frac{1}{r^2}\frac{\partial^2}{\partial\theta^2}\right]\psi+V(r,\theta)\psi=0 \tag{3.28}$$

The interaction has two different contributions, the first one is an isotropic term that we call $V_0(r)$, and the second one is an anisotropic term that we identify as $V_1(r,\theta)$. The contributions are defined as:

$$\begin{cases} V_0(r)=\frac{C_{dd}}{4\pi r^3} \\ V_1(r,\theta)=\frac{C_{dd}}{4\pi}\frac{3\cos^2\theta}{r^3} \end{cases} \tag{3.29}$$

With these definitions the potential can be rewritten as:

$$V(r,\theta)=V_0(r)-\lambda^2 V_1(r,\theta) \tag{3.30}$$

At this point we can write the Schrödinger equation in the following form:

$$-\frac{\hbar^2}{2\mu}\left[\frac{1}{r}\frac{\partial}{\partial r}\left(r\frac{\partial}{\partial r}\right)+\frac{1}{r^2}\frac{\partial^2}{\partial\theta^2}\right]\psi+V_0(r,\theta)\psi=\lambda^2 V_1(r,\theta)\psi \tag{3.31}$$

that can be understood as an inhomogeneous differential equation,

$$\left(-\frac{\hbar^2}{2\mu}\nabla^2+V_0(\mathbf{r})\right)\psi=\rho(\mathbf{r}) \tag{3.32}$$

where the source function $\rho(\mathbf{r})$ is given in this situation in a self-consistent form

$$\rho(\mathbf{r})=\lambda^2 V_1(\mathbf{r})\psi(\mathbf{r}) \tag{3.33}$$

causing that the source term depends on the wave function itself.

The solution of an inhomogeneous differential equation can be written in the form:

$$\psi(r,\theta)=\psi_0(r,\theta)+\psi_p(r,\theta) \tag{3.34}$$

where ψ_0 is the solution of the homogeneous equation and ψ_p is a particular solution due to the source term. From the previous section we know that the general homogeneous solution is the following:

$$\psi_0(r,\theta)=\sum_{m=0}^{\infty}B_m K_{2m}\left(\frac{\sqrt{2\mu C_{dd}}}{4\pi\hbar}\frac{2}{\sqrt{r}}\right)\cos m\theta \tag{3.35}$$

The particular solution $\psi_p(\mathbf{r})$ can be evaluated using Green's function theory [61, 62, 63] to obtain a perturbative solution in the form of a power series in the parameter λ as we show in the following.

Green's function perturbative solution

We can define a Green's function, $G(\mathbf{r}, \mathbf{r}')$, for the two body dipole problem using the following differential equation:

$$\left(\nabla^2 - \frac{2\mu}{\hbar^2} V_0(r)\right) G(\mathbf{r}, \mathbf{r}') = -\delta(\mathbf{r} - \mathbf{r}') \tag{3.36}$$

Solving this equation to obtain the Green's function allows us to transform the original differential equation into the following integral one:

$$\psi(\mathbf{r}) = \phi(\mathbf{r}) + \lambda^2 \int d\mathbf{r}' G(\mathbf{r}, \mathbf{r}') V_1(\mathbf{r}) \psi(\mathbf{r}') \tag{3.37}$$

where ϕ is a solution of the homogeneous part of the equation (3.31), or, in other words, a solution of the isotropic zero energy dipolar scattering.

Thus we expect that the solutions of the integral equation above are valid for low values of λ, i. e. low values of the polarisation angle. The solution of the integral equation can be written as a power series in the parameter λ,

$$\psi(\mathbf{r}) = \psi_0(\mathbf{r}) + \lambda^2 \psi_2(\mathbf{r}) + \lambda^4 \psi_4(\mathbf{r}) + \cdots = \sum_{n=0}^{\infty} \psi_n(\mathbf{r}) \lambda^{2n} \tag{3.38}$$

where we have defined $\psi_0(\mathbf{r}) \equiv \phi(\mathbf{r})$.

If one substitutes the perturbative expansion (3.38) on the integral equation (3.37) obtains:

$$\sum_{n=0}^{\infty} \psi_n(\mathbf{r}) \lambda^{2n} = \phi(\mathbf{r}) + \lambda^2 \int d\mathbf{r}' G(\mathbf{r}, \mathbf{r}') V_1(\mathbf{r}') \sum_{n=0}^{\infty} \psi_n(\mathbf{r}) \lambda^{2n} \tag{3.39}$$

From the last expression one can identify the terms that contribute at each order of the series expansion, which are given by the following recurring relations

$$\begin{cases} \psi_0(\mathbf{r}) = \phi(\mathbf{r}) \\ \psi_1(\mathbf{r}) = \int d\mathbf{r}' G(\mathbf{r}, \mathbf{r}') V_1(\mathbf{r}') \psi_0(\mathbf{r}') \\ \psi_2(\mathbf{r}) = \int d\mathbf{r}' G(\mathbf{r}, \mathbf{r}') V_1(\mathbf{r}') \psi_1(\mathbf{r}') \\ \quad \vdots \end{cases} \tag{3.40}$$

that can be written in general as

$$\psi_n(\mathbf{r}) = \int d\mathbf{r}' G(\mathbf{r}, \mathbf{r}') V_1(\mathbf{r}') \psi_{n-1}(\mathbf{r}') \tag{3.41}$$

Thus, we have to evaluate the Green's function of the two body dipolar problem and, using the previous integral relations, evaluate the different contributions at every λ order to build the complete solution of the problem.

Evaluation of the Green's function

The equation that defines Green's function given in (3.36) can be explicitly written in planar polar coordinates as:

$$\left[\frac{1}{r}\frac{\partial}{\partial r}\left(r\frac{\partial}{\partial r}\right)+\frac{1}{r^2}\frac{\partial^2}{\partial\theta^2}-\frac{2\mu}{\hbar^2}V_0(r)\right]G(\mathbf{r},\mathbf{r}')=-\frac{\delta(r-r')}{r}\delta(\theta-\theta') \quad (3.42)$$

In order to obtain a solution for this differential equation it is convenient to define the Fourier expansions of $G(\mathbf{r},\mathbf{r}')$ and $\delta(\theta-\theta')$ as [62]:

$$\begin{cases} G(\mathbf{r},\mathbf{r}')=\sum_{m=-\infty}^{\infty} g_m(r,r')\frac{e^{im(\theta-\theta')}}{2\pi} \\ \delta(\theta-\theta')=\sum_{m=-\infty}^{\infty}\frac{e^{im(\theta-\theta')}}{2\pi} \end{cases} \quad (3.43)$$

that can be introduced in the equation (3.42) to find the following expression:

$$\begin{aligned}\sum_{m=-\infty}^{\infty}\left[\frac{1}{r}\frac{d}{dr}\left(r\frac{d}{dr}\right)-\frac{m^2}{r^2}-\frac{2\mu}{\hbar^2}V_0(r)\right]g_m(r,r')\frac{e^{im(\theta-\theta')}}{2\pi}=\\ =-\sum_{m=-\infty}^{\infty}\frac{\delta(r-r')}{r}\frac{e^{im(\theta-\theta')}}{2\pi}\end{aligned} \quad (3.44)$$

The functions $e^{im\theta}$ form an orthonormal basis, this implies that the expansion above can be decoupled and converted in a system of ordinary differential equations given by:

$$\frac{1}{r}\frac{d}{dr}\left(r\frac{dg_m}{dr}\right)-\left(\frac{m^2}{r^2}+\frac{2\mu}{\hbar^2}\frac{C_{dd}}{4\pi r^3}\right)g_m=-\frac{\delta(r-r')}{r} \qquad \forall m\in\mathbb{Z} \quad (3.45)$$

where it can be seen that the partial Green's functions $g_m(r,r')=g_{-m}(r,r')$.

It is interesting to comment some issues independent of the particular form of $g_m(r,r')$. The Fourier decomposition of the Green's function implies a Fourier decomposition of the wave function itself, thus one could write the following expression for ψ:

$$\psi(r,\theta)=\sum_{m=-\infty}^{\infty}u_m(r)e^{im\theta} \quad (3.46)$$

If we suppose that the solution of the homogeneous part of the equation also supports a Fourier expansion given by:

$$\phi(r,\theta)=\sum_{m=-\infty}^{\infty}\phi_m(r)e^{im\theta} \quad (3.47)$$

we can write the following expression for the total wave function:

$$\begin{aligned}\sum_{m=-\infty}^{\infty}u_m(r)e^{im\theta}=\sum_{m=-\infty}^{\infty}\phi_m(r)e^{im\theta}+\\ \lambda^2\int d\mathbf{r}'G(\mathbf{r},\mathbf{r}')V_1(\mathbf{r}')\sum_{n=-\infty}^{\infty}u_n(r')e^{in\theta'}\end{aligned} \quad (3.48)$$

If we substitute the proposal for $G(\mathbf{r},\mathbf{r}')$ we can write:

$$\begin{aligned}\sum_{m=-\infty}^{\infty} u_m(r)e^{im\theta} &= \sum_{m=-\infty}^{\infty} \phi_m(r)e^{im\theta} + \\ \lambda^2 \int d\mathbf{r}' \sum_{m=-\infty}^{\infty} g_m(r,r')\frac{e^{im(\theta-\theta')}}{2\pi} V_1(\mathbf{r}') &\sum_{n=-\infty}^{\infty} u_n(r')e^{in\theta'}\end{aligned} \tag{3.49}$$

The potential in terms of imaginary exponentials is given by:

$$V_1(r,\theta) = \frac{2\mu C_{dd}}{4\pi\hbar^2}\frac{3\cos^2\theta}{r^3} = \frac{2\mu C_{dd}}{4\pi\hbar^2}\frac{3}{r^3}\frac{e^{i2\theta}+e^{-i2\theta}+2}{4} \tag{3.50}$$

If this expression for the potential is introduced in equation (3.49) we can write the following:

$$\begin{aligned}\sum_{m=-\infty}^{\infty} u_m(r)e^{im\theta} &= \sum_{m=-\infty}^{\infty} \phi_m(r)e^{im\theta} + \\ \frac{2\mu C_{dd}}{4\pi\hbar^2}\frac{3\lambda^2}{4} \sum_{m=-\infty}^{\infty}\sum_{n=-\infty}^{\infty} &\int_0^{\infty} dr' \frac{g_m(r,r')}{r'^2} u_n(r') \times \\ \times \int_0^{2\pi} d\theta' \frac{e^{im(\theta-\theta')}}{2\pi} &\left(e^{i2\theta'}+e^{-i2\theta'}+2\right) e^{in\theta'}\end{aligned} \tag{3.51}$$

where the angular integrals can be easily done considering that:

$$\int_0^{2\pi} d\theta' \frac{e^{-im\theta'}}{2\pi}\left(e^{i2\theta'}+e^{-i2\theta'}+2\right)e^{in\theta'} = \delta_{n,m-2}+\delta_{n,m+2}+2\delta_{n,m} \tag{3.52}$$

Using this last expression we can finally simplify the expression (3.51) as

$$\begin{aligned}\sum_{m=-\infty}^{\infty} u_m(r)e^{im\theta} &= \sum_{m=-\infty}^{\infty} \phi_m(r)e^{im\theta} + \frac{2\mu C_{dd}}{4\pi\hbar^2}\frac{3\lambda^2}{4}\times \\ \times \sum_{m=-\infty}^{\infty} \int_0^{\infty} dr' &\frac{g_m(r,r')}{r'^2}\left[u_{m+2}(r')+2u_m(r')+u_{m-2}(r')\right]e^{im\theta}.\end{aligned} \tag{3.53}$$

From this last equation we can write an integral equation for each partial wave of the solution,

$$\begin{aligned}u_m(r) = \phi_m(r) + \frac{2\mu C_{dd}}{4\pi\hbar^2}\frac{3\lambda^2}{4}\int_0^{\infty} dr' \times \\ \times \frac{g_m(r,r')}{r'^2}\left[u_{m+2}(r')+2u_m(r')+u_{m-2}(r')\right] \qquad \forall m\in\mathbb{Z}\end{aligned} \tag{3.54}$$

From this last expression one can see that the anisotropy of the dipolar interaction causes the coupling between partial waves corresponding to different

angular moment, and therefore, the angular moment it is no longer a good quantum number because the interparticle interaction can cause transitions between states of different angular moment.

Although we are considering a Fourier expansion in terms of imaginary exponentials it can be easily shown that this expansion simplifies and only the terms with $\cos m\theta$ with even m contribute. This simplification is due to the Bose symmetry of the wave function which leaves it unchanged under the transformation $\theta \to \theta + \pi$. If we apply this symmetry condition we obtain:

$$\begin{gathered}\psi(r,\theta) - \psi(r,\theta+\pi) = 0 \Rightarrow \\ \sum_{m=-\infty}^{\infty} u_m(r)\left(e^{im\theta} - e^{im(\theta+\pi)}\right) = 0 \Rightarrow \\ m\pi = 2k\pi \qquad \text{where } k \in \mathbb{Z}\end{gathered}$$

This condition, in addition with the symmetry of the partial contributions to the Green's function $g_m(r,r') = g_{-m}(r,r')$ that we have commented previously implies that we can write the wave function in terms of cosine Fourier series only:

$$\psi(r,\theta) = u_0(r) + 2\sum_{m=1}^{\infty} u_{2m} e^{i2m\theta} \tag{3.55}$$

After this consideration we come back to the evaluation of the Green's function. We have seen that the evaluation of the full Green's function $G(\mathbf{r},\mathbf{r}')$ can be reduced using a Fourier decomposition to the evaluation of a set of radial Green's functions $g_m(r,r')$ defined by the equation (3.45), that can be thought as the following operational relation:

$$\mathcal{L}_m g_m = -\delta(r-r') \tag{3.56}$$

where $\mathcal{L}_m$ is a self-adjoint operator given by:

$$\mathcal{L}_m \equiv \frac{d}{dr}\left(r\frac{d}{dr}\right) - \left(\frac{m^2}{r} + \frac{2\mu}{\hbar^2}\frac{C_{dd}}{4\pi r^2}\right). \tag{3.57}$$

The generic form of a self-adjoint operator in the Sturm-Liouville theory is given by:

$$L \equiv \frac{d}{dx}\left(p(x)\frac{d}{dx}\right) + q(x), \tag{3.58}$$

so identifying the different functions one can see that in our situation $p(r) = r$ and $q(r) = \left(\frac{m^2}{r} + \frac{2\mu}{\hbar^2}\frac{C_{dd}}{4\pi r^2}\right)$. The Green's function for a self-adjoint operator is given by [61, 62]:

$$g_m(r,r') = -\frac{1}{p(r')W(r')}\begin{cases} y_1(r)y_2(r') & 0 \le r < r' \le \infty \\ y_1(r')y_2(r) & 0 \le r' < r \le \infty \end{cases} \tag{3.59}$$

where $y_1(r)$ and $y_2(r)$ are two linearly independent solutions of the homogeneous differential equation

$$\mathcal{L}_m g_m(r,r') = 0 \tag{3.60}$$

and $W(r)$ is the Wronskian of these solutions, defined as:

$$W(r) = \begin{vmatrix} y_1(r) & y_2(r) \\ y_1'(r) & y_2'(r) \end{vmatrix}. \tag{3.61}$$

The Green's function must satisfy the same physical boundary condition

$$\lim_{r\to 0} g_m(r,r') = 0 \tag{3.62}$$

due to the divergence of the dipolar interaction at short distances.

We have seen in previous sections of this chapter that two independent solutions of the equation (3.60) are given by $y_1(r) = K_{2m}\left(\sqrt{\frac{2\mu C_{dd}}{4\pi\hbar^2}}\frac{2}{\sqrt{r}}\right)$ and $y_2(r) = I_{2m}\left(\sqrt{\frac{2\mu C_{dd}}{4\pi\hbar^2}}\frac{2}{\sqrt{r}}\right)$, and the Wronskian determinant is $W(r) = -\frac{1}{2r}$. From the two independent solutions and the Wronskian we can build the Green's function for each Fourier component as:

$$g_m(r,r') = \begin{cases} 2K_{2m}\left(\sqrt{\frac{2\mu C_{dd}}{4\pi\hbar^2}}\frac{2}{\sqrt{r}}\right) I_{2m}\left(\sqrt{\frac{2\mu C_{dd}}{4\pi\hbar^2}}\frac{2}{\sqrt{r'}}\right) & r < r' \\ 2K_{2m}\left(\sqrt{\frac{2\mu C_{dd}}{4\pi\hbar^2}}\frac{2}{\sqrt{r'}}\right) I_{2m}\left(\sqrt{\frac{2\mu C_{dd}}{4\pi\hbar^2}}\frac{2}{\sqrt{r}}\right) & r' < r \end{cases}. \tag{3.63}$$

It can be seen that the Green's function remains bounded for all the range $0 < r < \infty$, and, as a consequence of the short-ranged nature of the interaction potential in two dimensions, all anisotropic contributions ($m \neq 0$) vanish at large distances given that $\lim_{r\to\infty} I_{2m}\left(\sqrt{\frac{2\mu C_{dd}}{4\pi\hbar^2}}\frac{2}{\sqrt{r}}\right) = 0 \quad \forall m > 0$.

Once we have evaluated the Green's function of the problem we can use the recursive relations in (3.54) to evaluate the different Fourier components of the full wave function in a perturbative way supposing by means of an iterative process given by:

$$\begin{aligned} u_m^{(k+1)}(r) &= u_m^{(k)}(r) + \frac{2\mu C_{dd}}{4\pi\hbar^2}\frac{3\lambda^2}{4}\int_0^\infty dr' \times \\ &\times \frac{g_m(r,r')}{r'^2}\left[u_{m+2}^{(k)}(r') + 2u_m^{(k)}(r') + u_{m-2}^{(k)}(r')\right] \qquad \forall m \in \mathbb{Z} \end{aligned} \tag{3.64}$$

where $u_0^{(0)}(r) = \phi_0(r)$, $u_m^{(0)}(r) = 0$ if $m > 0$ and $\phi_0(r)$ is the zero angular momentum solution of the isotropic two body problem

$$\phi_0(r) = K_0\left(\sqrt{\frac{2\mu C_{dd}}{4\pi\hbar^2}}\frac{2}{\sqrt{r}}\right). \tag{3.65}$$

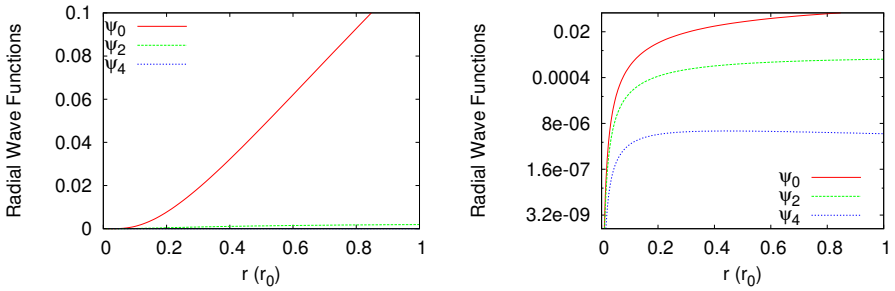

(a) Lowest angular momentum Fourier components for $\alpha = 0.2$.

(b) Same as panel (a) but in logarithmic scale on the y-axis.

Figure 3.5: Comparison between the lowest angular momentum partial contributions to the anisotropic wave function of the two dimensional dipolar problem with tilting angle $\alpha = 0.2$.

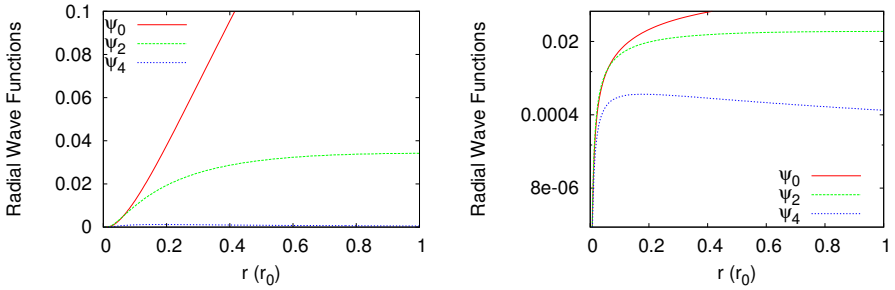

(a) Lowest angular momentum Fourier components for $\alpha = 0.6$.

(b) Same as panel (a) but in logarithmic scale on the y-axis.

Figure 3.6: Comparison between the lowest angular momentum partial contributions to the anisotropic wave function of the two dimensional dipolar problem with tilting angle $\alpha = 0.6$.

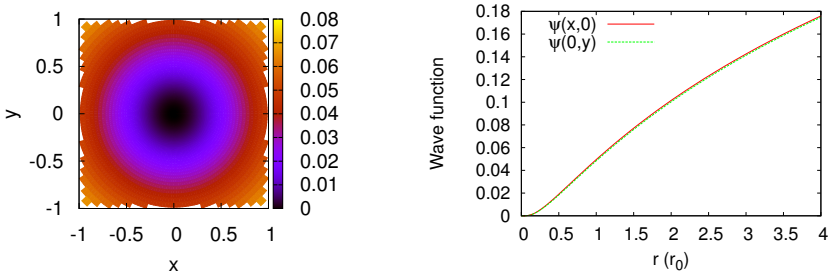

(a) Wave function for the two-dipole problem with $\alpha = 0.2$.

(b) Cuts of the wave function for the two-dipole problem with $\alpha = 0.2$ in the x (red) and y- directions.

Figure 3.7: Two-body wave function for the $\alpha = 0.2$ case.

From expression (3.64) one sees that by adding successive orders in λ^2 to the series expansion of $\psi(\mathbf{r})$, more angular momentum channels couple together. In fact, it can be shown from the previous expressions that $u_m^{(k)}(r) = 0$ for $m/2 > k$, and that therefore the lowest order contribution to the m-th Fourier component is $O(\lambda^m)$. By adding $u_m^{(k)}(r)$ for all k and fixed m one recovers the complete Fourier contribution of angular momentum m to the full wave function $\psi(\mathbf{r})$, given by:

$$u_m(r) = \sum_{k=m/2}^{\infty} \lambda^{2k} u_m^{(k)}(r) \tag{3.66}$$

which means that, up to a given order λ^{2k}, the total wave function $\psi(\mathbf{r})$ has contributions coming only from Fourier components $m = 0, 2, \cdots, 2k$

Figures 3.5 and 3.6 show the lowest order partial waves contributions to the two polarization angles $\alpha = 0.2$ and $\alpha = 0.6$ respectively. The latter angle is fairly close to the critical angle $\alpha_c = 0.615$ where the interaction starts to show attractive regions. At $\alpha = 0.6$ the contribution of the $m \neq 0$ angular momentum states is expected to be larger than for any lower angle. This is clearly seen from the figure, where the λ^2 corrections to the $m = 0$, $m = 2$ and $m = 4$ Fourier components are shown (red, green and blue lines respectively). It is clear from equations (3.63), (3.64) and the positiveness of the modified Bessel functions that every radial contribution to the two body wave function is also positive, as seen for the lowest angular momentum Fourier components shown in the figures. It is also clear that the lower the angle, the smaller the corrections due to high angular momentum states.

The effect of the anisotropy on the ground state wave function can be clearly seen in Figures 3.7 and 3.8 for $\alpha = 0.2$ and $\alpha = 0.6$ respectively.

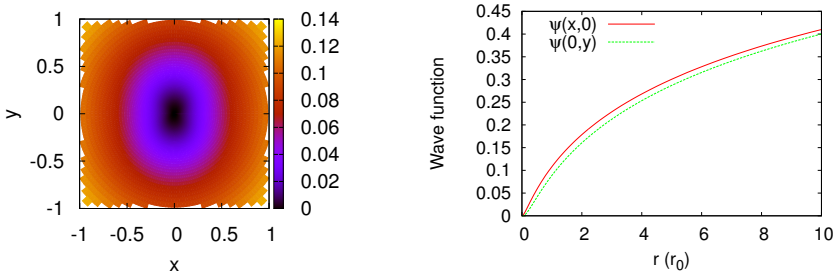

(a) [Wave function for the two-dipole problem with $\alpha = 0.6$.

(b) [Cuts of the wave function for the two-dipole problem with $\alpha = 0.6$ in the x (red) and y- directions.

Figure 3.8: Two-body wave function for the $\alpha = 0.6$ case.

It is shown in the figures a two dimensional map of the wave function (left panel in both figures) and the value of the wave function in to different cuts (right panel in both figures), one along the x-axis (contained in the plane formed by the angular momentum vector and the z-axis), and another in the perpendicular direction (y-axis) are depicted. The two cuts presented correspond to the directions where the interaction is the least and most repulsive respectively. As it can be seen, anisotropic effects can be appreciated in both situations but are much more pronounced at higher values of the tilting angle of the dipoles.

Scattering length for the two dimensional anisotropic interaction

A very important result that can be extracted from the zero energy scattering solution is the scattering length of the interaction that is a fundamental quantity in the theory of low density quantum gases. From the asymptotic behaviour of the zero-energy two-body wave function $\psi(\mathbf{r})$ we can extract an analytical approximate expression for the scattering length of the anisotropic dipolar interaction in two dimensions. The scattering length is given by the node of the asymptotic $r \to \infty$ form of the two body wave function.

As we have seen in the previous sections the $m \neq 0$ Fourier components of the full wave function vanish at large distances, so the asymptotic behaviour of the wave function is dominated by the $m = 0$ partial wave, which is determined by the following equation:

$$u_0(r) = \phi_0(r) + \frac{2\mu C_{dd}}{4\pi\hbar^2}\frac{3\lambda^2}{2}\int_0^\infty dr' \frac{g_0(r,r')}{r'^2}\left[u_0(r') + u_2(r')\right]. \qquad (3.67)$$

We want to analyse the behaviour of the the $u_0(r)$ function up to λ^2 order, which implies that the contribution of the $u_2(r)$ Fourier component can be

neglected in this approximation, so the equation that we want to study is

$$u_0(r) = \phi_0(r) + \frac{2\mu C_{dd}}{4\pi\hbar^2}\frac{3\lambda^2}{2}\int_0^\infty dr' \frac{g_0(r,r')}{r'^2} u_0(r') + O(\lambda^4) \tag{3.68}$$

If we introduce in this last expression the form of the Green's function given in (3.63), and the solution of the isotropic zero energy solution with $m = 0$ given by (3.65), we can write

$$\begin{aligned} u_0(r) =& K_0\left(\sqrt{\frac{2\mu C_{dd}}{4\pi\hbar^2}}\frac{2}{\sqrt{r}}\right) + \frac{2\mu C_{dd}}{4\pi\hbar^2}3\lambda^2 \times \\ \Bigg[& I_0\left(\sqrt{\frac{2\mu C_{dd}}{4\pi\hbar^2}}\frac{2}{\sqrt{r}}\right)\int_0^r dr' \frac{K_0\left(\sqrt{\frac{2\mu C_{dd}}{4\pi\hbar^2}}\frac{2}{\sqrt{r'}}\right)}{r'^2} K_0\left(\sqrt{\frac{2\mu C_{dd}}{4\pi\hbar^2}}\frac{2}{\sqrt{r'}}\right) + \\ & K_0\left(\sqrt{\frac{2\mu C_{dd}}{4\pi\hbar^2}}\frac{2}{\sqrt{r}}\right)\int_r^\infty dr' \frac{I_0\left(\sqrt{\frac{2\mu C_{dd}}{4\pi\hbar^2}}\frac{2}{\sqrt{r'}}\right)}{r'^2} K_0\left(\sqrt{\frac{2\mu C_{dd}}{4\pi\hbar^2}}\frac{2}{\sqrt{r'}}\right) \Bigg] \end{aligned} \tag{3.69}$$

We want to analyse the long range behavior of the $u_0(r)$ function, so we can safely neglect the second integral when $r \to \infty$ and consider only the first contribution where $r' < r$. The first integral can be extended to the range $[0, \infty)$ and will be given by:

$$\int_0^\infty dr' \frac{\left[K_0\left(\sqrt{\frac{2\mu C_{dd}}{4\pi\hbar^2}}\frac{2}{\sqrt{r'}}\right)\right]^2}{r'^2} = \frac{1}{4}\left(\frac{4\pi\hbar^2}{2\mu C_{dd}}\right) \tag{3.70}$$

Now, the asymptotic long range behaviour of the modified Bessel functions is given by:

$$K_0\left(\sqrt{\frac{2\mu C_{dd}}{4\pi\hbar^2}}\frac{2}{\sqrt{r}}\right) \approx \frac{1}{2}\log\left(\frac{r}{e^{2\gamma+\log\left(\frac{2\mu C_{dd}}{4\pi\hbar^2}\right)}}\right) \tag{3.71}$$

and

$$I_0\left(\sqrt{\frac{2\mu C_{dd}}{4\pi\hbar^2}}\frac{2}{\sqrt{r}}\right) \approx 1 \tag{3.72}$$

Finally we can introduce the asymptotic behaviours and the result (3.70) in (3.69) to find

$$u_0(r) \approx \frac{1}{2}\left[\log\left(\frac{r}{e^{2\gamma+\log\left(\frac{2\mu C_{dd}}{4\pi\hbar^2}\right)}}\right) + \frac{3\lambda^2}{2}\right] \tag{3.73}$$

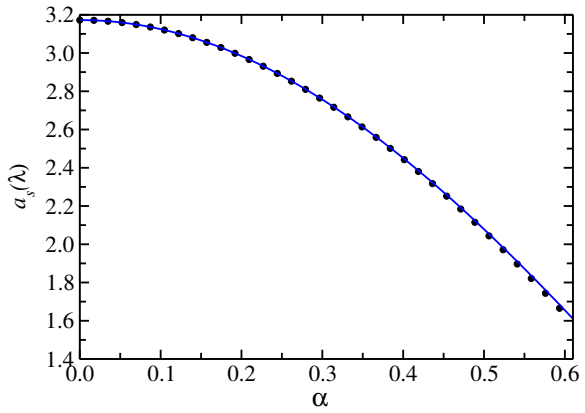

Figure 3.9: s-wave scattering length as a function of the tilting angle α. The line and the dots correspond to the λ^2 approximation and the exact numerical solution respectively.

that can be rearranged as:

$$u_0(r) \approx \frac{1}{2}\left[\log\left(\frac{r}{e^{2\gamma+\log\left(\frac{2\mu C_{dd}}{4\pi\hbar^2}\right)}e^{-\frac{3\lambda^2}{2}}}\right)\right] \tag{3.74}$$

To find the desired expression we must have in account that our approach is valid only up to an order $O(\lambda^2)$ so we can consider $e^{-\frac{3\lambda^2}{2}} \approx 1 - \frac{3\lambda^2}{2}$, and we can finally write the desired expression for the asymptotic behaviour of the $u_0(r)$ function as:

$$u_0(r) \approx \frac{1}{2}\log\left(\frac{r}{a_s(\lambda)}\right) \tag{3.75}$$

where $a_s(\lambda)$ is the lowest order approximation to the scattering length of the anisotropic dipolar scattering in two dimensions, given by:

$$a_s(\lambda) = e^{2\gamma+\log\left(\frac{2\mu C_{dd}}{4\pi\hbar^2}\right)}\left(1 - \frac{3\lambda^2}{2}\right). \tag{3.76}$$

It can be seen that the scattering length becomes smaller as the anisotropy of the dipole - dipole interaction increases, which is an expected behaviour given that the potential becomes less repulsive in average showing regions where the strength of the interaction is much lower than in the isotropic situation. As a conclusion of this section we have compared the scattering length evaluated using the equation (3.76) with the exact result obtained by numerically finding the node of the asymptotic $m = 0$ wave function, which is isotropic and dominates the large distance behaviour of the wave function $\psi(\mathbf{r})$. The results of this comparison are presented in figure As can be seen from the figure, the approximation works surprisingly well up to

the critical angle α_c where the interaction starts to show attractive regions. Deviations increase with increasing polarisation angle, but even at $\alpha = \alpha_c$ the separation between the approximation in equation (3.76) and the exact numerical estimation is less than 3%.

Chapter 4

Two dimensional dipolar Bose gas at low density

4.1 Introduction

The analysis of the low density equation of state of a gas of weakly interacting particles has historically attracted great interest. Corrections to the mean field prediction for three-dimensional [64] and one-dimensional [65] systems have been known for more that fifty years now. The two-dimensional case has been much more controversial as already the two-body problem presents logarithmic divergences in the leading scattering parameters that make series expansions difficult to carry out [22, 23]. In any case, the low density behaviour of a gas of weakly interacting particles in 2D has been widely discussed in the literature for the case of isotropic interactions. One of the most remarkable properties exhibited by these systems is the *universal* behaviour of the energy per particle, which admits a non–analytic series expansion in the gas parameter $x = na^2$, with n the density and a the $s-$wave scattering length. The leading order, mean-field term in this series has been derived by several authors [66, 67] and reads

$$\epsilon_{mf}(x) = \left(\frac{2ma^2}{\hbar^2}\right)\frac{E}{N} = \frac{4\pi x}{|\ln x|} \ . \tag{4.1}$$

The detailed form of the next-to-leading correction to this expression has been the subject of discussion and different authors proposed different forms in the past, see for instance Refs. [68, 69]. The correct expression was recently derived in Ref. [70] and checked against numerically intense Monte Carlo simulations in Ref. [71]. For the model system of hard disks, the mean field prediction of Equation (4.1) holds well starting at $x \sim 0.001$ and down to quite low but still experimentally affordable values of the gas parameter [72]. However, no particular attention has been paid in all these works to the special case of anisotropic interactions.

In this chapter we discuss to which extent the mean field law of Equation (4.1) holds for the special case of the spatially anisotropic dipole-dipole interaction when the polarisation angle varies between 0 and α_c. We are particularly interested in discerning whether the angular dependence of the interaction has a noticeable impact on the mean-field prediction of Eq. (4.1) and on other relevant ground state properties. In order to do that, we use the previously presented solution of the zero-energy two-body problem to build a variational many-body Jastrow wave function that will be used as an input to both variational Monte Carlo (VMC) and diffusion Monte Carlo (DMC) calculations from where we obtain the equation of state as a function of the gas parameter x. For the sake of completeness we also analyse structural properties of the dipolar Bose gas as the pair distribution function or the static structure factor. Additionally, we have also evaluated the one-body density matrix and the condensate fraction, and discuss how these quantities scale on the gas parameter for different polarisation angles and densities.

4.2 Many-Body description

We have used DMC and VMC methods in order to accurately evaluate the most relevant ground state properties of an homogeneous and anisotropic gas of bosonic dipoles with a polarisation angle α lower than the critical angle $\alpha_c = 0.615$. We stick to the low density limit where the system, characterised by a fully repulsive and anisotropic interaction, remains in a stable, gaseous phase. One of the most relevant quantities to analyse at low densities is the total energy per particle and its universal scaling properties. Quite a lot of work has been devoted in the past to that question, including both 3D [64, 73, 74, 75] and 2D [66, 67, 68, 69, 70, 71, 72] systems. However, little has been discussed about the same properties in anisotropic systems as the dipolar gas considered here. We analyse the impact of the polarisation angle α formed by the dipoles on the universality scaling law exhibited by other isotropic, short ranged interactions.

The Hamiltonian of the system of fully polarised dipoles, written in dipolar units, becomes

$$H = -\frac{1}{2}\sum_{j=1}^{N}\nabla_j^2 + \sum_{i<j}\frac{1-3\lambda^2\cos^2\theta_{ij}}{r_{ij}^3}\ , \tag{4.2}$$

with $\lambda = \sin\alpha$, and r_{ij} and θ_{ij} the distance and angle formed by dipoles i and j, respectively, measured on the plane.

The leading ground state quantities describing the low density static properties of the system can be obtained using different techniques. In this work we stick to diffusion and variational Monte Carlo methods, widely used nowadays in the analysis of weakly and strongly correlated systems.

The quality of the results is directly related to the quality of the wave function employed in the VMC case, while DMC is far less demanding and any reasonable guiding function can be used as long as it is not orthogonal to the true ground state. But even in DMC a high-quality wave function makes the method converge faster and with smaller variance towards the exact result. Consequently, seeking for a good trial many-body wave function $\Psi(\mathbf{r}_1, \mathbf{r}_2, \ldots, \mathbf{r}_N)$ is always desirable.

4.3 Many body wave function

In this work we use a model Bijl-Jastrow wave function

$$\Psi(\mathbf{r}_1, \mathbf{r}_2, \ldots, \mathbf{r}_N) = \prod_{i<j} f(\mathbf{r}_{ij}) \ , \tag{4.3}$$

where the two-body correlation factor $f(\mathbf{r}_{ij}) = f(\mathbf{r}_i - \mathbf{r}_j)$ depends on the position vector linking particles i and j. One significant difference between this Jastrow factor and the ones most commonly employed in the analysis of other condensed matter systems is that, due to the anisotropic character of the interaction, $f(\mathbf{r})$ depends explicitly on the whole $\mathbf{r}$ vector and not only on its magnitude. In this way, the wave function in Eq. (4.3) describes an homogeneous but anisotropic system as the one under study.

At low densities, the zero-energy scattering solution of the two-body problem greatly influences the structural properties of the gas. For that reason we use as a Jastrow factor the anisotropic solution of the relative motion of two dipoles on the plane derived in the previous chapter.

$$f(\mathbf{r}_{ij}) = \begin{cases} A\phi_{2B}(\mathbf{r}_{ij}) & \text{if } r_{ij} < R_m \\ Be^{-C\left(\frac{1}{r_{ij}} + \frac{1}{L - r_{ij}}\right)} & \text{if } r_{ij} \geq R_m \end{cases} \tag{4.4}$$

where ϕ_{2B} is the two body zero energy solution presented in the previous chapter. The $n = 0$ partial wave of this wave function is matched at some healing distance R_m with the symmetrized form of a phononic wave function [76], taking R_m as a variational parameter. By imposing the continuity of $f(r)$ and $f'(r)$ at $r = R_m$ the parameters A, B and C can be easily determined. The $n > 0$ partial waves of the two-body problem, inducing the anisotropy of $\Psi(\mathbf{r}_1, \mathbf{r}_2, \ldots, \mathbf{r}_N)$ in Eq. (4.3), decay to zero at large distances and so their influence at the boundaries of the simulation box is marginally small. Alternatively, the optimal Jastrow factor corresponding to the many-body problem can be obtained from the solution of the HNC/0 Euler-Lagrange equations [77]. Although not exact, the optimised HNC/0 solution gives an accurate variational description of quantum Bose systems and captures most of the short and long range features of the exact ground state wave function. For the sake of comparison, we show in Fig. 4.1 the

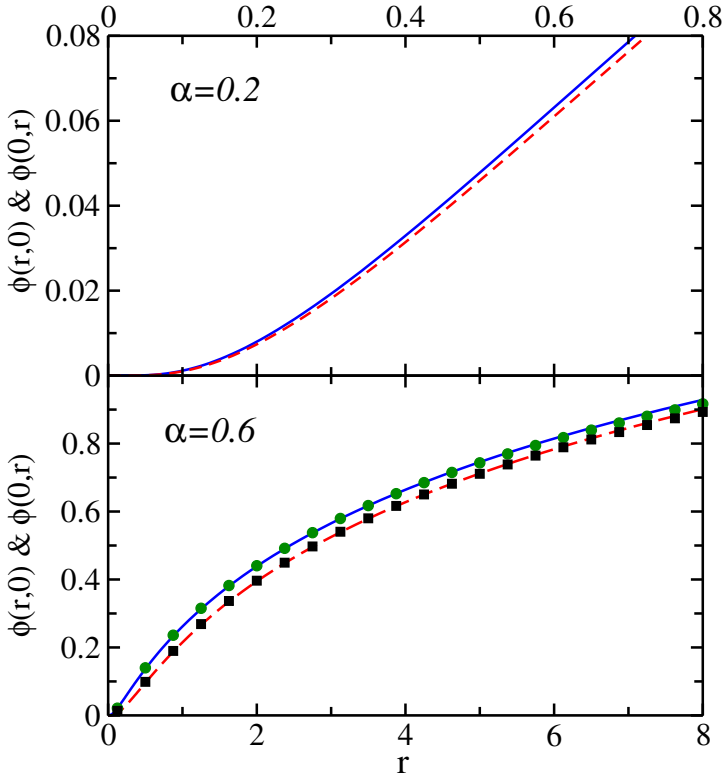

Figure 4.1: Cuts of the zero energy two-body scattering wave function describing the relative motion of two dipoles. The blue solid line and the red dashed line correspond to the cuts along the x and y axes, respectively. The green circles and black squares are the prediction of the optimal Jastrow factor obtained from the solution of the HNC/0 Euler equations for a value of the gas parameter $x = 0.01$.

x	$\alpha = 0.2$	$\alpha = 0.4$	$\alpha = 0.6$
10^{-7}	$4.268(61) \cdot 10^{-9}$	$6.490(24) \cdot 10^{-9}$	$1.429(75) \cdot 10^{-8}$
$5 \cdot 10^{-7}$	$2.389(90) \cdot 10^{-8}$	$3.633(91) \cdot 10^{-8}$	$7.931(45) \cdot 10^{-8}$
10^{-6}	$5.044(91) \cdot 10^{-8}$	$7.631(36) \cdot 10^{-8}$	$1.690(86) \cdot 10^{-7}$
$5 \cdot 10^{-6}$	$2.874(24) \cdot 10^{-7}$	$4.360(89) \cdot 10^{-7}$	$9.472(85) \cdot 10^{-7}$
10^{-5}	$6.135(87) \cdot 10^{-7}$	$9.312(22) \cdot 10^{-7}$	$2.011(92) \cdot 10^{-6}$
$5 \cdot 10^{-5}$	$3.596(27) \cdot 10^{-6}$	$5.450(94) \cdot 10^{-6}$	$1.199(81) \cdot 10^{-5}$
10^{-4}	$7.768(72) \cdot 10^{-6}$	$1.177(30) \cdot 10^{-5}$	$2.579(84) \cdot 10^{-5}$
$5 \cdot 10^{-4}$	$4.757(48) \cdot 10^{-5}$	$7.205(59) \cdot 10^{-5}$	$1.567(73) \cdot 10^{-4}$
10^{-3}	$1.051(31) \cdot 10^{-4}$	$1.590(58) \cdot 10^{-4}$	$3.467(23) \cdot 10^{-4}$
$5 \cdot 10^{-3}$	$6.807(74) \cdot 10^{-4}$	$1.029(58) \cdot 10^{-3}$	$2.240(26) \cdot 10^{-3}$
10^{-2}	$1.551(31) \cdot 10^{-3}$	$2.337(23) \cdot 10^{-3}$	$5.067(97) \cdot 10^{-3}$
$5 \cdot 10^{-2}$	$1.085(29) \cdot 10^{-2}$	$1.634(18) \cdot 10^{-2}$	$3.544(62) \cdot 10^{-2}$
10^{-1}	$2.572(67) \cdot 10^{-2}$	$3.840(66) \cdot 10^{-2}$	$8.292(21) \cdot 10^{-2}$
$5 \cdot 10^{-1}$	$1.962(54) \cdot 10^{-1}$	$2.938(41) \cdot 10^{-1}$	$6.347(32) \cdot 10^{-1}$

Table 4.1: VMC energies per particle as a function of the gas parameter $x = na^2$.

optimised HNC/0 Jastrow factor (black and green symbols) at $x = 0.01$ and polarisation angle $\alpha = 0.6$ [78]. The comparison indicates that the two-body solution provides an accurate description of the two-body correlation factor, which becomes even better as the gas parameter is reduced.

4.4 Equation of state

The most important part of the analysis of the low density Bose dipolar gas is the determination of the equation of state of the system. The results of the Monte Carlo simulations can be compared with the low density equation of state given in equation (4.1).

Tables 4.1 and 4.2 list both the VMC and DMC energies respectively obtained from the Jastrow trial wave function of Eq. (4.3) for the polarisation angles $\alpha = 0.2$, 0.4 and 0.6. Notice that the energies in the table are given for fixed x and different polarisation angles, and since the scattering length varies with α, the densities change accordingly. A direct measure of the quality of the variational model is given by the separation between these two measures (VMC and DMC), and one can check that the relative difference in energies is always of the order of 1% or 2%. Other than that, the energy is an increasing function of the gas parameter that yields appreciably different results for different polarisation angles. These energies can be used to check the influence of the anisotropic character of the dipolar interaction on the universality scaling property fulfilled by the energy per particle of

x	$\alpha = 0.2$	$\alpha = 0.4$	$\alpha = 0.6$
10^{-7}	$4.271(61) \cdot 10^{-9}$	$6.469(62) \cdot 10^{-9}$	$1.414(62) \cdot 10^{-8}$
$5 \cdot 10^{-7}$	$2.386(24) \cdot 10^{-8}$	$3.602(70) \cdot 10^{-8}$	$7.888(15) \cdot 10^{-8}$
10^{-6}	$5.030(32) \cdot 10^{-8}$	$7.614(21) \cdot 10^{-8}$	$1.664(50) \cdot 10^{-7}$
$5 \cdot 10^{-6}$	$2.868(24) \cdot 10^{-7}$	$4.317(70) \cdot 10^{-7}$	$9.448(93) \cdot 10^{-7}$
10^{-5}	$6.105(64) \cdot 10^{-7}$	$9.271(41) \cdot 10^{-7}$	$2.032(90) \cdot 10^{-6}$
$5 \cdot 10^{-5}$	$3.584(31) \cdot 10^{-6}$	$5.405(15) \cdot 10^{-6}$	$1.180(40) \cdot 10^{-5}$
10^{-4}	$7.744(61) \cdot 10^{-6}$	$1.170(41) \cdot 10^{-5}$	$2.542(88) \cdot 10^{-5}$
$5 \cdot 10^{-4}$	$4.734(49) \cdot 10^{-5}$	$7.124(93) \cdot 10^{-5}$	$1.555(62) \cdot 10^{-4}$
10^{-3}	$1.046(16) \cdot 10^{-4}$	$1.577(33) \cdot 10^{-4}$	$3.425(30) \cdot 10^{-4}$
$5 \cdot 10^{-3}$	$6.776(61) \cdot 10^{-4}$	$1.018(90) \cdot 10^{-3}$	$2.222(51) \cdot 10^{-3}$
10^{-2}	$1.532(20) \cdot 10^{-3}$	$2.316(31) \cdot 10^{-3}$	$5.036(55) \cdot 10^{-3}$
$5 \cdot 10^{-2}$	$1.077(11) \cdot 10^{-2}$	$1.616(9) \cdot 10^{-2}$	$3.517(74) \cdot 10^{-2}$
10^{-1}	$2.534(29) \cdot 10^{-2}$	$3.774(42) \cdot 10^{-2}$	$8.235(21) \cdot 10^{-2}$
$5 \cdot 10^{-1}$	$1.947(14) \cdot 10^{-1}$	$2.908(28) \cdot 10^{-1}$	$6.311(33) \cdot 10^{-1}$

Table 4.2: DMC energies per particle as a function of the gas parameter $x = na^2$.

homogeneous and isotropic systems in 2D. In order to do that, one has to express the total energy per particle in units of $\hbar^2/2ma^2$ with a the scattering length. This is achieved multiplying the energies in Table 4.2 (expressed in dipolar units) by $2a_s^2(\lambda)$, with $a_s(\lambda)$ the scattering length for the corresponding polarisation angle.

Figure 4.2 shows the ratio of the energy per particle in units of $\hbar^2/2ma^2$ to the mean field prediction of Eq. (4.1) for the three polarisation angles $\alpha = 0.2$, 0.4 and 0.6. As it can be seen, expressed in scattering length units, all curves corresponding to different polarisation angles merge into a single curve, with very small deviations that are not easily resolved even at the highest values of gas parameters x considered in this work. That means that the anisotropy of the interaction, present in the wave function, does not appreciably affect the energy per particle in the low density regime analysed in this work. We conclude that the difference in energy values shown in Table 4.2 for fixed x and varying polarisation angles are to be mostly attributed to the different density $n = x/a^2$ in each case. It is also shown in Figure 4.2 the universal curve including beyond mean field effects of Ref. [71] and the optimised HNC/0 prediction for a gas of hard disks of Ref. [72]. As it can be seen, the universal and the hard disks curves are close to each other while the dipole curves remain closer to the mean field prediction $\epsilon_{mf}(x)$ as the gas parameter is raised. Starting at $x \sim 0.05$ the dipole curves bend downwards and the energy deviates significantly from $\epsilon_{mf}(x)$. In any case, it is clear from the figure that the universality regime, where the energy per particle depends only on the gas parameter of the interaction, is left much

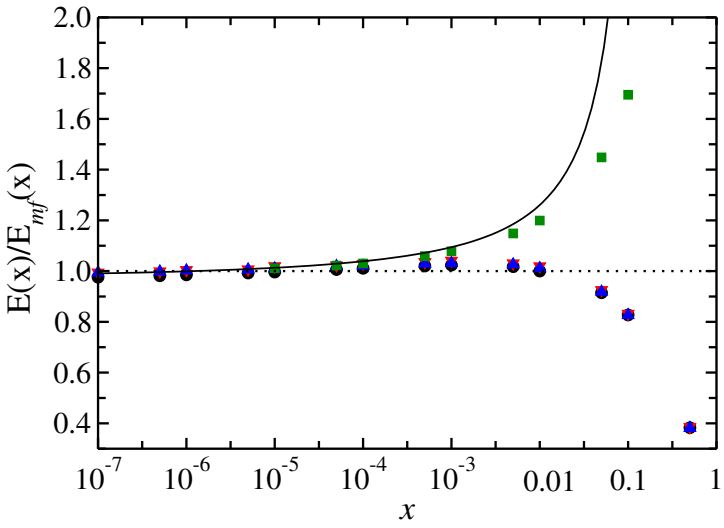

Figure 4.2: Ratio of the energy per particle of the gas of dipoles for different polarisation angles to the mean field prediction of Eq. (4.1). Black circles, red triangles and blue triangles correspond to $\alpha = 0.2, 0.4$ and 0.6, respectively. The green squares are the optimised HNC/EL energies for hard disks of Ref. [75], while the solid line is the universal curve of Ref. [79]. The dotted line corresponds to the mean field prediction.

before anisotropic effects have an appreciable impact on the energy of the dipolar gas.

4.5 Structural properties: pair distribution function and static structure factor

The anisotropic character of the dipolar interaction has a direct influence on the ground state wave function that is reflected in the ground state expectation value of any many-body operator.

Figures 4.3 and 4.4 show pure DMC estimations [80] of the pair distribution function $g(\mathbf{r})$ and its Fourier transform, the static structure factor $S(\mathbf{k})$, for two values of the polarisation angle $\alpha = 0.4$ and $\alpha = 0.6$ (left and right panels), and three values of the gas parameter $x = 10^{-5}, 10^{-3}$ and 10^{-1} (top to bottom). Notice that in both figures the horizontal axis has been scaled with the square root of the density for a better comparison. Due to the symmetries of the Hamiltonian, the complete $g(\mathbf{r})$ and $S(\mathbf{k})$ functions vary continuously on the plane but the pattern on the first quadrant is repeated and reflected on the other three. The figures show only the two cuts along the perpendicular and parallel directions with respect to the polarisation plane, corresponding to the lines where the interaction is

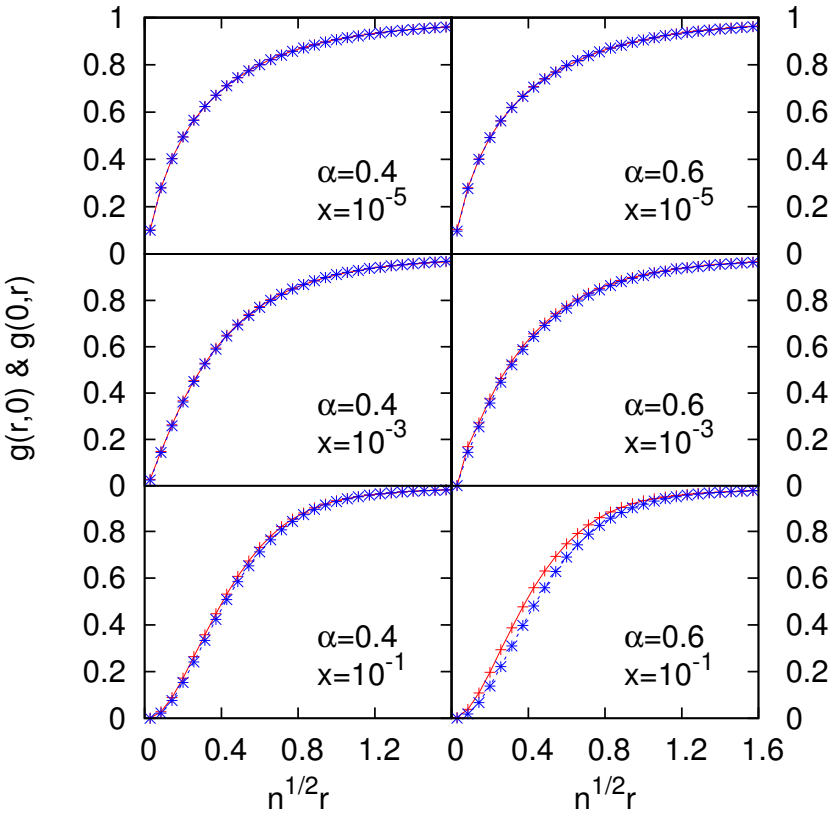

Figure 4.3: Pair distribution function for $\alpha = 0.4$ and $\alpha = 0.6$ and three values of the gas parameter. The red and blue curves show the two cuts $g(r, 0)$ and $g(0, r)$, respectively.

most and least repulsive, respectively. As it can be seen, and in agreement with what one would expect, the effect of the anisotropy is more clearly seen at higher polarisation angles and for large values of the gas parameter, being maximal for $\alpha = 0.6$ and $x = 10^{-1}$. For fixed α the separation between $g(r, 0)$ and $g(0, r)$ is enhanced with increasing x, as happens with $S(k, 0)$ and $S(0, k)$. Accordingly and for a given x, the separation between the curves also increases when the polarisation angle is raised. In any case it is remarkable how the anisotropy present in $g(\mathbf{r})$ and $S(\mathbf{k})$ changes with the polarisation angle as can be seen from the figures at large x, while the total energies per particle are almost the same when properly scaled with the scattering length. This points towards a delicate balance between the kinetic and potential contributions, which change with α but keep their sum constant once expressed in scattering length units.

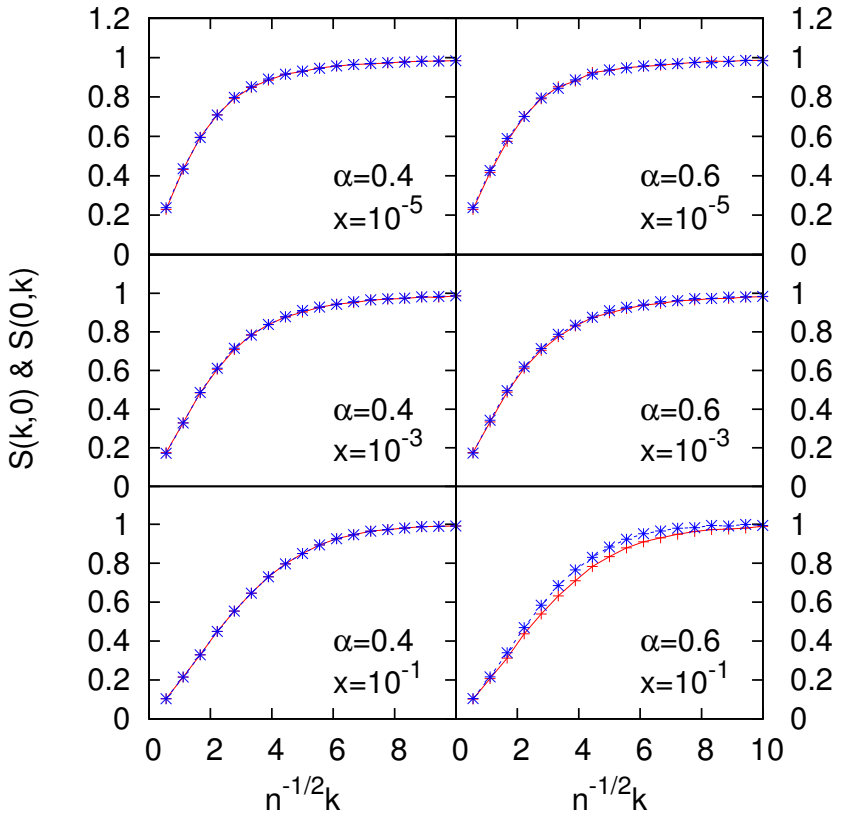

Figure 4.4: (Static structure function for polarisation angles $\alpha = 0.4$ and $\alpha = 0.6$ for $x = 10^{-5}, 10^{-3}$ and 10^{-1}. The red and blue curves show the two cuts $S(k, 0)$ and $S(0, k)$, respectively.

4.6 Excitation spectrum

A relevant issue in the study of tilted dipolar gases is the influence of the anisotropy of the interaction on the collective excitation spectrum. In this Section, we analyse this problem within two standard methods used currently in the study of Bose fluids: the Feynman and Bogoliubov approximations.

The Feynman spectrum is easy to derive from a simple sum rules argument and provides a single line in $(\mathbf{k}, \omega)$ space corresponding to a set of infinite lifetime excitations of energy [81]

$$\epsilon(\mathbf{k}) = \frac{\hbar^2 k^2}{2mS(\mathbf{k})} \ . \tag{4.5}$$

In this approximation, $\epsilon(\mathbf{k})$ depends directly on the static structure factor, the only non-trivial quantity, and provides an upper bound to the actual excitation spectrum [82]. In systems like liquid ^{4}He, this bound is closer to the experimental mode the lower the total momentum is.

On the other hand, we can study the excitation spectrum of the low density two-dimensional dipolar gas in the framework of the mean-field theory using the 2D time-dependent Gross-Pitaevskii equation,

$$i\hbar\frac{\partial\psi}{\partial t} = -\frac{\hbar^2}{2m}\nabla^2\psi + g|\psi|^2\psi \ , \tag{4.6}$$

where g is the 2D coupling constant $g = \frac{4\pi\hbar^2}{m}\frac{1}{|\log na^2|}$ [66]. Performing a standard Bogoliubov-deGennes linearization one finds the well-known Bogoiubov spectrum

$$\epsilon(\mathbf{k}) = \sqrt{\frac{\hbar^2 k^2}{2m}\left(\frac{\hbar^2 k^2}{2m} + 2gn\right)} \ . \tag{4.7}$$

Although the spectrum obtained using this approach has contributions coming from the anisotropic character of the interaction due to the polarisation angle dependence of the scattering length, not all contributions of the same order are taken into account. This simple Bogoliubov approach disregards the contribution coming from higher angular momentum channels, keeping only s-wave scattering processes. However, we know that different angular momentum channels couple in a non-trivial way in a dipolar system and so we have to take them into account. We know from the analysis of the zero-energy two-body problem that higher order partial wave contributions appear with higher orders in λ^2, so the leading corrections appear in d-wave. In order to consider the contribution of the d-wave we use the following pseudo-potential [83]

$$V_{ps}(\mathbf{r}) = g\delta^{(2)}(\mathbf{r}) - \frac{C_{dd}}{4\pi}\frac{3\lambda^2\cos 2\theta}{r^3} \tag{4.8}$$

that leads to the following Gross-Pitaevskii equation

$$\begin{aligned} i\hbar\frac{\partial\psi}{\partial t} = -\frac{\hbar^2}{2m}\nabla^2\psi + g|\psi|^2\psi - \\ \frac{C_{dd}}{4\pi}\left(\int d\mathbf{x}'\frac{3\lambda^2\cos 2\theta}{|\mathbf{x}-\mathbf{x}'|^3}|\psi(\mathbf{x}',t)|^2\right)\psi \ . \end{aligned} \tag{4.9}$$

The functional form of the pseudopotential $V_{ps}(\mathbf{r})$ (4.8) as a sum of two terms, one isotropic and another anisotropic, follows the same prescription used in the three-dimensional problem [84, 85]. One can consider a linear perturbation of the condensate wave function of the system of the form

$$\psi(\mathbf{x},t) = e^{-\frac{i}{\hbar}\mu t}(\sqrt{n} + \delta\psi(\mathbf{x},t)) \ , \tag{4.10}$$

where the perturbative term $\delta\psi(\mathbf{x},t)$ is given by

$$\delta\psi(\mathbf{x},t) = ce^{i(\mathbf{k}\cdot\mathbf{x}-\omega t)} \ , \tag{4.11}$$

where c is the (small) perturbation amplitude.

By inserting (4.10) into Eq. (4.9), and neglecting non-linear terms, one finds the equation fulfilled by the small perturbation $\delta\psi$,

$$\begin{aligned} i\hbar\frac{\partial\delta\psi}{\partial t} = -\frac{\hbar^2}{2m}\nabla^2\delta\psi + (2gn-\mu)\delta\psi + gn\delta\psi^* + \\ n(F(\mathbf{k})\delta\psi^* + F(-\mathbf{k})\delta\psi) \ , \end{aligned} \tag{4.12}$$

where $F(\mathbf{k})$ is given by

$$F(\mathbf{k}) = \frac{C_{dd}}{4\pi}\left(\int d\mathbf{y}\frac{3\lambda^2\cos 2\theta}{|\mathbf{y}|^3}e^{i\mathbf{k}\cdot\mathbf{y}}\right), \tag{4.13}$$

and $\mathbf{y} = \mathbf{r} - \mathbf{r}'$. Now, taking into account that for a dilute homogeneous system the chemical potential is $\mu = gn$ and that for the two-dimensional dipole-dipole interaction $F(\mathbf{k}) = F(-\mathbf{k})$, we finally arrive at the following expression for the Bogoliubov spectrum [83]

$$\epsilon(\mathbf{k}) = \sqrt{\frac{\hbar^2k^2}{2m}\left(\frac{\hbar^2k^2}{2m} + 2n(g + \pi k\lambda^2\cos 2\theta_{\mathbf{k}})\right)} \ , \tag{4.14}$$

where $\theta_{\mathbf{k}}$ is the angle formed by the momentum of the excitation and the x-axis.

The comparison between the Bogoliubov approximation given in this expression and the excitation spectrum obtained from DMC calculations using the Feynman approximation is shown in Fig. 4.5 for several values of the density and polarisation angle. We can see from the figure that, as expected, the Bogoliubov and Feynman approximations coincide at very

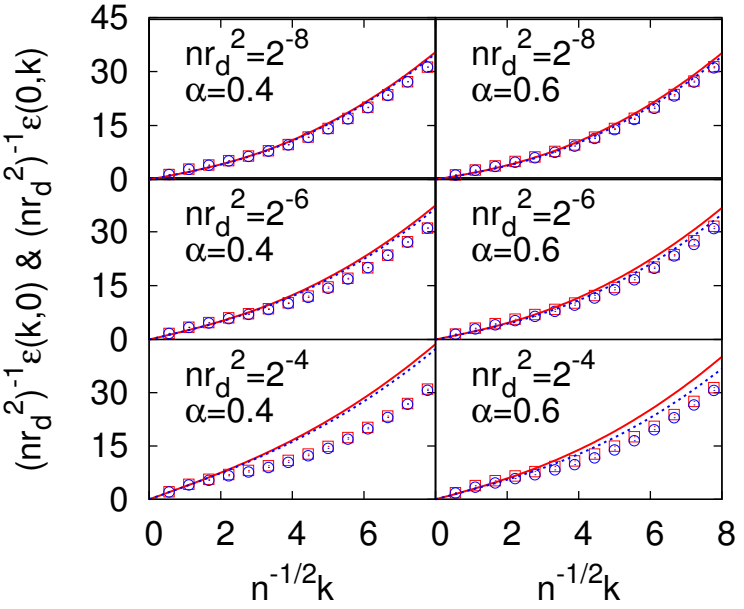

Figure 4.5: Comparison of Feynman (symbols) and Bogoliubov (lines) excitation spectrum for angles $\alpha = 0.4$ and $\alpha = 0.6$ and $nr_0^2 = 2^{-4}, 2^{-6}$ and 2^{-8}. Red solid and blue dashed curves show the two cuts $\epsilon(k, 0)$ and $\epsilon(0, k)$ corresponding to Bogoliubov approximation respectively. Red open squares and Blue open circles show $\epsilon(k, 0)$ and $\epsilon(0, k)$ corresponding to Feynman approximation respectively

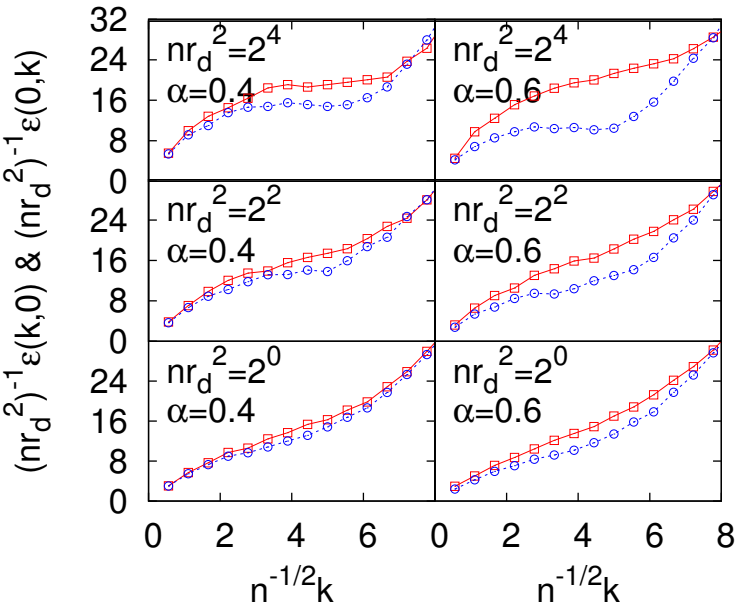

Figure 4.6: Feynman excitation spectrum for angles $\alpha = 0.4$ and $\alpha = 0.6$ for $nr_0^2 = 2^4, 2$ and 2^0. The red open squares and blue open circles show the two cuts $\epsilon(k, 0)$ and $\epsilon(0, k)$, respectively.

low densities. It is also noticeable the fact that, for a given value of the density, the Bogoliubov approximation is closer to the Feynman prediction at large polarisation angles. This stresses once again that the relevant quantity describing the low density dipolar Bose gas is the gas parameter $x = na^2$ that decreases with increasing polarisation angle. For a fixed density, x decreases when α increases, and the Feynman prediction gets closer to the Bogoliubov mode, which is know to successfully characterise the excitation spectrum of Bose gases when $x \to 0$. We can conclude from Fig. 4.5 that Feynman and Bogoliubov approximations are close to each other at small values of the momentum k. Finally, one also sees that the excitation spectrum becomes isotropic when $k \to 0$ indicating that the sound velocity of the system does not depend on the direction of the propagation.

Furthermore, the Bogoliubov approximation is expected to be valid only at very low densities while the Feynman approximation is known to provide an upper bound to the exact excitation spectrum of the system. To have some insight on how $\epsilon(\mathbf{k})$ evolves with the density we show in Figure 4.6 the Feynman mode at higher values of n. The results presented in the figure correspond to densities that are still far from the crystallisation point of the isotropic system [29, 30]. From Fig. 4.6, one can see that with increasing density the spectrum develops a roton-like minimum which for fixed density

and polarisation angle is deeper in the most repulsive direction. It is interesting to notice that as the anisotropy of the interaction is increased,i.e., when the polarisation angle grows, the roton minimum is deeper in the more repulsive direction while in the orthogonal direction the spectrum does not show any minimum in the range of considered densities. In fact, the emergence of the roton and its eventual zero-energy limit has been discussed as a clear signature of the instability of the system when the critical polarisation angle is higher than α_c [27, 86].

4.7 One body density matrix and condensate fraction

The last quantity analysed in this work is the one-body density matrix $\rho_1(\mathbf{r}_1, \mathbf{r}_1')$, which provides a measure of the overlap between two instances of the ground state wave function when one particle is shifted from its initial position at $\mathbf{r}_1$ to a new position at $\mathbf{r}_1'$

$$\rho_1(\mathbf{r}_1, \mathbf{r}_1') = N \frac{\int d\mathbf{r}_2 \cdots \mathbf{r}_N \Psi_0(\mathbf{r}_1, \mathbf{r}_2, \ldots, \mathbf{r}_N) \Psi_0(\mathbf{r}_1', \mathbf{r}_2, \ldots, \mathbf{r}_N)}{\int d\mathbf{r}_1 d\mathbf{r}_2 \cdots \mathbf{r}_N \Psi_0^2(\mathbf{r}_1, \mathbf{r}_2, \ldots, \mathbf{r}_N)} \ . \tag{4.15}$$

In the case of translationally invariant systems as the one under study, the one-body density matrix depends on its arguments only through their difference and thus $\rho_1(\mathbf{r}_1, \mathbf{r}_1') = \rho_1(\mathbf{r}_1 - \mathbf{r}_1', 0) \equiv \rho_1(\mathbf{r}_{11'})$ Additionally, if the interaction is isotropic, ρ_1 depends only on the magnitude of its argument $r_{11'} = |\mathbf{r}_{11'}|$ and its large-$r_{11'}$ limit measures directly the condensate fraction n_0 which is proportional to the number of particles in the Bose-Einstein condensate. In the present case, however, the system is homogeneous but not isotropic so $\rho_1(\mathbf{r}_{11'})$ will depend on the direction of $\mathbf{r}_{11'}$. Due to translational invariance, though, momentum is still a good quantum number and one expects condensation to appear at the zero momentum state. In that sense one can still write the relation between $\rho_1(\mathbf{r}_{11'})$ and the momentum distribution in the form

$$\rho_1(\mathbf{r}_{11'}) = \rho n_0 + \frac{1}{(2\pi)^2} \int d\mathbf{k}\, e^{i\mathbf{k}\mathbf{r}_{11'}} \tilde{n}(\mathbf{k}) \tag{4.16}$$

where $\tilde{n}(\mathbf{k})$ is the momentum distribution of the non-condensate atoms. The one-body density matrix of the anisotropic gas of Bose dipoles can be further expanded in partial waves

$$\rho_1(\mathbf{r}) = \sum_{m=0}^{\infty} \rho_{1m}(r) \cos(2m\,\theta) \ , \tag{4.17}$$

with $\rho_{1m}(r)$ the radial function corresponding to the m-th mode contribution. Notice that, as before, the Bose symmetry restricts the previous sum to even modes only.

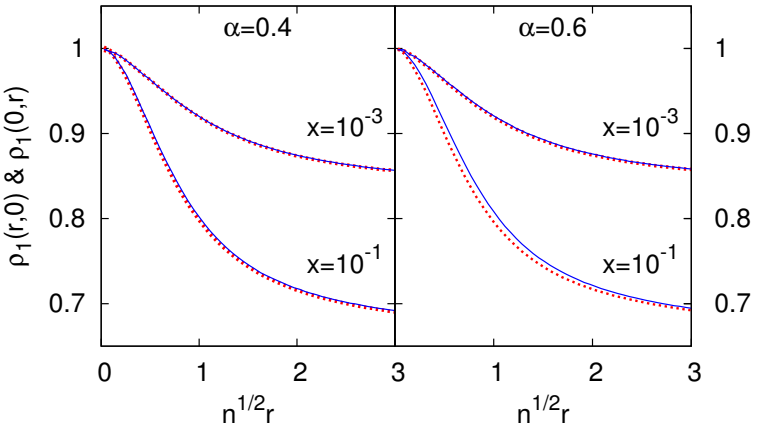

Figure 4.7: Cuts of the one-body density matrix along the x (red dotted lines) and y (blue lines) axes, for the gas parameter values $x = 10^{-3}$ and $x = 10^{-1}$ (top to bottom). The curves on the left and right panels correspond to $\alpha = 0.4$ and $\alpha = 0.6$, respectively.

Once enough modes $\rho_{1m}(r)$ are known, one can reconstruct the complete one-body density matrix for all points in the plane. In particular, the cuts along the two directions parallel and perpendicular to the polarisation plane, corresponding to $\theta = 0$ and $\pi/2$ in Eq. (4.17), turn out to be particularly easy to evaluate

$$\rho_1(r,0) = \sum_{m=0}^{\infty} \rho_{1m}(r) \quad , \quad \rho_1(0,r) = \sum_{m=0}^{\infty} (-1)^m \rho_{1m}(r) \tag{4.18}$$

and display the maximum difference two cuts along different directions can take at the low densities considered in this work.

Figure 4.7 shows the parallel and perpendicular cuts of $\rho_1(\mathbf{r})$ for the polarisation angles $\alpha = 0.4$ and $\alpha = 0.6$ (left and right panels). The upper and lower curves correspond to the gas parameter values $x = 10^{-3}$ and $x = 10^{-1}$, respectively. As before, the coordinates on the horizontal axis have been scaled with the density. Similarly to what happens to the other quantities analysed, only at the highest gas parameter values the effects of the anisotropy start to be visible. This stresses once again the minor role played by the anisotropy at low densities, even in a non-diagonal quantity like $\rho_1(\mathbf{r}_{11'})$.

The most significant differences in the one-body density matrix for different values of the gas parameter appear at large distances, where $\rho_1(\mathbf{r}_{11'})$ reaches an asymptotic value that can be identified with the condensate fraction n_0 in isotropic systems. When the anisotropic character of the interaction is taken into account, the presence of higher order partial waves in

Eqs. (4.17) and (4.18) could in principle change this behaviour, making the limiting value of $\rho_1(\mathbf{r}_{11'})$ depend on the direction. The role of the different partial waves in that limit can be determined by looking at the momentum distribution of the system, which can be obtained from $\rho_1(\mathbf{r}_{11'})$ by looking at the inverse of Eq. (4.16)

$$\begin{aligned}\tilde{n}(\mathbf{k}) = &\int_0^\infty dr\, r \int_0^{2\pi} d\theta e^{ikr\cos(\theta-\varphi)} \times \\ &\times \left[\Big(\rho_{10}(z) - \rho n_0\Big) + \sum_{m=1}^{\infty} \rho_{1m}(r)\cos(2m\theta) \right] ,\end{aligned} \tag{4.19}$$

with φ the angle formed by $\mathbf{k}$ and the x-axis. Changing variables $\alpha = \theta - \varphi$, using the Jacobi-Anger expansion of a plane wave in Bessel functions

$$e^{ikz\cos\alpha} = J_0(kz) + 2\sum_{m=1}^{\infty} i^m J_m(kz)\cos(m\alpha) \tag{4.20}$$

and taking into account the orthogonality of the cosine functions in the range $[0, 2\pi]$, one finally finds

$$\begin{aligned}\tilde{n}(\mathbf{k}) =& 2\pi \int_0^\infty J_0(kr)\Big(\rho_{10}(r) - n_0\Big) r dr + \\ &+ 2\pi \sum_{m=1}^{\infty} (-1)^m \cos(2m\varphi) \int_0^\infty J_{2m}(kr)\rho_{1m}(r)\, r dr\end{aligned} \tag{4.21}$$

where the first term on the right is isotropic and constitutes the $m = 0$ mode of $\tilde{n}(\mathbf{k})$, while the other terms stand for the $m > 0$ contributions. Notice once again that only even modes appear in this expansion.

Requiring $\tilde{n}(\mathbf{k})$ to be finite for all values of $\mathbf{k}$ implies all integrals appearing in Eq. (4.21) to be finite, a constraint that can only be fulfilled when the functions multiplying the Bessel functions decay to zero at large distances. This condition particularly means that n_0 can be obtained as the large r limit of the $m = 0$ mode of the one-body density matrix, which is the isotropic contribution to $\rho_1(\mathbf{r}_{11'})$. This is the direct generalisation of the usual procedure employed to determine n_0 in homogeneous and isotropic systems.

Figure 4.8 shows on the left panel the $m = 0$ mode contribution $\rho_{10}(r)$ for the three polarisation angles $\alpha = 0.2, 0.4$ and 0.6 in terms of the scaled distances $n^{1/2}r$ for $x = 0.1$. As can be seen from the figure, all three curves are hardly distinguishable, stressing once again that to a large extent the physics is governed by the scattering length, which makes the density change for different polarisation angles when x is fixed. The right panel in the figure shows the condensate fraction as a function of the gas parameter $x = na^2$, obtained from the $r \to \infty$ limit of a fit to the long range asymptotic limit

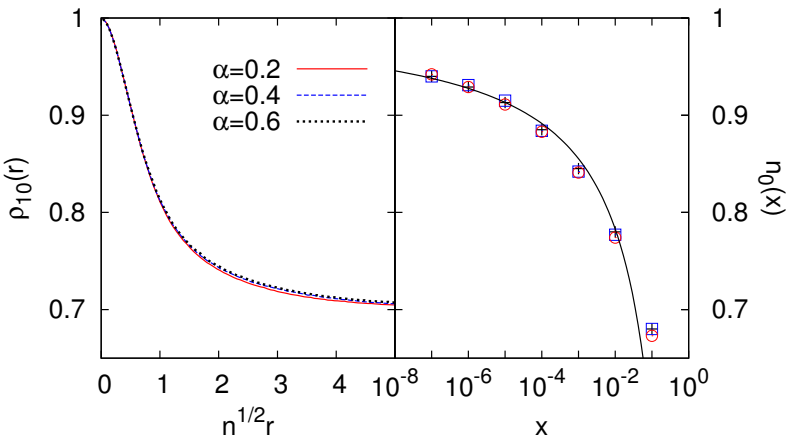

Figure 4.8: Left panel: isotropic ($m = 0$) contribution to the one-body density matrix at $x = 0.1$ for the three polarisation angles $\alpha = 0.2, 0.4$ and 0.6 (red solid, blue dashed and black dotted lines, respectively). Right panel: Condensate fraction n_0 as a function of the gas parameter for $\alpha = 0.2, 0.4$ and 0.6, compared with the Bogoliubov prediction (black line). The color coding for the symbols is the same as in the left panel.

of the $m = 0$ partial wave contribution of the one-body density matrix. Up to the highest value of x considered all three cases yield nearly the same prediction within statistical errors, while differences start to be significant only at $x \approx 0.1$. Therefore, the scaling on the gas parameter is preserved although moving from $\alpha = 0.2$ to $\alpha = 0.6$ for fixed x implies a change in density by almost a factor of 2. The figure also shows the Bogoliubov prediction for an isotropic gas of weakly interacting 2D bosons

$$n_0(x) = 1 - \frac{1}{|\ln x|} \tag{4.22}$$

which agrees reasonably well with the Monte Carlo prediction up to $x \approx 0.01$ where particle correlations seem to deplete the condensate less effectively than the mean field model.

4.8 Summary and Conclusions

To summarise, in this work we have described the ground state properties of a gas of fully polarised Bose dipoles moving on the XY plane, where the polarisation field forms an angle α with the normal direction. The projection of the polarisation vector on the XY plane defines the x-axis, where the potential is softer than in any other direction. In this context, the dipole-dipole interaction defines a critical angle $\alpha_c \approx 0.615$ where the potential starts to

have attractive contributions. We have solved the zero energy two-body scattering problem by means of a Green's function and a decomposition of the wave function in partial waves. We have then found the dependence of the s-wave scattering length on the polarisation angle by inspection of the $m = 0$ mode, which dominates at large distances. Equipped with the two-body solution, we have built a variational wave function of the Jastrow type that has been used as a guiding function in a DMC simulation of the gas of polarised dipoles at low densities. We have found that the scaling of the energy in the gas parameter is preserved up to values of x where other isotropic systems deviate significantly. This behaviour extends to other relevant ground state quantities like the pair distribution function, the static structure factor and the one-body density matrix, including the condensate fraction which can be determined from the large distance asymptotic behaviour of its isotropic part.

Chapter 5

Phase diagram of the anisotropic two dimensional dipolar system

5.1 Introduction

In the previous section we have analysed the behaviour of the anisotropic boson gas of dipoles in two dimensions at low densities and we have seen that the anisotropy in the interaction does not influence significantly neither the equation of state nor the structural properties of the system. In that case the equation of state can be well approximated by the mean-field approach using the scattering length of the anisotropic dipolar potential. In this section we want to study the behaviour of the strongly interacting dipolar gas where the anisotropy of the interaction will play a crucial role in the structure of the system and particularly in its phase diagram.

In order to study accurately the properties of the two dimensional dipolar Bose gas at high densities we have used a different approach than in the low density regime. As we have seen in the previous section, the wave function of the many-body system at low densities can be well approximated by means of a Jastrow wave function built on the zero-energy scattering solution of the two-body Schrödinger equation. Unfortunately, this simple ansatz does not work anymore at higher densities where the many-body system strongly interacts and the two-body scattering properties are no longer relevant in determining the macroscopic behaviour of the dipolar gas. For this reason it is difficult to use the diffusion Monte Carlo method to study the high density dipolar system properly. This difficulty is related to the necessity of a reasonable trial wave function for guiding the diffusion process, task which is not easy in the high density anisotropic system as the one we are interested in.

It is important to note that the fundamental reason to not use diffusion

Monte Carlo in this situation is the bias introduced by the guiding wave function in the evaluation of any observable that does not commute with the Hamiltonian of the system (mainly the pair correlation function and the static structure factor). We have used the path integral ground state method (PIGS) to study the high density dipolar gas. PIGS has a very important advantage over DMC in situations where a reliable approximation of the wave function of the system is not available, because the a priori knowledge of the wave function is much less important than in DMC. In fact, the guiding (or trial) wave function will only influence the speed of convergence in a PIGS simulation, i. e. the convergence of the results will be faster for a good trial wave function.

We are mainly interested in the study of the phase diagram of the two dimensional dipolar Bose gas with an anisotropic interaction between the particles of the system. It is known that in the isotropic case ($\alpha = 0$) the two-dimensional system shows a phase transition between gas and crystal phases at high density ($nr_0^2 \approx 290$) [29, 30]. In our situation, we have two parameters that can influence the phase diagram: the density and the tilting angle of the dipolar momenta of the particles respect to the orthogonal direction to the plane. As we have seen before, the tilting angle of the dipolar momenta causes that the interaction strength decreases in the direction of the projection of the dipole moments in the plane, as we will see in the present chapter this anisotropy enriches the phase diagram of the system.

5.2 Numerical approach to the high density two dimensional dipolar gas

The numerical study of the high density dipolar gas is performed by means of the path integral ground state method (PIGS), that allows us to obtain unbiased estimations for the physical observables that we used to characterise the macroscopic phase of the system. As we have seen in previous chapters of this work, the PIGS method works by propagating an initial trial wave function (that is introduced as an input in the simulation procedure) in imaginary time in order to wipe out all the non ground state contributions to the wave function of the system.

For the analysis of this problem we chose a standard Jastrow wave function of the form

$$\Psi_T(\mathbf{r}_1, ..., \mathbf{r}_N) = \prod_{i<j} f(\mathbf{r}_{i,j}) \tag{5.1}$$

where the two body correlation factor is given by

$$f(\mathbf{r}_{ij}) = \begin{cases} AK_0\left(\frac{2}{\sqrt{r}}\right) & \text{if } r \leq R_M \\ B\exp\left(-\left(\frac{C}{r} + \frac{C}{L-r}\right)\right) & \text{if } r > R_M \end{cases}, \tag{5.2}$$

with K_0 the modified Bessel function of the second kind and zero order. In the two body correlation factor (5.2) we distinguish between two different regions. At small distances the correlation factor corresponds to the solution of the zero-energy Schrödinger equation for two dipoles in two dimensions with zero tilting angle ($\alpha = 0$). At large distances, the correlation factor is a symmetrized form of the phononic long range part of the wave function in a two dimensional system [76]. The parameter L is the length of the simulation box (that will be determined by the density and the number of particles in the simulation) and the constants A, B and C are determined by imposing the following two conditions:

- The two body correlation and its first derivative must be continuous at the matching distance R_M.
- The two body correlation value at the edge of the simulation box is $f(L/2) = 1$.

Finally the parameter R_M it is chosen by minimising the variational energy of the many body system.

We notice that the phononic part of the wave function is introduced in a symmetrized form to ensure that $f'(L/2) = 0$. This is a generally required condition in any Monte Carlo simulation in order to guarantee that the contribution to the kinetic energy vanishes at distances larger than $\frac{L}{2}$.

In order to give a description of the full phase diagram we need a systematic method to identify the macroscopic state of the system and to characterise the transitions between the different phases. A commonly used method for this puspose is to use the static structure factor ($S(\mathbf{k})$) of the system [30]. It is known that the static structure factor in a crystal phase must show Bragg peaks for $\mathbf{k}$ values corresponding to the nodes of the reciprocal lattice of the system, contrarily, there is no such Bragg peaks in the gas phase. In the thermodynamic limit these Bragg peaks are delta peaks, but in a system with a finite number of particles this is no longer true. For a finite size system in a crystalline phase one can see that these Bragg peaks grow linearly with the number of particles, i. e. $S(\mathbf{k}_{Peak}) \propto N$, this fact gives us a method to distinguish a gas phase where there are no Bragg peaks in the structure factor ($\frac{S(\mathbf{k}_{Peak})}{N_P} \to 0$ if $N_P \to \infty$) and an ordered phase ($\frac{S(\mathbf{k}_{Peak})}{N} \to$ constant if $N \to \infty$). Therefore, we can extract information about the long range ordering of the particles of the system using the strength of the peaks of the static structure factor as the order parameter of the system. Moreover, this is a quantity that can be easily evaluated in the PIGS simulation without any kind of bias coming from the chosen trial wave function.

In the following sections, we will show the results obtained by the numerical study of the phase diagram of the system. First we will provide a description of the transition from the gas phase to the crystal that happens

at high densities ($nr_0^2 \geq 290$) and values of the tilting angle $0 \leq \alpha \lesssim 0.45$. After analysing the crystallisation of the system, we will study the transition from the gas phase to the stripe phase, that occurs for values of the tilting angle $\alpha \gtrsim 0.45$, and finally we will study the crystal to stripe phase transition, that happens at high densities ($nr_0^2 \gtrsim 420$) and large tilting angles ($\alpha \gtrsim 0.45$).

5.3 Gas - Crystalline solid phase transition

The fully isotropic ($\alpha = 0.0$) dipolar Bose gas present a first order phase transition from a gas phase to a crystal at high densities [29, 30]. In the crystal phase the particles of the system are arranged on the nodes of a triangular lattice, the spatial configuration that minimises the potential energy in two dimensions. Along this section we will see how the anisotropy of the interaction potential influences the crystallisation of the system.

The characterisation of the crystal phase of the system using PIGS is done in a different way that using diffusion Monte Carlo. In the DMC analysis we must use two different trial wave functions: a Jastrow wave function for the gas phase and a Nosanov-Jastrow function, that includes the localisation of the particles in the lattice, for the crystal phase. In the PIGS study we only have used the Jastrow wave function (5.2). In the PIGS simulation, we start the calculation from a perfect crystal configuration in a triangular lattice and let the system relax under the path integral algorithm. When the stationary state of the Monte Carlo sampling is achieved, the system will be in its ground state and the crystalline ordering can be broken if it is not the preferred configuration under the given conditions.

The dipolar interaction is no longer isotropic if the tilting angle of the dipolar momenta is non-zero, so one can expect that the crystal lattice of the system reflects the anisotropy of the interparticle potential showing an elongation in the direction where dipolar interaction is stronger (the y-axis in our model). In order to study the deformation of the lattice we need to generalise the initial crystalline configuration of the system.

The positions of the particles in a crystalline lattice can be generated using

$$\mathbf{r} = n_1\mathbf{a}_1 + n_2\mathbf{a}_2 \tag{5.3}$$

where $\mathbf{a}_1$ and $\mathbf{a}_2$ are the primitive vectors of the Bravais lattice considered. For a perfect triangular lattice the primitive vectors are:

$$\mathbf{a}_1 = a\hat{\imath} \tag{5.4}$$

$$\mathbf{a}_2 = a\left(\frac{1}{2}\hat{\imath} + \frac{\sqrt{3}}{2}\hat{\jmath}\right) \tag{5.5}$$

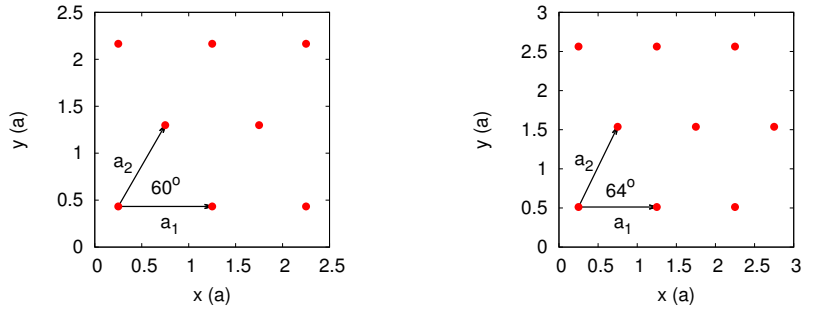

(a) Perfect triangular lattice (b) Deformed triangular lattice

Figure 5.1: Comparison between the perfect triangular lattice that represents the crystalline phase of the two dimensional system of dipoles with tilting angle equal to zero (a) and the deformed triangular lattice that is elongated in the direction where the general anisotropic dipolar potential is stronger (b).

a being the lattice spacing, that will be directly related with the system density in our simulation.

In the general situation we consider a deformed triangular lattice where it is allowed that the primitive vectors have different modulus. Specifically we consider primitive vectors that does not form an angle of 60^o, this can be easily done by supposing that the vectors that generates the lattice are given by:

$$\mathbf{a}_1 = a\hat{\imath} \tag{5.6}$$

$$\mathbf{a}_2 = a\left(\frac{1}{2}\hat{\imath} + \frac{\tan\beta}{2}\hat{\jmath}\right) \tag{5.7}$$

In this case we have two lattice parameters, the distance between particles along the x-axis, given by a, and the oblique distance given by $\frac{a}{2}\sqrt{1+\tan^2\beta}$. β is the angle between the two primitive vectors $\mathbf{a}_1$ and $\mathbf{a}_2$. In figure 5.1 it is shown a comparison between the perfect triangular lattice and the deformed lattice with an angle $\beta = 64^0$.

Solid state theory tells us that the static structure factor $S(\mathbf{k})$ in the solid phase must show Bragg peaks for $\mathbf{k}$ values corresponding to the nodes of the reciprocal lattice. For a general triangular lattice in two dimensions the primitive vectors of the reciprocal lattice are simply obtained by considering that if $\mathbf{b}_1$ and $\mathbf{b}_2$ are the vectors that generate the reciprocal lattice, they must verify the following relation:

$$\mathbf{a}_i \cdot \mathbf{b}_j = 2\pi\delta_{ij} \tag{5.8}$$

that means that reciprocal lattice's primitive vectors are orthogonal to the

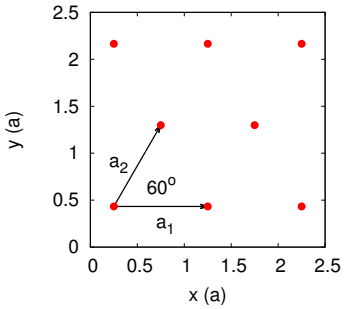

(a) Perfect triangular lattice.

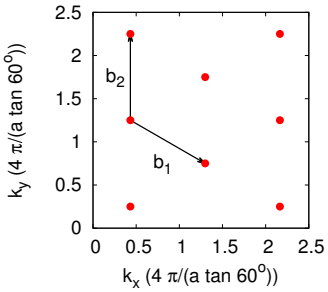

(b) Reciprocal lattice of a perfect triangular lattice.

Figure 5.2: Comparison between the perfect triangular lattice that represents the crystalline phase of the two dimensional system of dipoles with tilting angle equal to zero (a) and the corresponding reciprocal lattice (b).

primitive vectors of the crystalline lattice. This relation gives us the following pair of vectors:

$$\mathbf{b}_1 = \frac{2\pi}{a\tan\beta}\left(\tan\beta\hat{\imath} - \hat{\jmath}\right) \tag{5.9}$$

$$\mathbf{b}_2 = \frac{4\pi}{a\tan\beta}\hat{\jmath} \tag{5.10}$$

In figure 5.2 we show the direct and reciprocal lattice for a perfect triangular lattice. In order to determine the deformation of the lattice for each value of the tilting angle we have analysed the stability of the crystalline phase, i. e., we performed PIGS simulations for several values of the deformation angle and then we have chosen the lattice that melts at lower density.

As we have commented in the previous section we will use the strength of the main peak of the static structure factor as the order parameter of the phase transition, and, given that the transition between gas and crystal phases is first order we expect that the order parameter changes in a non-continuous way. As a test of this statement we have revisited the fully isotropic two dimensional dipolar system using our PIGS simulation. In figure 5.3 we show the static structure factor for an isotropic two-dimensional dipolar Bose system for the gas (left panel) and crystal phases (right panel). One can see a large difference in the strength of the peak: in both figures there is a clear peak in $S(\mathbf{k})$, the difference between both situations is that in the gas phase the strength of the peak does not increase when the number of particles is increased in the simulation while in the crystal phase there is an enhancement when the number of particles is increased.

We have used the isotropic ($\alpha = 0$) dipolar gas as a test of the method to determine the phase of the system and characterise the phase transition

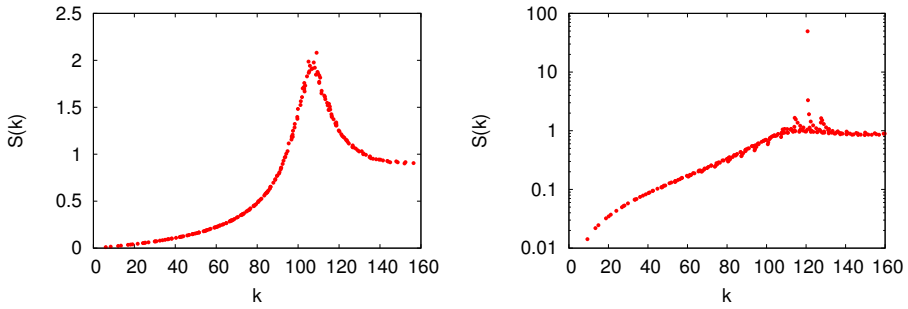

(a) Static structure factor for the two dimensional dipolar gas at density $nr_0^2 = 260$ and tilting angle $\alpha = 0$.

(b) Static structure factor for the two dimensional dipolar gas at density $nr_0^2 = 320$ and tilting angle $\alpha = 0$.

Figure 5.3: Comparison between the static structure factor of the isotropic ($\alpha = 0$) dipolar gas in gas phase (left panel) and solid phase (right panel).

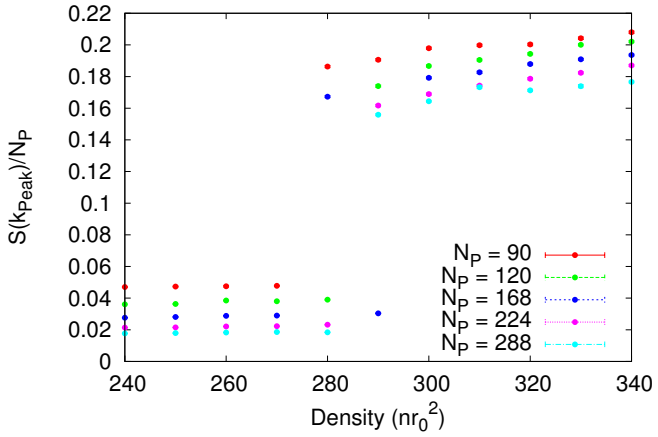

Figure 5.4: Evolution of the order parameter $S(\mathbf{k}_{Peak})/N_P$ with the density for different number of particles in a two dimensional dipolar system with tilting angle $\alpha = 0.0$.

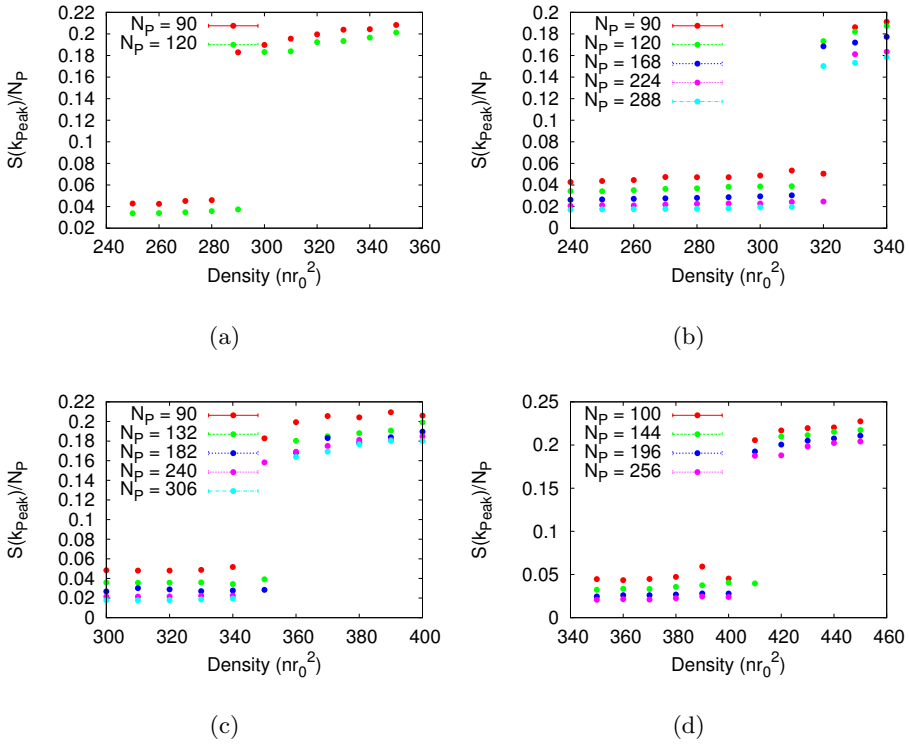

Figure 5.5: Evolution of the order parameter of the system for several tilting angles: (a) $\alpha = 0.1$, (b) $\alpha = 0.2$, (c) $\alpha = 0.3$ and (d) $\alpha = 0.4$.

between the gas and crystal phases. In figure 5.4 we show the dependence of the order parameter $(S(\mathbf{k}_{Peak})/N_P)$ for different system sizes. We can see in the figure that for the isotropic situation the order parameter shows a clear discontinuity at a density $nr_0^2 \approx 280$ for all the system sizes analysed. These results are in good agreement with the studies in Refs. [29, 30] and indicate the existence of a first-order phase transition in the system.

The anisotropic dipolar interaction has a weaker strength as the tilting angle of the dipoles increases. Therefore, additionally to the elongation of the crystalline lattice, the crystallisation density it is also larger for larger tilting angles. In figure 5.5 we show the evolution of the order parameter in terms of the density for several values of the tilting angle $(\alpha = 0.1, 0.2, 0.3, 0.4)$ and different system sizes. One can see that the discontinuity in the order parameter is nearly independent of the system size for all α values.

We can also see that the number of particles influences the order parameter by reducing its value, in agreement with the expected behaviour of the

α	β	n_c
0.0	60°	280(20)
0.1	60°	290(20)
0.2	60°	320(20)
0.3	62°	350(20)
0.4	64°	410(20)

Table 5.1: Results for the crystallisation density (n_c) and the deformation angle of the lattice (β) for the two dimensional dipolar system in terms of the tilting angle (α).

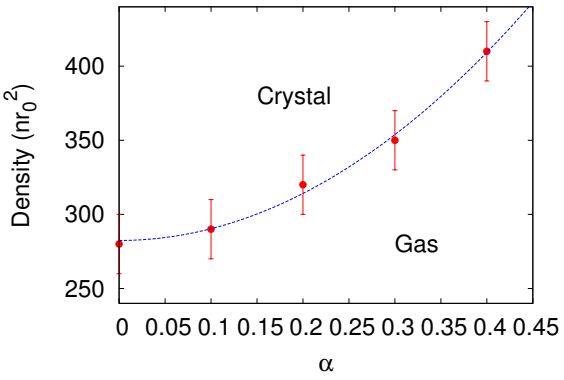

Figure 5.6: Crystallisation curve.

order parameter in the thermodynamic limit is given by:

$$\lim_{N_P\to\infty} \frac{S(\mathbf{k}_{Peak})}{N_P} = \begin{cases} 0 & \text{if } n < n_c \\ \text{Constant} & \text{if } n > n_c \end{cases} \tag{5.11}$$

In Table 5.1, we show the results of the Monte Carlo study of the crystallisation transition of the system. It can be seen that the lattice shows an increasing elongation in the y-direction that is the direction where the interaction is stiffer. At low tilting angles the crystalline lattice does not show a significant deviation from the perfect triangular lattice, while for large tilts there is a difference that can be resolved using our simulation method.

As a final comment on the gas - crystal phase transition we may note that, being a first order phase transition, must have two relevant density values: the freezing and melting densities. However, our numerical study does not have enough resolution to evaluate separately these quantities. The obtained results allows us to find a crystallisation curve of the system in the parameter space (n, α). In figure 5.6 we show the results obtained for the

gas - crystal transition of the two dimensional dipolar system. We also show a fit to the data of the form

$$n_c(\alpha) = a + b \sin^2 \alpha. \tag{5.12}$$

that gives an approximate crystallisation density of the system in the range of densities studied. The parameters obtained from the fit are $a = 281.75 \pm 2.76$ and $b = 836.41 \pm 34.38$.

5.4 Gas - Stripe phase transition

As we have seen in the previous section the tilt of the dipole moments of the particles introduces a new degree of freedom in the Hamiltonian that strongly influences the high density behaviour of the system. In the previous sections we have considered relatively large tilting angles, but quite far from the critical value that makes the system collapse ($\alpha \approx 0.61$). In this section, we want to study the large tilting angle regime of the system, and the consequences of the high degree of anisotropy of the dipole - dipole interaction in the phase diagram.

There are several previous approaches to this gas - stripe phase transition in the context of Fermi dipolar gases in two dimensions using mean field and other analytical techniques [34, 35, 36], or even in a bilayer configuration [37]. Those studies on Fermi dipolar gases predict the emergence of a density wave in the system along the direction where the dipolar potential is stronger. The development of this density wave is related with the strength of the interaction (the analogous quantity in our work is the density of the system) and the value of the tilting angle. The most interesting point of those studies is the prediction that the density wave phase (stripe phase in the following) appears even in the isotropic ($\alpha = 0$) situation if the strength of the interaction is large enough. However, a recent Monte Carlo study of the isotropic two-dimensional Fermi gas at large densities seems to indicate that the stripe phase is not energetically favourable, independently of the strength of the interaction [32]. Concerning bosonic systems, this stripe phase has been recently found in numerical calculations using Monte Carlo methods in homogeneous [87] and trapped systems [38], but only in the regime of large tilting angles and high densities.

In a dipolar Bose gas the stripe phase is a clear consequence of the high degree of anisotropy of the interaction. When the tilting angle is close to the critical angle the interaction is extremely soft in the direction of the projection of the dipolar moments in the plane (x-direction) while, in the orthogonal direction (y-direction), there is no reduction of the stiffness of the potential. This fact implies that it is easy for the particles to be tightly confined in well localised stripes parallel to the x-axis, but with a certain freedom to move inside each stripe, so particles in a stripe can move along the

stripe itself. Thus, one clear signature of this stripe phase is the emergence of spatial long range order in the system, but only in the direction of maximum strength of the potential.

As in the previous section we used the static structure factor to characterise the phase of the system. Due to he existence of long range order in the system $S(\mathbf{k})$ must present a strong peak (a "Bragg-like" peak) in the y-direction but not in any other. $S(\mathbf{k})$ can show also some structure in the x-direction but it must be completely different from the peak that we can find in a crystal, in the sense that this peak in the x-direction does not grow with the number of particles and therefore it is not a Bragg peak. With these considerations we can conclude that the overall behaviour of the order parameter of the system is similar to the gas - crystal transition. We have a disordered phase where the order parameter is very small (the gas phase) and an ordered one that has a non-vanishing order parameter (the stripe phase).

From the static structure factor one can evaluate the excitation spectrum of the system in the Feynman approximation, given by

$$\epsilon(\mathbf{k}) = \frac{\hbar^2}{2mS(\mathbf{k})}, \tag{5.13}$$

that is an upper bound of the exact excitation spectrum of the system. It is known that the excitation spectrum of the dipolar Bose gas shows a deep roton-like minimum at high densities, but in our situation it is interesting to study what is the behaviour of this roton as the tilting angle is increased and the interactions become highly anisotropic. In Figure 5.7, we can see the evolution of the Feynman excitation spectrum of the system in the x and y directions as the tilting angle is increased. It can be seen that the roton minimum in the y direction becomes deeper as the tilting angle grows and eventually it will touch zero. When this happens the system has two different states with the same energy, which means that the ground state of the system becomes degenerate. Another interesting point is that this new ground state has non zero momentum, which means that it is a standing wave in the y direction, corresponding to the stripe phase.

Using correlated basis function theory the full dynamic structure factor $S(\mathbf{k}, E)$ can be evaluated in an perturbative way. We are interested in the dependence of $S(\mathbf{k}, E)$ on the polarization angle α and, for a given $\alpha > 0$, its dependence on the direction of $\mathbf{k}$. In Fig. 5.8, we show $S(\mathbf{k}, E)$ for $n = 128$ and $\alpha = 0.20; 0.50; 0.58$ in order to illustrate the evolution from an isotropic to an anisotropic excitation spectrum and the approach to the stability limit. The wave vector $\mathbf{k}$ is pointing in the y and x-direction (i.e. the direction of strongest and weakest interaction) in the left and right panels. Also shown is the Feynman approximation of the spectrum (solid line).

For $\alpha = 0.20$ the dispersion is almost independent on the direction of $\mathbf{k}$, with only a slight slope of the Pitaevskii plateau [88], which for isotropic

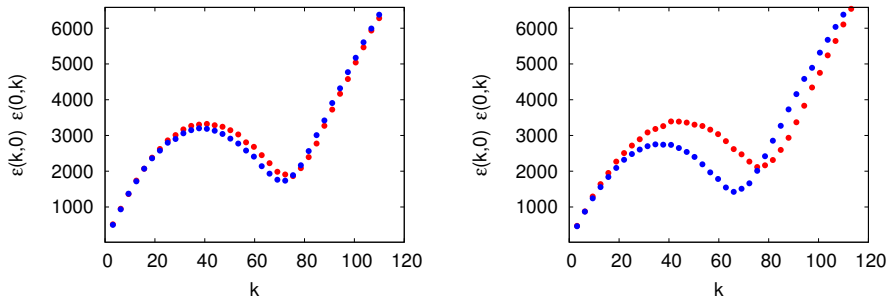

(a) $\alpha = 0.20$.

(b) $\alpha = 0.40$.

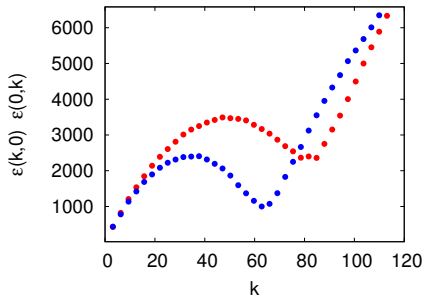

(c) $\alpha = 0.50$.

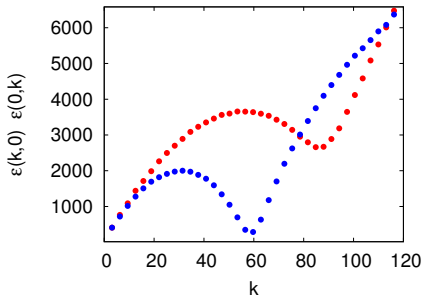

(d) $\alpha = 0.58$.

Figure 5.7: Feynman excitation spectrum for density $nr_0^2 = 128$ and different values of the tilting angle. Blue symbols correspond to the cut $\epsilon(0, k)$ and red symbols to the orthogonal direction $\epsilon(k, 0)$.

systems denotes the sudden onset of damping at twice the roton energy due to decay into two rotons. As α is increased, $S(\mathbf{k}, E)$ becomes very different in the y- and x-direction and features a highly anisotropic dispersion relation for $\alpha = 0.58$. The wave number of the roton depends on the direction of $\mathbf{k}$, but most strikingly its energy decays almost to zero in the y-direction for $\alpha = 0.58$, indicating that the system is close to the limit where the homogeneous gas phase in unstable against infinitesimal density fluctuations. Since the restriction to pair correlation fluctuations used here typically gives an upper bound to the excitation energy [89], the exact roton energy in y-direction is expected to be even smaller. Furthermore, at twice the wave number of the roton, $S(\mathbf{k}, E)$ has another roton-like peak for $\alpha = 0.58$, following a quadratic dispersion, albeit broadened and with smaller spectral weight. In the y-direction, the dispersion relation thus resembles that of a solid, continued beyond the first Brillouin zone. While for $n = 128$ and $\alpha = 0.58$ the system is still in the gas phase, our PIGS results presented below indeed predict a stripe phase at even higher density.

The dotted lines in Fig. 5.8 depict the damping limit $E_c(\mathbf{k})$ above which decay into two excitations of lower energy is kinematically allowed, hence excitations below $E_c(\mathbf{k})$ have infinite lifetime corresponding to peaks in $S(\mathbf{k}, E)$ with zero linewidth. The kinematics of an anisotropic dispersion is different from the isotropic case, as evidenced e.g. by the lack of a constant Pitaevskii plateau. The decay into two rotons is very efficient in an isotropic system because of the high density of states at the roton energy. For the anisotropic phonon-roton dispersion, the roton energy depends on the direction of $\mathbf{k}$, thus the roton energies are spread out leading to a smoother density of states than in the isotropic limit. For example, decay of the maxon in the y-direction is not allowed, although its energy is higher than twice the roton energy.

We have done a similar analysis to that of the gas - crystal phase transition, i. e. we have evaluated the static structure factor and have found a strong peak in the y-direction, that can be used to characterise the ordering of the system. We show some of the obtained results in figure 5.9.

The first main difference between the behaviour of the order parameter in this situation respect to the gas - crystal case is that in this situation the change from the disordered to ordered phases is done in a continuous way, this fact indicating that we are facing a different kind of phase transition: in this case, a second-order phase transition. Besides the continuity in the transition between the two phases, second-order phase transitions are characterised by the strong dependence of the physical quantities of the system on its size. Near a second-order phase transition the correlation length (ξ) of the fluctuations in the magnitudes of the system is divergent in the thermodynamic limit, indicating that near the transition point the system becomes invariant under scale transformations and has no characteristic length scales. The behaviour of the correlation length of the system

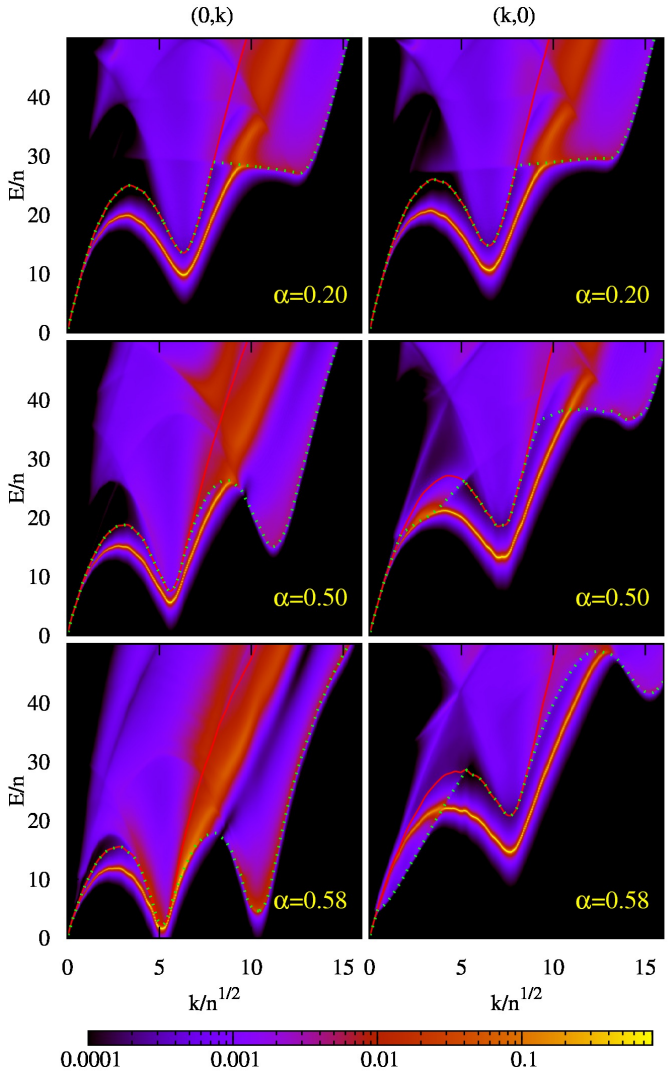

Figure 5.8: $S(\mathbf{k}, E)$ for $\mathbf{k} = (0, k)$ (left panels) and $(k, 0)$ (right panels) for polarization angles $\alpha = 0.20; 0.50; 0.58$ at density $n = 128$. The spectrum in Feynman approximation is shown as a solid line, and the dotted line denotes the damping limit $E_c(\mathbf{k})$.

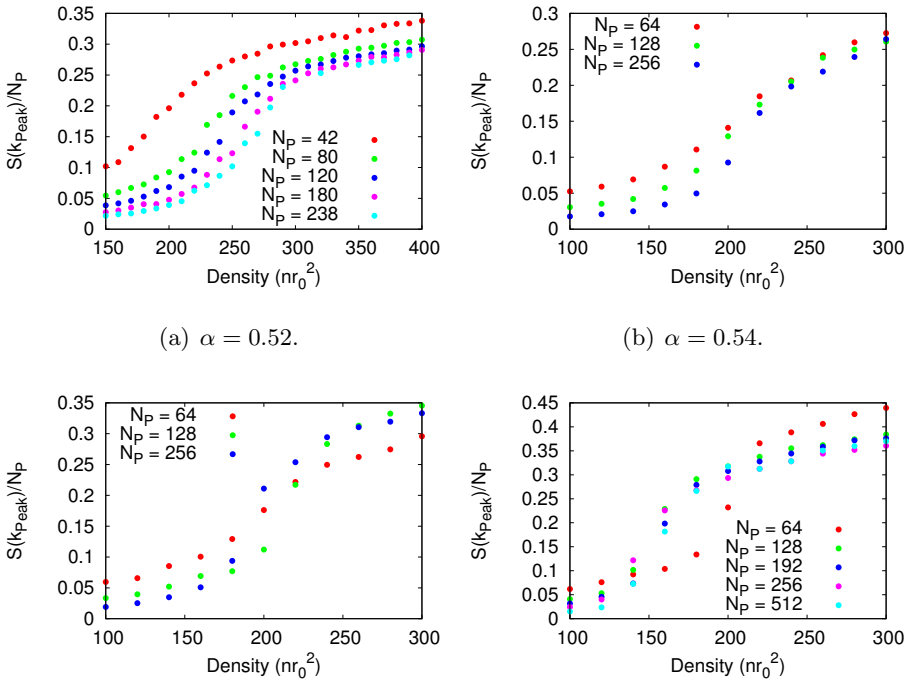

(a) $\alpha = 0.52$.

(b) $\alpha = 0.54$.

(c) $\alpha = 0.56$.

(d) $\alpha = 0.58$.

Figure 5.9: Order parameter variation in terms of the density of the system for different tilting angles and different system sizes.

in a second-order phase transition is given by [90]

$$\xi(t) \sim t^{-\nu}, \tag{5.14}$$

where ν is one of the critical exponents of the system and t is the reduced density given by:

$$t \equiv \frac{n - n_C}{n_C}. \tag{5.15}$$

The behaviour of the order parameter close to a second order phase transition is given also in terms of a critical exponent usually called β, so near the phase transition we have

$$\eta \sim \begin{cases} (-t)^{\beta} & \text{if } t < 0 \\ 0 & \text{if } t > 0 \end{cases}. \tag{5.16}$$

These relations are only valid for a system in the thermodynamic limit. In the case of a finite-size system, as the one used in Monte Carlo simulations, is, of course, not possible to have an infinite correlation length because the use of periodic boundary conditions forces that all physical quantities are evaluated within the limits of the simulation box. When the correlation length is $\xi \sim L$ the system is effectively ordered and the correlations are of infinite range. L is the size of the simulation box, determined by the density of the system and the number of particles used in the PIGS simulation.

In order to give a proper description of a second-order phase transition it is usual to apply the finite-size scaling, which is a method based on the homogeneity properties of the thermodynamic functions of the system and, from these properties, to define the corresponding functions for the finite size system. This relation allows us to do the reverse road and to study the behaviour of the order parameter in terms of the size of the system.

The order parameter η is defined as before:

$$\eta \equiv \frac{S(\mathbf{k}_{Peak})}{N_P}. \tag{5.17}$$

But in this case we use the peak that emerges in the direction where the dipolar interaction is stronger, the y direction. The scaled form of the order parameter of the system can be written as [90]:

$$\eta_L(t) = L^{-\beta/\nu}\tilde{\eta}(L^{1/\nu}t) \tag{5.18}$$

where η_L is the order parameter for the system of size L, and β and ν are the critical exponents of the order parameter and the correlation length respectively. $\tilde{\eta}$ is the scaling function for the order parameter, which is constructed to be independent of the system size, but strongly dependent on the parameters t, ν and β. If the correct values for the parameters are

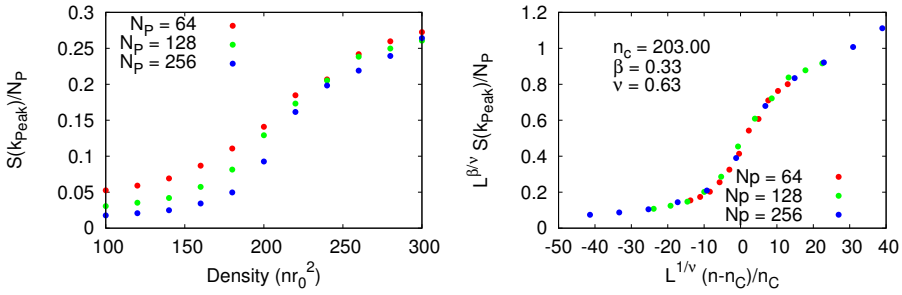

(a) Order parameter in terms of the density for $\alpha = 0.54$.

(b) Scaled order parameter in terms of the reduced density for $\alpha = 0.54$.

Figure 5.10: Collapse of the curves corresponding to the order parameter of the system with $\alpha = 0.54$ for different number of particles under a scaling transformation.

chosen, the data obtained for different system sizes will collapse onto a single curve.

In figures 5.10 and 5.11 we show the scaling of the PIGS data under the application of the relation (5.18) for $\alpha = 0.54$ and $\alpha = 0.58$ respectively. It can be seen in both examples the collapse of the different curves corresponding to different sizes of the system to a single scale invariant curve that corresponds to the function $\tilde{\eta}$ in equation (5.18). The accuracy of the collapse of the curves for different number of particles allows us to give a good estimation for the critical density of the gas - stripe phase transition and also for the values of the critical exponents that describe the behaviour of the thermodynamic variables near the transition point.

The first interesting result provided by the finite size scaling study of the system is that the values of the critical exponents do not show a significant dependence with the tilting angle of the system within the accuracy of our results. The values of the critical exponents are related with the broken symmetry of the transition and, for the gas - stripe phase transition the symmetry breaking does not depend on the value of the tilting angle if the tilting angle exceeds a threshold value of $\alpha_{th} \sim 0.45$. The only relevant parameter that controls the behaviour of the system is the density of the system, or equivalently the strength of the interaction since we are working in dimensionless units.

The second important result given by the finite size analysis concerns the values of the critical exponents obtained. The numerical values of the critical exponents are compatible with various known universality classes, namely the 3D Ising and 3D XY model universality classes. It is known that the critical behaviour of a quantum system in d dimensions it is equiv-

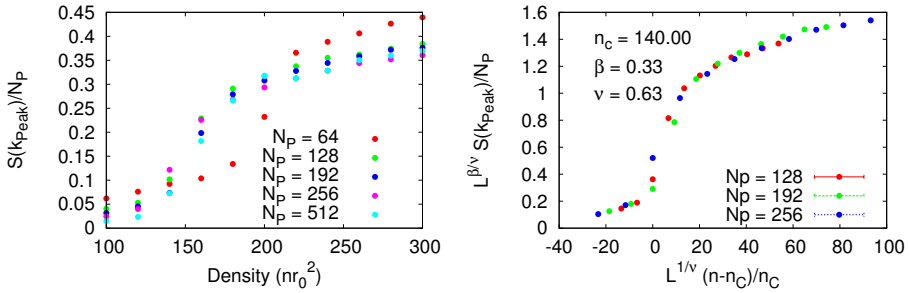

(a) Order parameter in terms of the density for $\alpha = 0.58$.

(b) Scaled order parameter in terms of the reduced density for $\alpha = 0.58$.

Figure 5.11: Collapse of the curves corresponding to the order parameter of the system with $\alpha = 0.58$ for different number of particles under a scaling transformation.

α	n_c
0.52	260(20)
0.54	205(20)
0.56	160(20)
0.58	140(20)
0.60	125(20)

Table 5.2: Critical density of the gas - stripe transition in terms of the tilting angle.

alent to the behaviour of the same classical system in $d+1$ dimensions [91]. Unfortunately the accuracy of the obtained results is not high enough to distinguish the universality class. However, in this situation the symmetry breaking of the phase transition is $U(1)/Z_2$ which means that the critical exponents must be in the 3D Ising universality class.

From the finite-size scaling analysis of the PIGS results for several tilting angles we can write the transition curve for the gas - stripe transition in the parameter space (nr_0^2, α). The critical density of the transition is given in table 5.2 in terms of the tilting angle.

Using the data in table 5.2 we can plot the critical density transition curve in terms of the tilting angle, in figure 5.12 we show the numerical evaluated data and a fit to that data of the form:

$$n_c(\alpha) = n_0 + a \sin^2(\alpha - \alpha_0). \tag{5.19}$$

The results obtained for the coefficients of the fit are the following $n_0 = 125.59 \pm 3.70$, $a = 18750 \pm 2113$ and $\alpha_0 = 0.6047 \pm 0.0052$. It can be

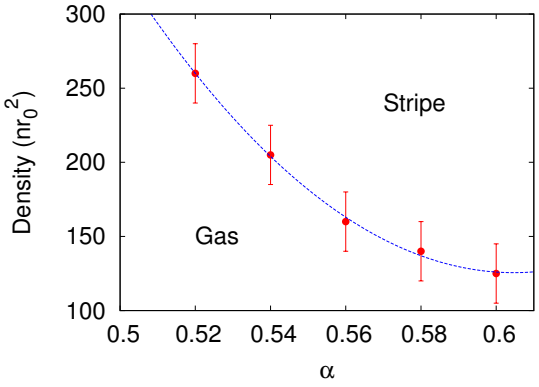

Figure 5.12: Gas to stripe phase transition curve in terms of the density and the tilting angle of the dipole moments of the system.

observed from the figure that another interesting point involving the stripe phase is that its emergence requires a minimum density and tilting angle of the dipoles. For low densities we have not observed any kind of ordering of the system, it stays on gas phase for all values of tilting angles up to the collapse limit.

5.5 Crystal - Stripe phase transition

In this section we present the last part of the study of the phase diagram of the two dimensional system of bosonic dipoles, the high density and high tilting angle regime. The main interest of this region of the parameter space is obviously the study of the transition between the stripe and crystal phases and its properties. This regime is the most difficult to analyse due to the extremely high densities involved and the limitations of the simulation methods used in this work. In two dimensions the dipole-dipole interaction is short ranged (this is different of three dimensions where the dipolar interaction is long ranged and therefore requires specific techniques to perform a numerical simulation), but it is near the limit of long range interactions. This fact implies that the approximations involved in our Monte Carlo simulation become less accurate as the density is increased, requiring the use of much larger system sizes to describe properly the physics of the dipolar system. But working with a large number of particles in a PIGS simulation implies that the evolution and relaxation of the system is slower and then we need a much longer computation time in order to equilibrate the system to obtain reliable results for the physical observables of interest.

Another problem that we have to address to study the crystal - stripe phase transition is that the criterion to distinguish between phases that we

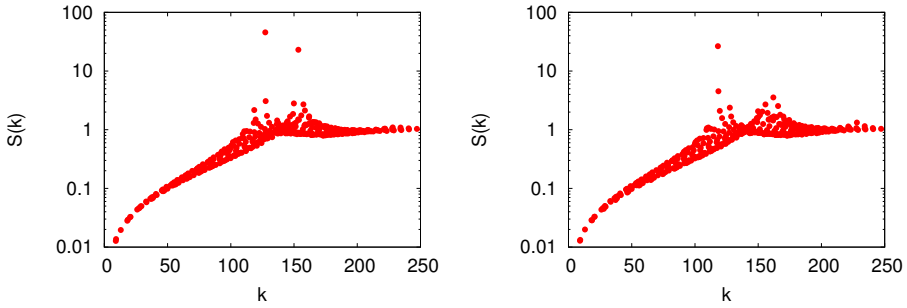

(a) Structure factor for density $nr_0^2 = 450$ and tilting angle $\alpha = 0.48$.

(b) Structure factor for density $nr_0^2 = 450$ and tilting angle $\alpha = 0.48125$.

Figure 5.13: Static structure factor of the high density dipolar system at a density $nr_0^2 = 450$ for two different tilting angles. The case (a) corresponds to the crystal phase while the (b) situation corresponds to the stripe phase.

have used in the previous sections cannot be used in this situation. As we have seen the transitions from a disordered phase to a ordered one can be well described using the largest peak of $S(\mathbf{k})$ as the order parameter of the transition. This is not possible in this situation because we are facing a transition between two ordered phases, so we must find a different order parameter that allows us to distinguish the two different phases. In order to do that it is convenient to evaluate the full static structure factor $S(k_x, k_y)$ that contains all the information about the ordering of the particles of the system. If we consider the structure factor for a two dimensional crystalline solid, as the one depicted in figure 5.2, it is obvious that it shows Bragg peaks for each $\mathbf{k}$ value that corresponds to a node of the reciprocal lattice, so in the situation of the figure $S(\mathbf{k})$ will have a Bragg peak in the y direction and another one in the oblique direction. The structure factor for a stripe phase will be different in the sense that it has only a peak in the y direction. So the criterion to distinguish between the solid and stripe phase involves the emergence of a second peak in the structure factor.

In order to describe the phase transition between the crystal and the stripe phase we performed PIGS simulations with slightly different tilting angles for each value of the density and we have determined through the analysis of the peak structure of $S(k_x, k_y)$ the tilting angle that makes the system lose crystalline order. In figures 5.13 and 5.14 we show the change in the structure factor for two different values of the density, $nr_0^2 = 450$ for $\alpha = 0.48$ and $\alpha = 0.48125$ in figure 5.13 and $nr_0^2 = 550$ for $\alpha = 0.483$ and $\alpha = 0.485$ in figure 5.13 . It is evident from these figures that the second peak of the structure factor in the solid situation ((a) panel in both figures) disappears by slightly increasing the tilting angle, indicating the loss

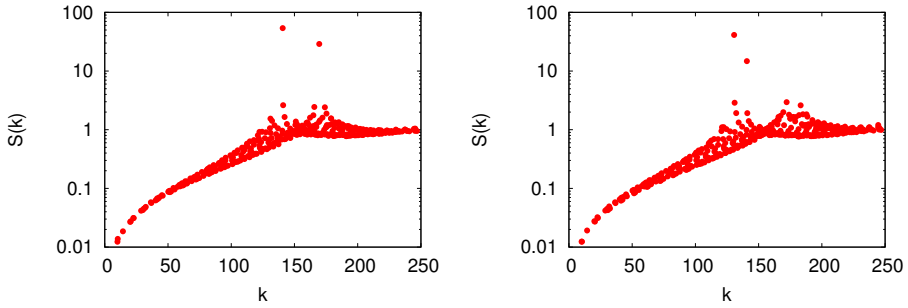

(a) Structure factor for density $nr_0^2 = 550$ and tilting angle $\alpha = 0.483$.

(b) Structure factor for density $nr_0^2 = 550$ and tilting angle $\alpha = 0.485$.

Figure 5.14: Static structure factor of the high density dipolar system at a density $nr_0^2 = 550$ for two different tilting angles. The case (a) corresponds to the crystal phase while the (b) situation corresponds to the stripe phase.

n	α_c
450	0.4806(1)
480	0.4819(1)
500	0.4819(1)
550	0.4838(1)

Table 5.3: Critical tilting angle for the crystal to stripe phase transition in terms of the density of the system.

of crystalline order in the system and the emergence of the stripe phase.

An obvious question that we must answer about the crystal to stripe phase transition is about the order of the transition, as we have seen in the previous sections the gas to stripe transition is second order while the gas to crystal transition is first order. In the present case we have not seen a smooth decay of the second peak of the static structure factor by increasing the tilt of the dipoles, contrarily, as we have shown the second crystalline Bragg peak sudden disappears as we make a little variation of the tilting angle indicating that the crystal to stripe phase transition is probably first order. In spite of this argument, a definite conclusion would require a more careful analysis due to the technical problems that we have commented previously. By looking for the loss of crystalline order for several densities we can evaluate the crystal to stripe phase transition tilting angles in terms of the density of the system. Table 5.3 summarises the results that we have obtained from our simulations. In figure 5.15, we show the transition curve. From the figure it can be shown that the slope of the curve is very large. This fact implies that if the tilting angle is larger than $\alpha \sim 0.47$ the stability

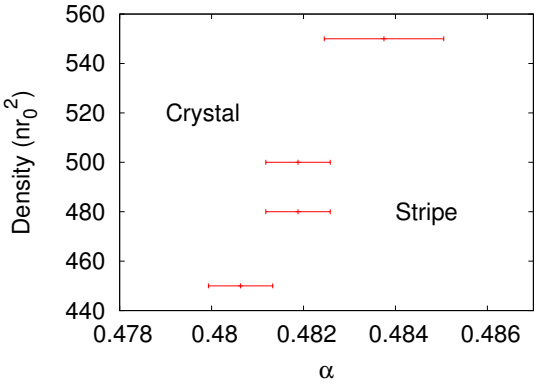

Figure 5.15: Crystal to stripe phase transition curve in terms of the density and the tilting angle of the dipole moments of the system.

of the crystalline phase requires extremely high density.

5.6 Summary and conclusions

In this chapter we have studied the phase diagram of the two dimensional system of bosonic dipoles with a non zero tilting angle. Figure 5.16 summarises the results obtained in this work. As we can see from the figure, at low densities the system is in the gas phase. When the density is increased and the tilting angle is below $\alpha \sim 0.45$ the system undergoes a first order phase transition between the gas and crystal phases. The anisotropy of the interaction influences the shape of the crystal lattice of the system by elongating the interparticle distance in the direction where the dipole - dipole potential is larger. If the density is between the crystallisation density of the isotropic ($\alpha = 0.0$) system and a threshold density of $n_{th} r_0^2 \sim 125$ the system shows a second order phase transition between the gas and the stripe phase. Interestingly, the critical exponents of this second order transition are nearly independent of the tilting angle and are compatible with the 3D Ising and 3D XY model universality classes within the statistical uncertainty of our simulations. An accurate numerical determination of the universality class of the gas - stripe phase transition would require a more accurate evaluation of the order parameter of the system and probably the use of larger systems than the ones used along this work. Finally, at high densities and large tilting angles the system shows a first order phase transition between the crystal and stripe phases. The slope of this transition curve is extremely large indicating that, due to the anisotropy of the interaction, the crystal phase of the system is no longer stable if the dipole - dipole potential is highly anisotropic.

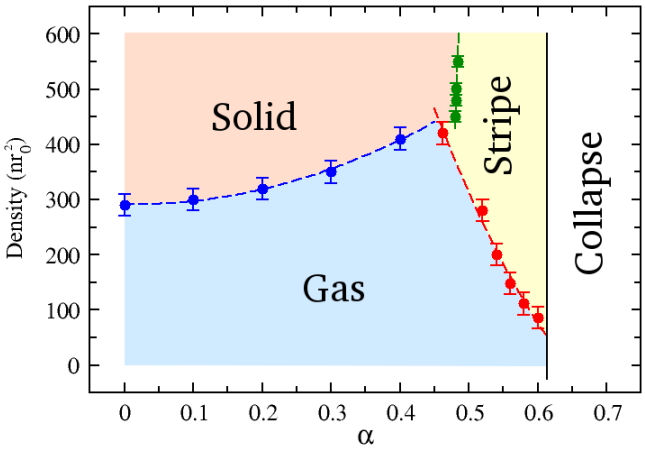

Figure 5.16: Phase diagram for the two dimensional system of anisotropic bosonic dipoles obtained from PIGS simulations.

Chapter 6

Bosonic dipolar gas in a bilayer configuration

6.1 Introduction

A configuration where the anisotropy of the dipole - dipole interaction becomes crucial in the physical properties of the system is the dipolar gas in a bilayer configuration. We consider an homogeneous distribution of bosonic dipoles confined by an external potential in two parallel two dimensional layers separated by a distance h as it is shown in Figure 6.1.

The general dipole - dipole potential when we consider the two - body interaction between particles in different layers reduces to the following form

$$V_{Inter}(r) = \frac{C_{dd}}{4\pi} \frac{r^2 - 2h^2}{(r^2 + h^2)^{5/2}}. \tag{6.1}$$

This form of the dipolar interaction, contrarily to the interaction between tilted dipoles in a single two dimensional layer, has axial symmetry. In this situation the interaction shows an azimuthal anisotropy which means that the interaction between particles in different layers is different that the interaction between particles in the same layer and shows an strong dependence with the separation between the layers h.

The inter-layer potential shows an attractive well for values of the in-plane distance $r < r_0\sqrt{2}h$. At large distances, the potential has a repulsive long range tail of the form $V_{Inter}(r) \sim r^{-3}$. Between these two limiting distances there is a potential barrier whose height is proportional to h^{-3} for a distance $r = 2h$. With all this information about the inter-layer interaction potential we can conclude that its shape is strongly dependent on the inter-layer distance, as we can see in the right panel of Figure 6.2. It can be seen from the figure that the attractive region is deeper and narrower for small values of h while the potential is flatter at low values of the inter-layer distance.

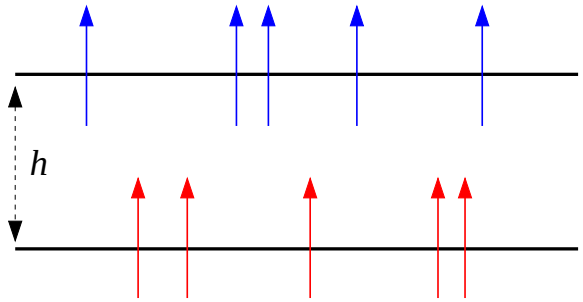

Figure 6.1: Dipoles in two paralel layers separated by a distance h.

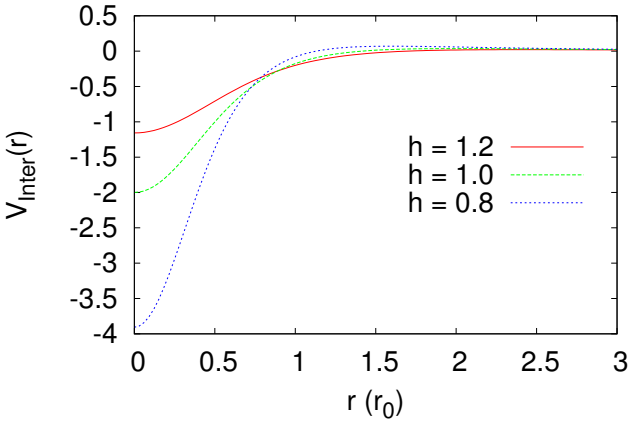

Figure 6.2: Dipole - dipole interaction between particles in different layers for several values of the inter-layer distance h.

For particles being in the same layer the interaction is the usual two dimensional isotropic dipolar interaction given by

$$V_{Intra}(r) = \frac{C_{dd}}{4\pi}\frac{1}{r^3}. \tag{6.2}$$

Due to the presence of inter-layer and intra-layer interactions there are also two different effects that compete in the system. On one side, the attractive region of the inter-layer interaction tries to pair particles in different layers. On the other side, the repulsive part of the inter-layer interaction and the fully repulsive intralayer interaction prevents the dimerization of the system. The relative importance of these two effects at fixed density is only determined by the inter-layer distance that allows us to control the strength of the inter-layer interaction.

We model the many - body system by considering N dipolar bosons in

two planes separated by a distance h; the particles are equally distributed between the two layers with a density n on each of them. We also consider that the confinement of the dipoles in the layers is strong enough to suppress the tunnelling between them, so the number of particles on each layer remains fixed. The Hamiltonian of such a system is given by:

$$\begin{aligned} H = &- \frac{\hbar^2}{2m}\sum_{i=1}^{N/2}\nabla_i^2 - \frac{\hbar^2}{2m}\sum_{\alpha=1}^{N/2}\nabla_\alpha^2 \\ &+ \sum_{i<j}\frac{C_{dd}}{4\pi}\frac{1}{r_{ij}^3} + \sum_{\alpha<\beta}\frac{C_{dd}}{4\pi}\frac{1}{r_{\alpha\beta}^3} + \sum_{i,\alpha}\frac{C_{dd}}{4\pi}\frac{(r_{i\alpha}^2 - 2h^2)}{(r_{i\alpha}^2 + h^2)^{5/2}}, \end{aligned} \tag{6.3}$$

where Latin (i, j) and Greek (α, β) indexes refer to particles on top and bottom layers respectively. Here, $r_{ij(\alpha\beta)} = |\mathbf{r}_{i(\alpha)} - \mathbf{r}_{j(\beta)}|$ denotes the in-plane distance between pairs of particles in the top (bottom) layer, and $r_{\alpha i} = |\mathbf{r}_\alpha - \mathbf{r}_i|$ is the distance between the projections onto any of the layers of the positions of the α-th and i-th particle.

In the rest of the present chapter we will analyse the physics of the bilayer system of dipoles. We will study the two body problem of dipoles in different layers that, as we will see, always show a bound state. We will use the two body solution for inter-layer and intralayer interaction to build a many-body wave function that contains the key ingredients for the physics of the system and finally we use this many-body wave function to perform Monte Carlo simulations and evaluate physical observables that can help us to clarify the physical behaviour of the system.

6.2 Two body problem for the inter-layer potential

It is a well known fact that any attractive potential in two dimensions, $V(r)$ that verifies

$$\int_{\mathcal{R}^2} V(r)d\mathbf{r} < 0, \tag{6.4}$$

supports at least one bound state [93, 94] with a binding energy that can be approximated by:

$$E_B \sim \exp\left[\frac{4\pi}{\int_{\mathcal{R}^2} V(r)d\mathbf{r}}\right] \tag{6.5}$$

The inter-layer interaction however, does not verify (6.4), instead it belongs to the special family of potentials that verify

$$\int_{\mathcal{R}^2} V_{Inter}(r)d\mathbf{r} = 0 \tag{6.6}$$

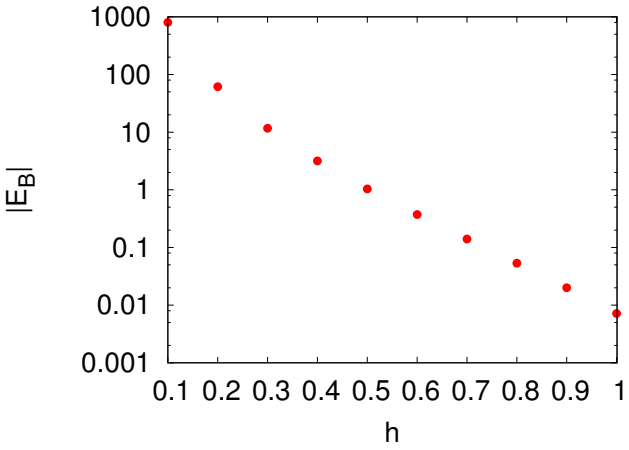

Figure 6.3: Binding energy of the ground state of inter-layer two dipole problem in terms of the distance between layers h.

In [93] it is shown that such a potential also present a bound state whose binding energy can be approximated by the expression:

$$E_B \sim -\exp\left(\frac{1}{c}\left(\frac{4\pi\hbar^2 h}{mC_{dd}}\right)^2\right) \tag{6.7}$$

with $c = -\frac{1}{8}$ [39]. However, this last expression is only valid for $h \to 0$ so in order to obtain accurate values for the binding energies we must solve the two body Schrödinger equation numerically. The Schrödinger equation for the two body inter-layer problem is given by

$$-\frac{\hbar^2}{2m}\nabla^2\psi + \frac{C_{dd}}{4\pi}\frac{r^2 - 2h^2}{(r^2+h^2)^{5/2}}\psi = E_b\psi. \tag{6.8}$$

In Figure 6.3 it is shown the absolute value of the energy for the lowest energy bound state of the system. It can be seen in the figure that the energy shows an exponential dependence with the inter-layer potential.

In the following sections we will show how the physics of the system is affected by the existence of the two body bound state between particles in different layers.

6.3 Numerical solution of the many body problem

The many body problem of quantum dipoles in a bilayer configuration has been addressed using different techniques. One of the first attempts to describe the phase diagram for a system of bosons is given in [46]. Interest

has been also devoted to the study of the bilayer system of fermionic dipoles [41, 42]. In the case of fermionic dipoles it is known that the existence of the attractive inter layer interaction makes the system undergo a BCS-BEC crossover and therefore it exhibits pair superfluidity for strong inter-layer interaction. In the bosonic situation there is a phase transition between two atomic superfluids for weak interactions (large h values) and a molecular superfluid at small values of h.

In order to give an accurate description of the physics of the bilayer dipolar system we have performed Monte Carlo simulations at zero temperature using the diffusion Monte Carlo method. As we have seen in previous chapters a central element in a DMC simulation is the many body wave function that must be used to improve the accuracy and to accelerate the convergence of the numerical calculation.

In order to describe the phase transition of the system we have chosen a many body wave function that has the following properties:

- The many body wave function is symmetric if we exchange the position of two particles in the same layer.
- The many body wave function is symmetric under the exchange of the two layers, i. e. this means that we can permute the upper and lower layers and the physics of the system is the same.
- The many body wave function is symmetric under the exchange of a pair of particles in different layers.

All these properties are a consequence of the bosonic symmetry. Having into account all these requirements our variational guess for the wave function of the system is [95]:

$$\Psi_T^{\text{pair}}(\mathbf{r}_1,\ldots,\mathbf{r}_N) = \prod_{i<j} f_1(r_{ij}) \prod_{\alpha<\beta} f_1(r_{\alpha\beta}) \times \\ \times \left(\prod_{i=1}^{N/2} \sum_{\alpha=1}^{N/2} f_2(r_{i\alpha}) + \prod_{\alpha=1}^{N/2} \sum_{i=1}^{N/2} f_2(r_{i\alpha}) \right),$$

where, again, Latin (i, j) and Greek (α, β) indexes refer to particles on top and bottom layers respectively. The two body correlation factor for particles in the same layer, $f_1(r)$, is given by

$$f(\mathbf{r}_{ij}) = \begin{cases} AK_0\left(\frac{2}{\sqrt{r}}\right) & \text{if } r \leq R_M \\ B\exp\left(-\left(\frac{C}{r}+\frac{C}{L-r}\right)\right) & \text{if } r > R_M \end{cases}. \tag{6.9}$$

while the two body correlation factor for particles in different layers, $f_2(r)$, is

$$f_2(r) = \exp\left(-\frac{ar^2}{1+br}\right). \tag{6.10}$$

a, b and R_M are free parameters that must be determined variationally while A, B and C are determined using the continuity conditions of the intralayer two - body wave function at $r = R_M$. The structure of the many - body wave function strongly favours the emergence of a bound state between pairs of particles in different layers and, at the same time, it is flexible enough to allow the system to break the dimers for an accurate choice of the variational parameters.

6.4 Qualitative description of the phase diagram

As we have commented in the previous section, the system of bosonic dipoles in a bilayer configuration undergoes a quantum phase transition between a dimer (or molecular) superfluid for small values of the inter-layer distance and another phase consisting in two coupled superfluids at large values of h. The phase transition is modulated by the strength of the dipolar inter-layer interaction.

A qualitative description of the physics of the system can be done by analysing the behaviour of the many - body wave function and the two - body physics of the system. The binding energy of the inter - layer bound state depends, as we have also seen, exponentially with the inter - layer distance. A rough estimation of the size (or typical length) of this bound state can be obtained by considering the following approximation for the bound state wave function:

$$\phi(r) \sim e^{-\sqrt{\frac{m|E_B|}{\hbar^2}}r} \tag{6.11}$$

where the bound state energy is, of course, negative. From this approximate wave function we can estimate the typical size of the bound state as:

$$r_B \sim \sqrt{\frac{\hbar^2}{m|E_B|}} \tag{6.12}$$

Additionally, we have another typical length scale that defines the many - body physics of the system: the length scale associated with the density of particles on each layer which is given by:

$$r_0 \sim \frac{1}{n^{1/2}} \tag{6.13}$$

It is clear that the physics of the system is strongly influenced by the these two length scales or, more precisely, by the competition between both length scales.

Having the two relevant length scales in our system we can distinguish three different situations:

- $r_B << r_0$

  In this situation the physics of the system is completely dominated by the interaction between particles in different layers. This strong interaction causes the dimerization of the system. The separation between dimers will be $\sim r_0$, much larger than the typical size of a dimer and, therefore, the energy of the collisions between dimers is much lower than the energy required to break a dimer.

  In this limit we can obtain a simple approximation to the interaction between dipoles in the system by considering the complete interaction between two pairs of particles as:

$$U(r) = 2\frac{C_{dd}}{4\pi}\frac{1}{r^3} + 2\frac{C_{dd}}{4\pi}\frac{r^2 - 2h^2}{(r^2+h^2)^{5/2}}. \tag{6.14}$$

  The distance between layers h will be much smaller that the typical distance between particles because we are studying the situation where the inter-layer interaction is very strong. With this consideration we can safely consider the limit $h \to 0$ to obtain the approximate interaction between dimers:

$$U(r) \sim 4\frac{C_{dd}}{4\pi}\frac{1}{r^3} \tag{6.15}$$

  So in this regime we expect that the bilayer dipolar system behaves as a single layer dipolar gas of particles with $\tilde{d} = 2d$, $\tilde{m} = 2m$ and density $\tilde{n} = \frac{n}{2}$, which implies an effective dipolar length $\tilde{r}_0 = 8r_0$.

  We can also consider what the trial wave function of the system (6.9) tells us in this regime. The two Jastrow terms corresponding to particles on the same layer are independent of the strength of the inter - layer interaction. The term involving particles on different layers will try to form dimers between particles on the up and down layers, and the size of these dimers is very small because the binding energy is very large. In this situation there is no overlap between the two body wave functions for the different possible pairs of particles in the system, and the many body wave function can be approximated by:

$$\Psi_T^{\text{pair}}(\mathbf{r}_1, \ldots, \mathbf{r}_N) = \prod_{i<j} f_1(r_{ij}) \prod_{\alpha<\beta} f_1(r_{\alpha\beta}) \times \prod_{i=\alpha=1}^{N/2} f_2(r_{i\alpha}) \tag{6.16}$$

  This many body wave function is only symmetric under the exchange of a pair of particles in different layers (one of them in the up layer and the other in the down layer), so we can see that due to the strength of the inter - layer interaction we have lost the symmetry under the exchange of a single particle in one of the layers of the system. The

change on the symmetry implies that in this regime the system can only present a Bose - Einstein condensation of dimers, which means that the system can exhibit pair superfluidity but without showing single layer superfluidity.

- $r_B >> r_0$

  When the size of the bound state of the inter - layer interaction is much larger than the typical distance between particles in the same layer we can consider that the correlation between layers is very small. We have seen in a previous section that the inter - layer dipole - dipole potential supports always a bound state independently of the strength of the interaction. However, in this regime the binding energy of the bound state will be exponentially small and any collision will break any eventual dimer.

  In this limitting situation the size of the bound state increases exponentially and the two - body wave function $f_2(r)$ in (6.9) can be safely approximated by $f_2(r) \sim 1$. In this situation the wave function Ψ_T has all the symmetry properties that we have shown in the previous section, but, no correlations between particles in different layers are negligible. In this regime, the system may present single layer superfluidity but there is no pair superfluidity.

- $r_B \sim r_0$

  This is the most interesting situation in the physical study of the bilayer dipolar system. For this range of the parameters the physics of the system is no longer dominated by one of the interactions. Contrarily, in this case both interactions play a crucial role in the behaviour of the system.

  We have an inter-layer interaction that is strong enough to allow for the existence of dimers and we have also a intra-layer interaction causing collisions between dimers that are strong enough to allow the exchange of one of the particles of a dimer. In this regime we can not make any kind of simplification on the wave function of the system, so we have to consider the full Ψ_T given in (6.9). According to the form and the symmetries of the wave function, the system can exhibit simultaneously pair and single layer superfluidity.

In the following sections we will present the results of the numerical simulations that we have performed for the bilayer dipolar system and we will show that there are some results that may indicate a second order quantum phase transition between a pair superfluid phase (with no single layer superfluidity) and another phase that exhibits pair superfluidity and single

layer superfluidity simultaneously. We have found from our simulations that Bose condensation of pairs seems to vanish as the strength of the inter - layer interaction is reduced.

6.5 Equation of state of the bilayer dipolar gas

In this section we will present the results of the Monte Carlo simulations for the energy per particle of the system in terms of the inter-layer distance for two different densities of the system. We have analysed a wide range of values of h that allows us to explore the two different regimes of the system (dimer and atomic superfluids) and also the transition between them.

We also want to compare the limiting cases $h \to 0$ and $h \to \infty$ with the dimerized dipolar gas and the atomic dipolar gas respectively. In the situation $h \to 0$ the energy of the bound state goes to $-\infty$ and the size of the bound state is exponentially small, in this situation the bilayer dipolar gas can be described using an equivalent single layer dipolar gas with an equivalent dipole moment $\tilde{d} = 2d$ and equivalent mass $\tilde{m} = 2m$ as we have seen in the previous section.

In order to obtain results for the equation of state that can be compared directly with the atomic dipolar gases equivalent of these cases we have evaluated the quantity $\frac{E}{N} - \frac{E_B}{2}$ where E_B is the energy of the bound state of the inter-layer potential. This subtraction allows us to extract the contribution to the energy per particle coming from the inter-layer interaction and allows us to study, mainly in the $h << r_0$ regime, the effective interaction between the bound pairs of particles.

In Figures 6.4 and 6.5 we show the results of the Monte Carlo simulations for the quantity $\frac{E}{N} - \frac{E_B}{2}$ at densities $n = 1.0$ and $n = 10^{-2}$ respectively in terms of the inter-layer distance h. Red symbols correspond to the results of the simulations extrapolated to the thermodynamic limit using the standard tail correction, assuming that the pair correlation function equals one for inter-particle distances larger than the size of the simulation box. We notice that E/N becomes negative when the inter-layer distance gets small enough and approaches the dimer binding energy in the limit $h << r_0$. An important remark is that in this regime the energy difference $\frac{E}{N} - \frac{E_B}{2}$ is found to be positive, indicating that dimers feel an effective repulsive interaction which stabilises the pair phase.

Pairing between dipoles is in fact a strong effect when $h << r_0$, forming tightly bound dimers which behave as composite objects featuring twice the mass and dipole moment as compared to single dipoles. The horizontal lines in figures 6.4 and 6.5 correspond to the energies per particle of a single layer of dipolar bosons with an effective interaction strength $\tilde{n}\tilde{r}_0^2$, as obtained using the results of [29], where $\tilde{n} = \frac{n}{2}$ and the dipolar length takes the two values $\tilde{r}_0 = r_0$ and $\tilde{r}_0 = 8r_0$. The first value corresponds to the limiting case

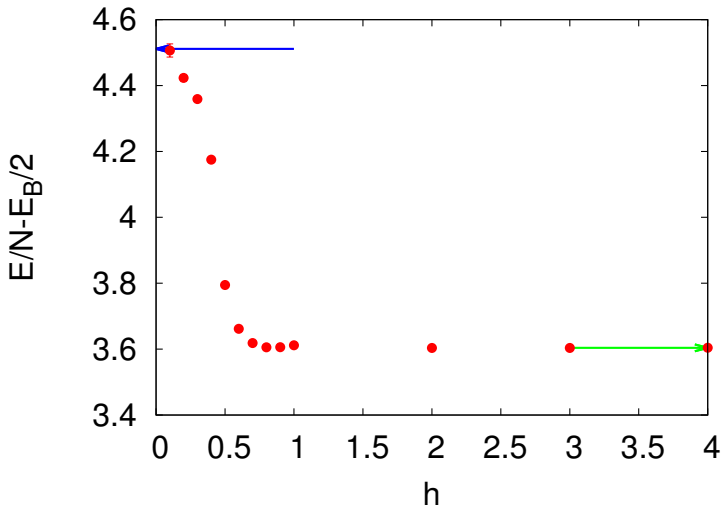

Figure 6.4: Energy per particle with half of the dimer binding energy subtracted as a function of the reduced inter-layer distance h/r_0 for $nr_0^2 = 1$. Red symbols correspond to the results obtained using the diffusion Monte Carlo simulations. The horizontal lines correspond to the energies of a single layer of dipoles with effective interaction strength $\tilde{n}\tilde{r}_0^2 = 0.5$ and $\tilde{n}\tilde{r}_0^2 = 32$

.

$h >> r_0$ of independent layers, whereas the second value refers to the opposite regime, $h << r_0$, where the system behaves as a single layer of particles having dipole moment $\tilde{d} = 2d$ and mass $\tilde{m} = 2m$ as have commented before.

6.6 Atomic and Dimer condensate fraction

After discussing the equation of state we analyse the one - body and two - body density matrices as a function of the inter-layer distance and, from their behaviours, the nature of the transition between atomic and dimerized superfluid regimes. The one - body density matrix within each layer is defined as usual

$$\rho_1(\mathbf{r}) = N \frac{\int \cdots \int \Psi^*(\mathbf{r}_1, \mathbf{r}_2, \cdots, \mathbf{r}_N)\Psi(\mathbf{r}_1 + \mathbf{r}, \mathbf{r}_2, \cdots, \mathbf{r}_N) d\mathbf{r}_2 \cdots d\mathbf{r}_N}{\int \cdots \int |\Psi(\mathbf{r}, \cdots, \mathbf{r}_N)|^2 d\mathbf{r}_1 \cdots d\mathbf{r}_N} \quad (6.17)$$

The relevant contribution to the two - body density matrix involves instead a pair of particles residing in different layers [96]

$$\rho_2(\mathbf{r}_1 + \mathbf{r}, \mathbf{r}_2 + \mathbf{r}; \mathbf{r}_1, \mathbf{r}_2) = N \frac{\int \cdots \int \Psi^*(\mathbf{r}_1, \mathbf{r}_2, \cdots, \mathbf{r}_N)\Psi(\mathbf{r}_1 + \mathbf{r}, \mathbf{r}_2 + \mathbf{r}, \cdots, \mathbf{r}_N) d\mathbf{r}_3 \cdots d\mathbf{r}_N}{\int \cdots \int |\Psi(\mathbf{r}, \cdots, \mathbf{r}_N)|^2 d\mathbf{r}_1 \cdots d\mathbf{r}_N} \quad (6.18)$$

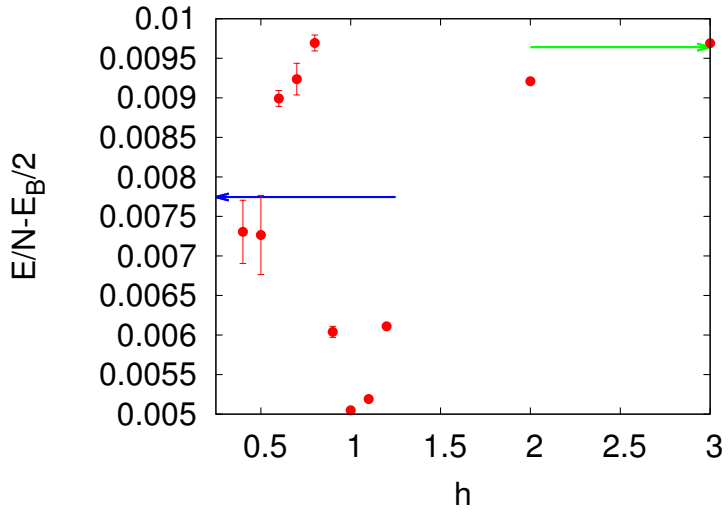

Figure 6.5: Energy per particle with half of the dimer binding energy subtracted as a function of the reduced inter-layer distance h/r_0 for $nr_0^2 = 10^{-2}$. Red symbols correspond to the results obtained using the diffusion Monte Carlo simulations. The horizontal lines correspond to the energies of a single layer of dipoles with effective interaction strength $\tilde{n}\tilde{r}_0^2 = 0.005$ and $\tilde{n}\tilde{r}_0^2 = 0.32$

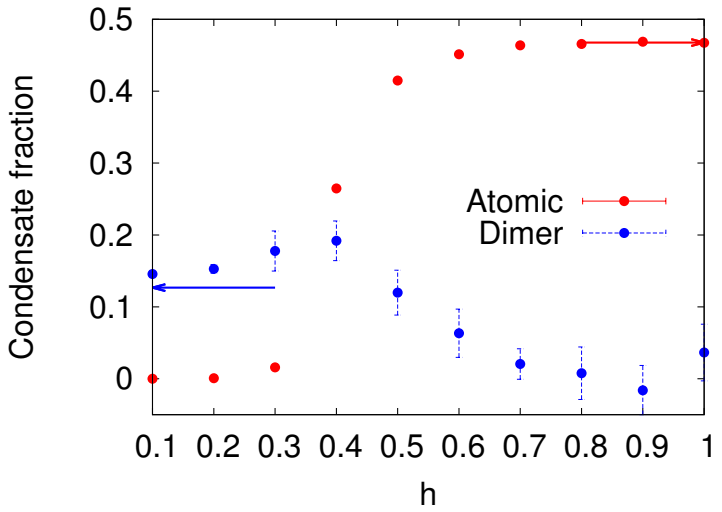

Figure 6.6: Atomic condensate n_0 and molecular condensate n_0^{mol} as a function of h/r_0 at the density $nr_0^2 = 1$. Arrows correspond to the condensate fraction of a single layer of dipoles at the effective interaction strength $\tilde{n}\tilde{r}_0^2 = 0.5$ (red arrow) and $\tilde{n}\tilde{r}_0^2 = 32$ (blue arrow).

From this last expression we can define the projected two - body density matrix as:

$$h(\mathbf{r}) = \frac{1}{N} \int \int d\mathbf{r}_1 d\mathbf{r}_2 \rho_2(\mathbf{r}_1 + \mathbf{r}, \mathbf{r}_2 + \mathbf{r}; \mathbf{r}_1, \mathbf{r}_2) \tag{6.19}$$

It is important to note that the two density matrices that we have defined are not normalised in the same way, at $r = 0$ their normalisation is given by: $\rho_1(0) = 1$ and $h(0) = \frac{N}{2}$. As we have seen in previous chapters, for homogeneous systems, off - diagonal long range order in the one - body density matrix implies a finite value of eq. (6.17) at large separations:

$$\lim_{r\to\infty} \rho_1(r) = n_0, \tag{6.20}$$

where $n_0 \leq 1$ is the fraction of atoms in the condensate of each layer. In an analogous way, off - diagonal long range order in the two - body density matrix entails

$$\lim_{r\to\infty} h(r) = \alpha. \tag{6.21}$$

One should notice that a non - zero asymptotic value at the level of the one - body density matrix implies also a non - zero at the level of the two - body density matrix and, in this case, $\alpha = \frac{N}{2} n_0^2$, which is macroscopically large. However, even if $n_0 = 0$, we can have $\alpha \neq 0$ (with $\alpha < 1$) that can be interpreted as the condensate fraction of pairs [97]. We can define an intrinsic order parameter related to the two - body density matrix as [98]:

$$n_0^{\text{mol}} = \alpha - \frac{N}{2} n_0^2 \tag{6.22}$$

The molecular condensate fraction n_0^{mol} coincides with the long - range behaviour α of the two - body density matrix when the atomic condensate n_0 vanishes and one removes from it the largest contribution, which scales as the total number of particles, when $n_0 \neq 0$.

The calculation of the two different density matrices using the DMC method relies on the usual extrapolation technique based on both DMC and VMC results in order to extract the pure expectation value of the relevant operator on the ground state of the system. It is known that, if the guiding wave function is similar enough to the exact ground state wave function of the system, the extrapolation technique helps us to eliminate the bias in the results for the physical observables.

Results for the one - body and two - body density matrices are shown in Figures 6.6 and 6.7 for densities $nr_0^2 = 1$ and $nr_0^2 = 10^{-2}$. The particle condensate is clearly vanishing for inter - layer distances smaller than a critical value, and grows continuously until it reaches the value corresponding to a single layer of dipoles at the density $nr_0^2/2$ [29]. The molecular condensate fraction n_0^{mol} is extremely small (but finite) in the regime of weak pairing which means large inter - layer separations, and increases smoothly in the

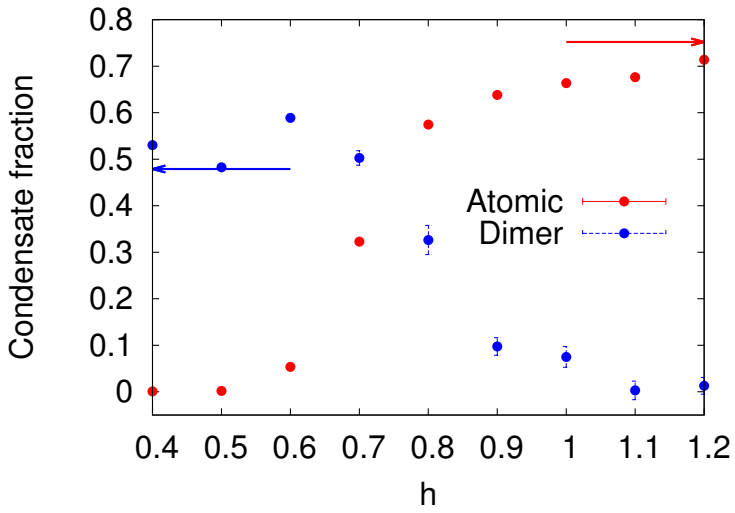

Figure 6.7: Atomic condensate n_0 and molecular condensate $n_0^{\rm mol}$ as a function of h/r_0 at the density $nr_0^2 = 10^{-2}$. Arrows correspond to the condensate fraction of a single layer of dipoles at the effective interaction strength $\tilde{n}\tilde{r}_0^2 = 0.005$ (red arrow) and $\tilde{n}\tilde{r}_0^2 = 0.32$ (blue arrow).

region of the transition to the molecular regime until it reaches the expected condensate fraction for a single layer of dipolar dimers. We notice that for the two different densities that we have studied there is a significant range of h values where n_0 and $n_0^{\rm mol}$ are simultaneously different from zero.

It is important to note that the behaviour of the atomic condensate fraction in terms of the inter-layer distance is compatible with the behaviour of the order parameter in a second order phase transition. In fact, it is predicted in [46] that the phase transition between the dimer and atomic superfluids belongs to the Ising universality class, as in the situations studied in [99, 100]. In these references it is shown the existence of a second order phase transition between a phase where n_0 and $n_0^{\rm mol}$ are both non zero and another one with $n_0 = 0$ and $n_0^{\rm mol} \neq 0$, and this is an Ising like phase transition according to the spontaneously broken symmetry.

6.7 Pair correlation function

In order to emphasize the existence of a continuous phase transition in the bilayer dipolar system we show in this section the results obtained by the Monte Carlo simulations for the radial distribution function. In this system one can define two different correlation functions: the one corresponding to pairs of particles in the same layer, and the other one corresponding particles in different layers. We denote each contribution as $g_{ud}(r)$ and $g_{uu}(r)$ for the

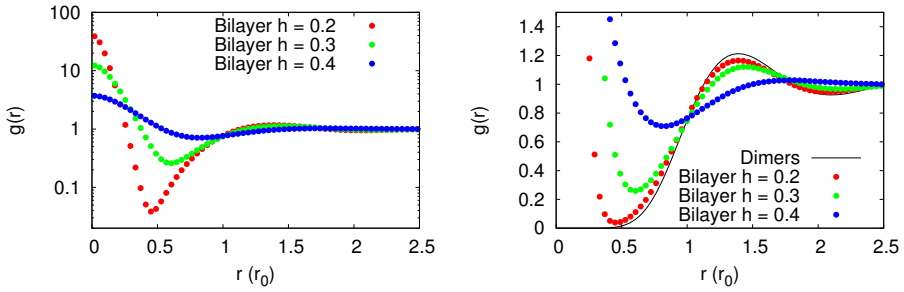

(a) (b)

Figure 6.8: (a) Pair correlation functions corresponding to particles on different layers for several values of the inter - layer distance. (b) Same pair correlation functions compared with the radial distribution function of a system of dimers with $\tilde{r}_0 = 8r_0$.

inter and intra - layer radial distribution functions respectively.

It is expected that the pair correlation function reflects the fact that the physics of the system will change when the value of the inter - layer distance changes. We have performed Monte Carlo simulations for a fixed density of $nr_0^2 = 1$ and several values of h and we have observed qualitative differences along the transition range.

At large values of h ($h \gtrsim 0.5$) the pair correlation function for particles in the same layer ($g_{uu}(r)$) is similar to the one corresponding to a single two dimensional layer; the pair correlation function for particles in different layers ($g_{ud}(r)$) shows a small peak at $r = 0$ indicating the existence of a force that tries to put the particles of the system in the dimer configuration, but despite of this $r = 0$ peak the shape of the radial distribution function is shallow. In fact, for values of the inter - layer distance $h > 1$ the pair correlation function is approximately flat.

At low values of h ($h \lesssim 0.3$) we have a completely different situation, the inter - layer interaction strength is large enough to have an strongly bound state and to cause the dimerization of the system. In this situation it is clear that the inter - layer pair correlation function will have a very steep peak at $r = 0$ that indicates the preference of the system to form dimers. At distances larger than the typical size of the bound state the shape of $g_{ud}(r)$ approaches the expected pair correlation function for a system of dimers. Concerning the intra - layer distribution function, the situation is completely analogous, the typical distance between particles on the same layer changes during the transition due to the differences between the dipole - dipole interaction and the dimer - dimer interaction.

Figures 6.8 and 6.9 summarise the results of the Monte Carlo simulations. In left panel of Figure 6.8 we can clearly see the large peak at $r = 0$ indicating

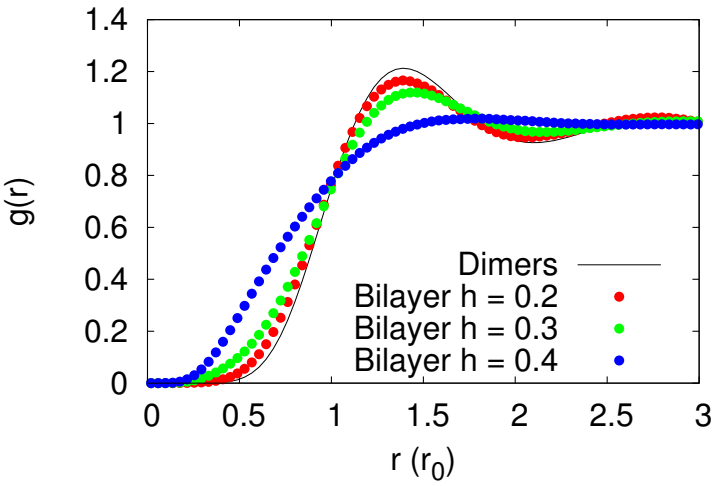

Figure 6.9: Pair correlation function for particles in the same layer and several inter-layer distances. It is also shown the pair correlation function for the system of dimers with $\tilde{r}_0 = 8r_0$.

the dimerization transition of the system. In right panel of Figure 6.8 and in Figure 6.9 it can be seen that the large scale physical properties of the system are completely dominated by the interaction between dimers. This change in the dominant interaction in the system can be understood as a clear sign that indicates the existence of a phase transition in the system.

6.8 Conclusions

We have presented the results of the Monte Carlo study performed over the dipolar gas of bosons in a bilayer configuration. In this chapter we have evaluated some physical quantities that could help us to clarify the physical behaviour of the system as the interaction between layers is changed. We have found that all the physical observables studied are compatible with the existence of a second order phase transition modulated by the inter-layer distance h. In this sense, the results presented in this work are in good agreement with some previous studies of dipolar gases in a bilayer.

Unfortunately the results obtained with our Monte Carlo simulations are not accurate enough to allows us to find solid numerical evidence of the existence of this second order phase transition. We have not been able to find a dependence of the order parameter (the atomic condensate fraction) with the number of particles because in order to obtain an accurate enough result a very large system must be analysed. The main problem with this is that the structure of the guiding wave function implies that the evaluation

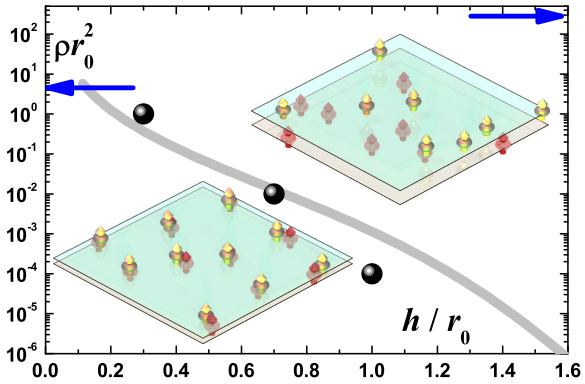

Figure 6.10: Schematic phase diagram featuring the single-particle (upper region) and the pair superfluid (lower region). The dots correspond to the transition points as obtained from DMC simulations. The two arrows show the freezing density of a single layer of particles (right) and of dimers (left). The line separates the region where $|E_B|/2 < \mu$ (weak pairing) from the region where $|E_B|/2 > \mu$ (strong pairing)

of the derivatives (needed to evaluate the energy of the system) scale as N^3 rather that the usual N^2 scaling that we have in an standard Jastrow function simulation. A possible solution to that problem could be to find a Jastrow wave function that is able to reproduce the key ingredients of the physics of the system.

Despite of the lack of precission of our numerical simulations we can give an approximate description of the phase diagram of the bilayer dipolar gas in terms of the density n and the inter-layer distance h. The schematic phase diagram is shown in Figure 6.10. It can be shown from the figure that the estimated transition line obtained using mean-field arguments gives a good estimation of the transition point for low values of the density, while for large values of density the mean-field results and the numerically evaluated point starts to deviate from each other.

Chapter 7

Conclusions and outlook

In this Thesis we have presented an exhaustive study of the physics of two-dimensional bosonic dipolar quantum gases. In order to provide an accurate description of the system, we have developed different quantum Monte Carlo codes that have been applied to the study of different situations of the system. The use of different Monte Carlo methods allows us to choose the best suited technique for each situation. We present results for different properties of the system spanning a wide range of densities and tilting angles. In this sense, the most relevant result obtained in this work is the phase diagram of two dimensional dipoles in a single layer with a tilting angle, although other aspects have been also explored.

In addition to the study of the single layer two-dimensional dipolar system, we have also started to analyse the physics of the bilayer configuration. As a starting point, we have chosen the simplest situation where the dipolar moments of all the particles are polarised orthogonally to the layers.

In the following sections we summarize the main conclusions of this Thesis.

7.1 Two-body dipolar problem and low density dipolar gas

In Chapter 3 we have solved the zero-energy two-body scattering problem by means of a Green's function and a decomposition of the wave function in partial waves. Using the Green's function we have built a perturbative solution for the two-body wave function. From the asymptotic behavior of the $m = 0$ angular momentum contribution to the wave function we have found the dependence of the s-wave scattering length on the polarisation angle, which dominates at large distances.

In Chapter 4 we have built a variational Jastrow many-body wave function from the solution of the two-body problem that has been used as a guiding function in a diffusion Monte Carlo simulation of the gas of polarised

dipoles at low densities. We have found that the scaling of the energy in the gas parameter is preserved up to values of x where other isotropic systems deviate significantly. This behaviour extends to other relevant ground state quantities like the pair distribution function, the static structure factor and the one-body density matrix, including the condensate fraction which can be determined from the large distance asymptotic behaviour of its isotropic part ($m = 0$ partial wave). We have also compared the excitation spectrum of the system coming from Bogoliubov theory with the Feynman approximation obtained from the numerical simulations. We have seen that, as the other observables studied, the Bogoliubov approach provides an accurate estimation of the excitation spectrum at low densities and, as the density is increased, it starts to deviate from the numerical results.

7.2 Phase diagram of two dimensional dipolar system with a tilt

In Chapter 5 we have studied the phase diagram of the two dimensional system of bosonic dipoles with a non zero tilting angle. As it is expected, at low densities the system is in the gas phase. When the density is increased and the tilting angle is below $\alpha \sim 0.45$ the system undergoes a first-order phase transition from the gas to the crystal phase. The anisotropy of the interaction influences the shape of the crystalline lattice by elongating the interparticle separation in the direction where the dipole-dipole potential is stronger.

Between the crystallisation density of the isotropic ($\alpha = 0.0$) system and a threshold density of $n_{th} r_0^2 \sim 125$ the system undergoes a second-order phase transition from the gas to the stripe phase. Interestingly, the critical exponents of this second order transition are nearly independent of the tilting angle and are compatible with the 3D Ising and 3D XY model universality classes within the statistical uncertainties of our simulations. Remarkably, our results show that for large polarization angles the stripe phase can be observed experimentally at densities significantly lower than those required to reach the solid phase although still quite large compared to what it is usually achieved in typical BEC experiments. An accurate determination of the universality class of the gas - stripe phase transition requires a more accurate evaluation of the order parameter of the system and probably the use of larger systems than the used along this work.

Finally, at high densities and large tilting angles the system shows a first order phase transition between the crystal and stripe phases. The slope of this transition curve is extremely high, indicating that due to the anisotropy of the interaction, the crystal phase of the system it is no longer stable if the dipole-dipole potential is highly anisotropic, at least for the range of densities analysed.

7.3 Quantum phase transition in a bilayer system of dipoles

Chapter 6 contains the results of the Quantum Monte Carlo study of the dipolar gas of bosons in a bilayer configuration. In this chapter, we have evaluated some of the physical quantities that could help to clarify the physical behaviour of the system as the interaction between layers varies. We have found that all the physical observables studied are compatible with the existence of a second order phase transition modulated by the inter-layer distance h. In this sense, the results presented in this work are in good agreement with previous studies of dipolar gases in bilayer configurations.

Unfortunately the results obtained with our Monte Carlo simulations are not accurate enough to allows us to find a solid numerical evidence of the existence of this second order phase transition. We have not been able to find a dependence of the order parameter (the atomic condensate fraction) on the number of particles because very large system sizes are required in that analysis, much larger that those directly available in our simulations. The main problem with this is that the structure of the guiding wave function employed implies that the evaluation of the derivatives (needed to evaluate the energy of the system) scale as N^3 rather that the usual N^2 scaling that one has in standard Jastrow function simulation. A possible solution to that problem could be to find a Jastrow wave function that is able to reproduce the key ingredients of the physics of the system.

Bibliography

[1] M. H. Anderson, J. R. Ensher, M. R. Mathews, C. E. Wieman and E. Cornell, Science **269**, 198 (1995).

[2] K. B. Davis, M. O. Mewes, M. R. Andrews, N. J. Vandruten, D. S. Durfee, D. M. Kurn and W. Ketterle, Phys. Rev. Lett. **75**, 3969 (1995).

[3] B. DeMarco and D. S. Jin, Science, **285**, 1703 (1999).

[4] A. G. Truscott, K. E. Strecker, W. I. McAlexander, G. B. Partridge and R. G. Hulet, Science, **291**, 2570 (2001).

[5] F. Schreck, L. Khaykovich, K. Corwin, G. Ferrari, T. Bourdel, J. Cubizolles and C. Salomon, Phys. Rev. Lett. **87**, 080403 (2001).

[6] Z. Hadzibabic, C. Stan, K. Dieckmann, S. Gupta, M. Zwierlein, A. Görlitz and W. Ketterle, Phys. Rev. Lett. **88**, 160401 (2002).

[7] C. J. Pethick and H. Smith, "Bose-Einstein condensation in dilute gases", Cambridge University Press (2002).

[8] T. Köhler, K. Góral and P. S. Julienne, Rev. Mod. Phys. **78**, 1311 (2006).

[9] C. Chin, R. Grimm, P. S. Julienne and E. Tiesinga, Rev. Mod. Phys. **82**, 1225 (2010).

[10] A. Griesmaier, J. Werner, S.Hensler, J.Stuhler, and T. Pfau, Phys. Rev. Lett. **94**, 160401 (2005).

[11] J. Stuhler, A. Griesmaier, T. Koch, M. Fattori, T. Pfau, S. Giovanazzi, P. Pedri, and L. Santos, Phys. Rev. Lett. **95**, 150406 (2005).

[12] K. K. Ni, S. Ospelkaus, M. H. G. de Miranda, A. Pe'er, B. Neyenhuis, J. J. Zirbel, S. Kotochigova, P. S. Julienne, D. S. Jin, and J. Ye, Science **322**, 231 (2008).

[13] S. Ospelkaus, A. Pe'er, K. K. Ni, J. J. Zirbel, B. Neyenhuis, S. Kotochigova, P. S. Julienne, J. Ye and D. S. Jin, Nature Phys. **4**, 622 (2009).

[14] K. K. Ni, S. Ospelkaus, D. Wang, G. Quémner, B. Neyenhuis, M. H. G. de Miranda, J. L. Bohn, J. Ye and D. S. Jin, Nature **464**, 1324 (2010).

[15] A. D. Lercher, T. Takekoshi, M. Debatin, B. Schuster, R. Rameshan, F. Ferlaino, R. Grimm and H. C. Nägerl, Eur. Phys. J. D (2011), arXiv:1101.1409v1.

[16] M. Lu, N. Q. Burdick, S. H. Youn, and B. L. Lev, Phys. Rev. Lett. **107**, 190401 (2011).

[17] M. Lu, N. Q. Burdick and B. L. Lev, Phys. Rev. Lett. **108**, 215301 (2012).

[18] T. Takekoshi, M. Debatin, R. Rameshan, F. Ferlaino, R. Grimm, H.-C. Nägerl, C. R. Le Sueur, J. M. Hutson, P. S. Julienne, S. Kotochigova, and E. Tiemann, Phys. Rev. A **85**, 032506 (2012).

[19] C. Ticknor, Phys. Rev. A **80**, 052702 (2009).

[20] C. Ticknor, Phys. Rev. A **81**, 042708 (2010).

[21] C. Ticknor, Phys. Rev. A **84**, 032702 (2011).

[22] I. R. Lapidus, Am. J. Phys. **50**, 45 (1982).

[23] S. K. Adhikari, Am. J. Phys. **54**, 362 (1986).

[24] K. Kanjilal, J. L. Bohn and D. Blume, Phys. Rev. A **75**, 052705 (2007).

[25] D. H. J. O'Dell, S. Giovanazzi and G. Kurizki, Phys. Rev. Lett. **90**, 110402 (2003).

[26] R. M. Wilson, S. Ronen, J. L. Bohn, and H. Pu, Phys. Rev. Lett. **100**, 245302 (2008).

[27] L. Santos, G. V. Shlyapnikov, and M. Lewenstein, Phys. Rev. Lett. **90**, 250403 (2003).

[28] F. Mazzanti, R. E. Zillich, G. E. Astrakharchik, and J. Boronat, Phys. Rev. Lett. **102**, 110405 (2009).

[29] G. E. Astrakharchik, J. Boronat, I. L. Kurbakov, and Yu. E. Lozovik, Phys. Rev. Lett. **98**, 060405 (2007).

[30] H. P. Buchler, E. Demler, M. Lukin, A. Micheli, N. Prokof'ev, G. Pupillo, and P. Zoller, Phys. Rev. Lett. **98** 060404 (2007).

[31] A. Filinov, N. V. Prokof'ev, and M. Bonitz, Phys. Rev. Lett. **105**, 070401 (2010).

[32] N. Matveeva and S. Giorgini, Phys. Rev. Lett. **109**, 200401 (2012).

[33] C. Ticknor, R. M. Wilson, and J. L. Bohn, Phys. Rev. Lett. **106**, 065301 (2011).

[34] K. Sun, C. Wu and S. Das Sarma, Phys. Rev. B **82**, 075105 (2010).

[35] Y. Yamaguchi, T. Sogo, T. Ito and T. Miyakawa, Phys. Rev. A **82**, 013643 (2010).

[36] M. M. Parish and F. M. Marchetti, Phys. Rev. Lett. **108**, 145304 (2012).

[37] F. M. Marchetti and M. M. Parish, Phys. Rev. B **87**, 045110, (2013).

[38] M. Ruggeri, arXiv:1305.6007 [cond-mat.quant-gas] (2014).

[39] M. Klawunn, A. Pikovski, and L. Santos, Phys. Rev. A **82**, 044701 (2010).

[40] A. Pikovski, M. Klawunn, G. V. Shlyapnikov, and L. Santos, Phys. Rev. Lett. **105**, 215302 (2010).

[41] M. A. Baranov, A. Micheli, S. Ronen and P. Zoller, Phys. Rev. A **83**, 043602 (2011).

[42] N. T. Zinner, B. Wunsch, D. Pekker, and D.-W. Wang, Phys. Rev. A **85**, 013603 (2012).

[43] N. Matveeva and S. Giorgini, preprint, arXiv:1405.7588.

[44] C. Trefzger, C. Menotti, and M. Lewenstein, Phys. Rev. Lett. **103**, 035304 (2009).

[45] A. Safavi-Naini, S. G. Soyler, G. Pupillo, H. R. Sadeghpour, and B. Capogrosso-Sansone, New J. Phys. **15**, 013036 (2013)

[46] D. W. Wang, Phys. Rev. Lett. **98**, 060403 (2007).

[47] B. L. Hammond, W. A. Lester Jr. and P. J. Reynolds *Monte Carlo methods in ab initio quantum chemistry*, World Scientific (1994).

[48] J. Boronat and J. Casulleras, Phys. Rev. B **49**, 8920 (1994).

[49] S. A. Chin, Phys. Rev. A **42**, 6991 (1991).

[50] D. M. Ceperley, Rev. Mod. Phys. **67**, 279 (1995).

[51] A. Sarsa, K. E. Schmidt and W. R. Magro, J. Chem. Phys. **113**, 1366 (2000).

[52] J. E. Cuervo, P.-N. Roy and M. Boninsegni, J. Chem. Phys. **122**, 114504 (2005).

[53] M. Rossi, M. Nava, L. Reatto and D. E. Galli, J. Chem. Phys. **131**, 154108 (2009).

[54] R. Rota, J. Casulleras, J. Boronat and F. Mazzanti, Phys. Rev. E **81**, 016707 (2010).

[55] M. Sprik, M. L. Klein and D. Chandler, Phys. Rev. B **31**, 4234 (1995).

[56] M. Suzuki, Phys. Lett. A **201**, 425 (1995).

[57] S. A. Chin, Phys. Lett. A **226**, 344 (1997).

[58] S. A. Chin and C. R. Chen, J. Chem. Phys. **117**, 1409 (2002).

[59] T. Lahaye, C. Menotti, L. Santos, M. Lewenstein, T.Pfau. *The physics of dipolar quantum gases*, arXiv: 0905.0386v1.

[60] M. Abramowitz, I. A. Stegun. *Handbook of mathematical functions with formulas, graphs, and mathematical tables.*

[61] G. B. Arfken, H. J. Weber. *Mathematical methods for physicists*, Elsevier Academic Press.

[62] D. G. Duffy. *Green's functions with applications*, Chapman & Hall/CRC

[63] J. J. Sakurai, S. F. Tuan. *Modern quantum mechanics*, Addison-Wesley Publishing company

[64] T. D. Lee and C. N. Yang, Phys. Rev. **105**, 1119 (1957); T. D. Lee, K. Huang, and C. N. Yang, *ibid.* **106**, 1135 (1957).

[65] M. Girardeau, J. Math. Phys. **1**, 516 (1960).

[66] M. Schick, Phys. Rev. A **3**, 1067 (1971).

[67] E. H. Lieb and J. Yngvason, J. Stat. Phys. **103**, 509 (2001).

[68] E. B. Kolomeisky and J. P. Straley, Phys. Rev. B **46**, 11749 (1992).

[69] A. Yu. Cherny and A. A. Shanenko, Phys. Rev. E **64**, 027105 (2001).

[70] C. Mora and Y. Castin, Phys. Rev. Lett. **102** 180404 (2009).

[71] G. E. Astrakharchik, J. Boronat, J. Casulleras, I. L. Kurbakov, and Yu. E. Lozovik, Phys. Rev. A **79**, 051602(R) (2009).

[72] F. Mazzanti, A. Polls, and A. Fabrocini, Phys. Rev. A **71**, 033615 (2005).

[73] A. L. Fetter and J. D. Walecka, *Quantum Theory of Many-Particle Systems* (McGraw-Hill, New York, 1971).

[74] S. Giorgini, J. Boronat, and J. Casulleras, Phys. Rev. **A60**, 5129 (1999).

[75] F. Mazzanti, A. Polls, and A. Fabrocini, Phys. Rev. **A67**, 063615 (2003).

[76] L. Reatto and G. V. Chester, Phys. Rev. 155, 88 (1967).

[77] E. Krotscheck, in *Microscopic quantum many-body theories and their applications*, Proc. European Summer School, Ed. J. Navarro and A. Polls, Springer (1998).

[78] A. Macia, F. Mazzanti, J. Boronat, and R. E. Zillich, Phys. Rev. A **84**, 033625 (2011).

[79] G. E. Astrakharchik, J. Boronat, I. L. Kurbakov, Yu. E. Lozovik, and F. Mazzanti, Phys. Rev. A **81**, 013612 (2010).

[80] J. Casulleras and J. Boronat, Phys. Rev. B **52**, 3654 (1995).

[81] R. P. Feynman, Phys. Rev. **94**, 262 (1954).

[82] J. Boronat, J. Casulleras, F. Dalfovo, S. Stringari and S. Moroni, Phys. Rev. B **52**, 1236 (1995).

[83] A. Macia, F. Mazzanti and J. Boronat, The Eur. Phys. J. D, **66**, 301, (2012).

[84] S. Yi and L. You, Phys. rev. A **63**, 053607 (2000).

[85] A. Derevianko, Phys. Rev. A **67**, 033607 (2003).

[86] D. Hufnagl, R. Kaltseis, V. Apaja and R. E. Zillich, Phys. Rev. Lett. **107**, 065303 (2011).

[87] A. Macia, D. Hufnagl, F. Mazzanti, J. Boronat and R. E. Zillich, Phys. Rev. Lett. **109**, 235307, (2012).

[88] L. P. Pitaevskii, Zh. Eksp. Teor. Fiz. **36**, 1169 (1958)

[89] C. E. Campbell and E. Krotscheck, J. of Low Temp. Phys. **158**, 226 (2010).

[90] H. E. Stanley, *Introduction to phase transitions and critical phenomena*, Oxford University Press (1971).

[91] S. Sachdev. *Quantum phase transitions*, Cambridge University Press, (2011)

[92] M. Ruggeri, arXiv:1305.6007v2 [cond-mat.quant-gas], (2013)

[93] B. Simon, Ann. Phys. **97**, 279 (1976).

[94] K. Yang, M. de Llano, American Journal of Physics **57**, 85 (1989).

[95] A. Macia, G. E. Astrakharchik, F. Mazzanti, S. Giorgini and J. Boronat, Phys. Rev. A **90**, 043623 (2014).

[96] G. E. Astrakharchik, J. Boronat, J. Casulleras, and S. Giorgini, Phys. Rev. Lett. **95**, 230405 (2005).

[97] C. N. Yang, Rev. Mod. Phys. **34**, 694 (1962).

[98] D. H. Kobe, J. Math. Phys. **10**, 1507 (1969).

[99] L. Radzihovsky, J. Park and P. B. Weichman, Phys. Rev. Lett. **92**, 160402 (2004).

[100] M. W. J. Romans, R. A. Duine, S. Sachdev and H. T. C. Stoof, Phys. Rev. Lett. **93**, 020405 (2004).